AD-A243 674

C
E
391
D
D

CRREL REPORT 91-19

The Role of Thermal Convection in Heat and Mass Transport in the Subarctic Snow Cover

Matthew Sturm

October 1991

This document has been approved for public release and sale; its distribution is unlimited.

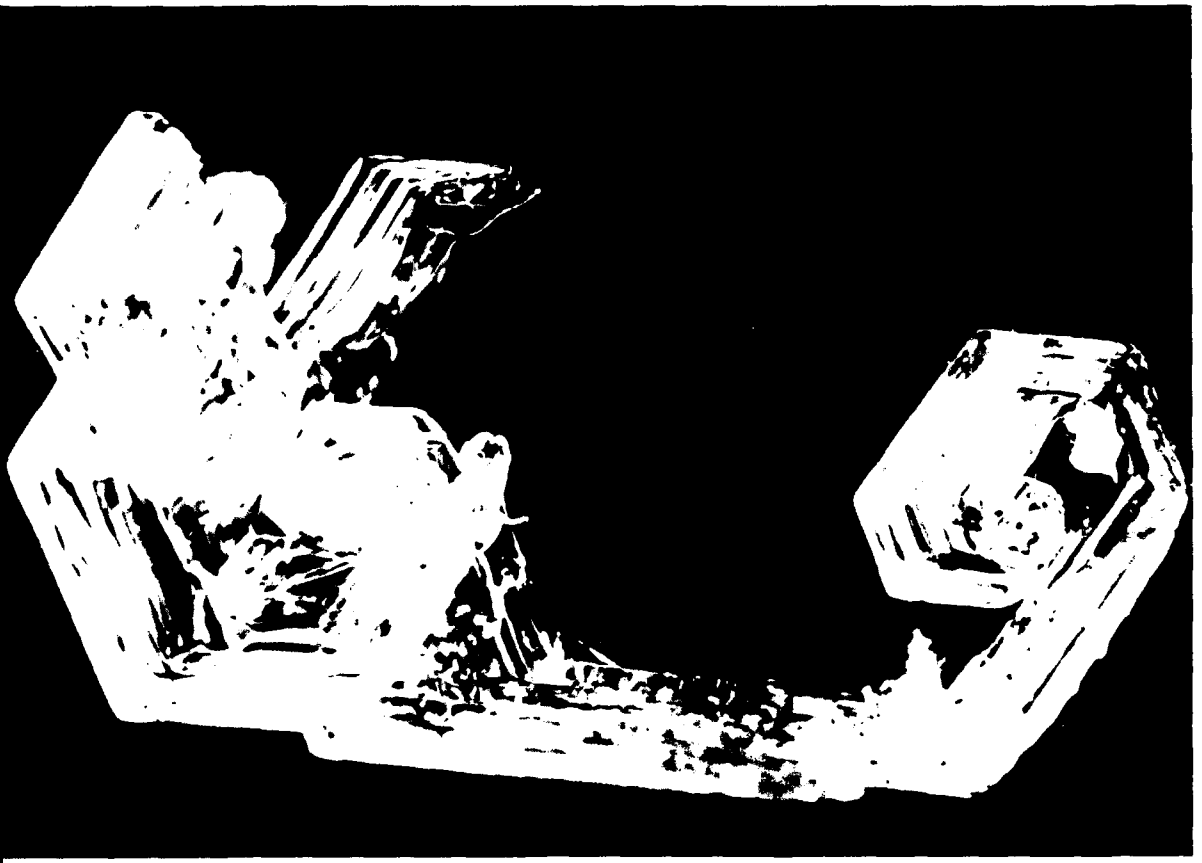

91-18772

91 12 23 116

For conversion of SI metric units to U.S./British customary units of measurement consult ASTM Standard E380, Metric Practice Guide, *published by the American Society for Testing and Materials, 1916 Race St., Philadelphia, Pa. 19103.*

Cover: A depth hoar crystal from the Fairbanks snow cover, magnified approximately 11.5x. The crystal is a scrolled cup crystal from near the base of the snow. Striae and steps on cups are typical of the depth hoar found in the subarctic snow cover.

CRREL Report 91-19

U.S. Army Corps of Engineers
Cold Regions Research & Engineering Laboratory

The Role of Thermal Convection in Heat and Mass Transport in the Subarctic Snow Cover

Matthew Sturm

October 1991

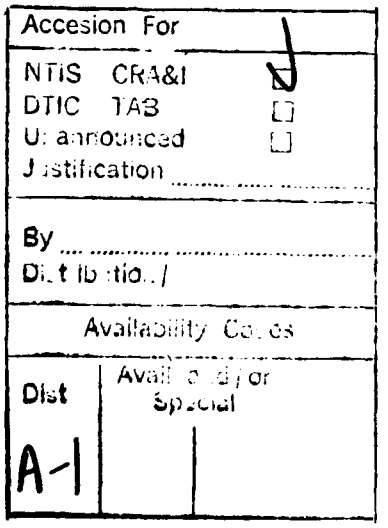

Approved for public release; distribution is unlimited.

PREFACE

This report was prepared by Dr. Matthew Sturm, Research Physical Scientist, USA Cold Regions Research and Engineering Laboratory. This study was supported by the In-House Laboratory Independent Research (ILIR) program, Project No. 4A161101A91D, Work Unit 524, *Development of a System to Measure Wind Pumping and Pressure Pumping in Natural Snow Covers.*

The report was technically reviewed by Dr. Wilford F. Weeks, University of Alaska, Geophysical Institute, and Dr. Donald Perovich, USACRREL, and it benefited from the help and guidance of many others. Dr. Carl Benson was an inspiration, exasperation, and mentor during the research and writing. Thirty years of working in the snow has not dampened his enthusiasm. Dr. Jerome Johnson helped initiate this project, supplied physical insight when it was most needed, and insulated the author from the demands of work to have the time to write up the results. Drs. Sue Ann Bowling, Lewis Shapiro, and William Harrison all contributed to the maturation of the work. Edward Chacho coordinated his permeability measurements. Dr. Donald Perovich analyzed the data from 1984–1985 and provided good, skeptical comments at the right time. Stephen Perkins wrote computer operating and analysis programs that were critical to the success of the work. Monique Fouchet and James Morse fabricated many of the thermistor strings. Max Stark, Joseph Holty, and Lawrence Burke at the University of Alaska farm helped in many ways.

The contents of this report are not to be used for advertising or promotional purposes. Citation of brand names does not constitute an official endorsement or approval of the use of such commercial products.

CONTENTS

ILLUSTRATIONS

Figure

TABLES

Table | Page

NOMENCLATURE

A	coefficient of exponential relationship
a_1, a_2, etc.	coefficients of polynomial fit to data
B	exponent of exponential relationship
b_1, b_2, etc.	intercepts of linear fit to data
c	specific heat capacity (J kg^{-1} °C^{-1})
c_t	specific heat capacity of thermistor (J kg^{-1} °C^{-1})
$\overline{d}$	mean "grain size" from sieving or photography (mm)
$\overline{D}_{j,j+1}$	central sieve mesh diagonal (mm)
D_o	diffusion coefficient of water vapor in air (m^2 s^{-1})
e	total uncertainty in calculated result
e_h	uncertainty in measurement of layer thickness (m)
e_{Dh}	uncertainty in change in layer thickness (m)
e_r	uncertainty in measurement of density (kg m^{-3})
e_{Dr}	uncertainty in change in density (kg m^{-3})
$\dot{e}$	strain rate (s^{-1})
$\dot{e}_{zz}$	vertical strain rate (s^{-1})
F	enhancement factor
g	acceleration of gravity (m s^{-2})
h	total snow depth or total snow layer thickness (m)
h_b	basal snow layer thickness (m)
H	geometric characteristic parameter of heat flow meter
i	electrical current (amp)
J	mass flux per unit area per unit time (kg s^{-1} m^{-2})
$\nabla \cdot \vec{J}$	mass flux divergence (kg m^{-2} s^{-1} m^{-1})
k	thermal conductivity of snow (W m^{-1} K^{-1})
k_{dry}	thermal conductivity without latent heat transfer (W m^{-1} K^{-1})
k_{eff}	bulk effective thermal conductivity including heat transport by convection (W m^{-1} K^{-1})
k_m	thermal conductivity of HFM (heat flow meter) (W m^{-1} K^{-1})
k_s	thermal conductivity of material around HFM (W m^{-1} K^{-1})
L	number of sieves; also depth below snow surface
L_s	latent heat of sublimation (J kg^{-1})
m	mass (kg)
$\overline{m}_j$	average mass of a grain in the jth sieve (kg)
m_t	mass of thermistor (kg)
M_j	weight fraction in the jth sieve (kg)
n	number of observations
N	number of grains per unit volume
N_j	total number of grains in the jth sieve
N_T	total number of grains in a sample
Nu	Nusselt number
P	electrical power (W)
Pe_h	Peclet number for heat
Q_m	heat flow measured by heat flow meter (J m^{-2} s^{-1})
Q_s	heat flow at the snow/soil interface (J m^{-2} s^{-1})
r	correlation coefficient; also radial coordinate
R	radius of cylindrical hole

Ra	Rayleigh number
Ra_{cr}	critical Rayleigh number (onset of convection)
t	time (s)
T	temperature (°C)
ΔT	change in temperature (°C)
$\vec{v}$	air flow velocity (m s^{-1})
v_z	vertical air flow velocity (m s^{-1})
V	volume (m^3)
z	vertical coordinate (m)
z_t	thermistor height above ground (m)
$\partial J/\partial z$	vertical mass flux gradient (kg m^{-2} s^{-1} m^{-1})
$\partial T/\partial z$	temperature gradient (°C m^{-1})
$\partial^2 T/\partial z^2$	curvature in vertical temperature profile (°C m^{-2})
α	thermal diffusivity (m^2 s^{-1})
α_{air}	thermal diffusivity of air (m^2 s^{-1})
α_{ice}	thermal diffusivity of ice (m^2 s^{-1})
α_{snow}	thermal diffusivity of snow (m^2 s^{-1})
α_{dry}	thermal diffusivity without latent heat transfer (m^2 s^{-1})
β	isobaric coefficient of thermal expansion ($°C^{-1}$)
ΔV	small control volume (m^3)
κ_i	intrinsic permeability (m s^{-1} N^{-1} m^{-2})
ν	kinematic viscosity (m^2 s^{-1})
ρ	bulk snow density or bulk density of a snow layer (kg m^{-3})
ρ_v	water vapor density (kg m^{-3})
$\partial\rho/\partial t$	bulk densification rate including compaction (kg m^{-3} s^{-1})
$(\partial\rho/\partial t)_v$	densification from vapor flux only (kg m^{-3} s^{-1})
ρc	volumetric heat capacity (J m^{-3} $°C^{-1}$)
$(\rho c)_f$	volumetric heat capacity of air (J m^{-3} $°C^{-1}$)
$(\rho c)_m$	volumetric heat capacity of porous medium (J m^{-3} $°C^{-1}$)
$(\rho c)_s$	volumetric heat capacity of ice (J m^{-3} $°C^{-1}$)
τ	response time of snow to temperature change (s)
ϕ	porosity, or grain size measure if associated with sieving

The Role of Thermal Convection in Heat and Mass Transport in the Subarctic Snow Cover

MATTHEW STURM

1. INTRODUCTION

The purpose of this study was to determine if air convects in a natural snow cover and, if it does, to evaluate its importance in moving heat and water vapor through the snow. To do this, measurements of temperature and density, from which heat and mass flow could be calculated, were made in the dry, cold snow cover near Fairbanks, Alaska.

The question of whether convection occurs in natural snow covers has been debated for decades. Seasonal snow covers lie on ground that is generally warmer than the air. This condition creates an unstable density stratification in the air in the snow that is necessary, but may not be sufficient, to cause thermal convection. Early investigators suspected that convection occurred, basing their speculation on inconclusive field tests and the failure of their diffusive mass transport models to predict the observed mass flux in the snow (Bader et al. 1939) or the relatively rapid rate at which the snow temperature changed (Bey 1951). More recently, attempts to induce convection in laboratory experiments have had mixed results, with convection occurring in some experiments (Powers et al. 1985a, 1985b) but not in others (Akitaya 1974, Brun and Touvier 1987). Theoretical studies have been equally inconclusive, suggesting that convection was likely to occur only in deep, highly permeable snow covers (Palm and Tveitereid 1979, Powers et al. 1985a, 1985b).

The only germane field studies were done by Trabant and Benson (1972) and Gjessing (1977). These authors concluded from their measurements that convection occurs in natural snow covers, but in both cases the presence of convection was inferred from indirect evidence. For example, Trabant and Benson (1972) based their conclusion on the fact that the measured mass transport in the Fairbanks snow cover was too great to be accounted for by existing theories of diffusive mass transport. Recent diffusion models (Sommerfeld 1983, Colbeck 1983a, Gubler 1985), however, can account for the greater transport. The present study was undertaken because the existing evidence for convection in the snow, both theoretical and experimental, was contradictory and inconclusive.

The subarctic snow found near Fairbanks, with its extreme temperature gradients and permeability (Fig. 1, 2), appeared to be the ideal place to make the measurements necessary to determine if convection occurs in natural snow covers. Though of moderate depth (Fig. 3), the Fairbanks snow cover is subjected to temperature gradients many times stronger than those found in other snow covers (Fig. 1), generating highly unstable density stratification of the air in the snow. The snow completely

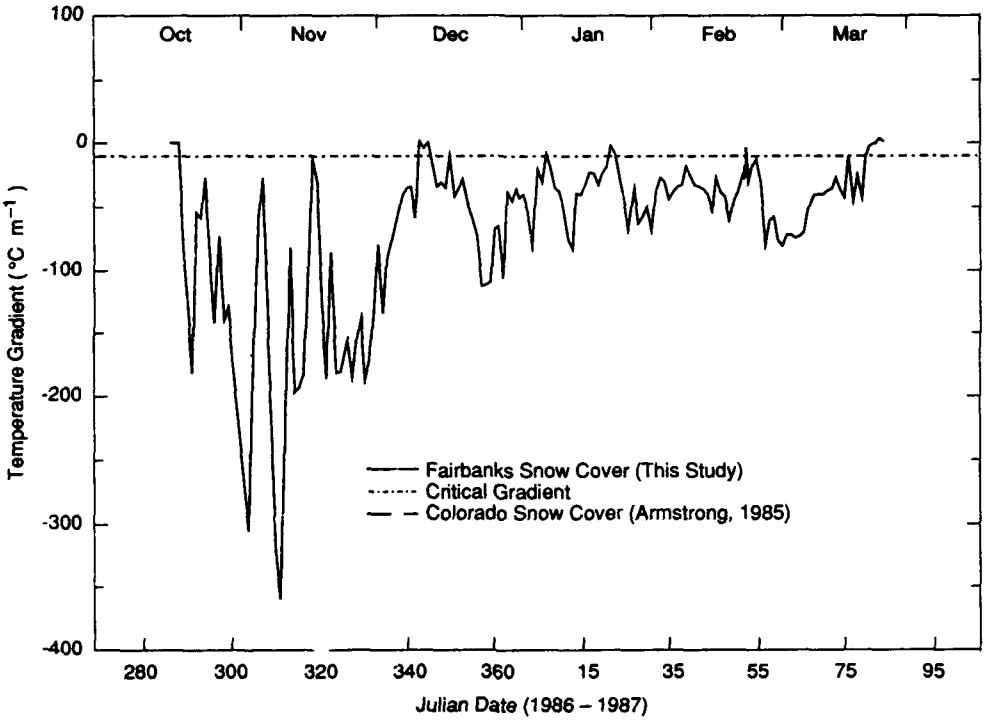

Figure 1. Average vertical temperature gradient across the Fairbanks snow cover during 1986–1987. For comparison, the temperature gradient for a snow cover in Colorado is also shown. The critical temperature gradient necessary for the formation of depth hoar is approximately 10 °C m^{-1}, shown by the dot-dash line. Temperature gradients in the Fairbanks snow cover exceed the critical gradient for more than 150 days.

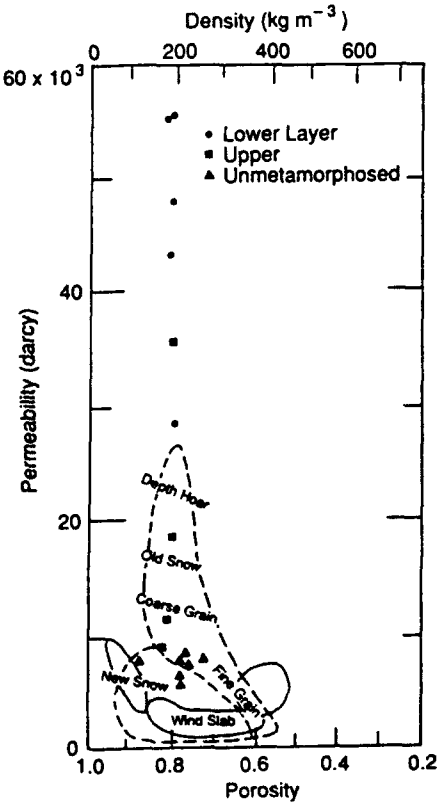

Figure 2. Air permeability of Fairbanks snow. Other snow types are shown by fields enclosed by solid lines (Shimizu 1970) and dashed lines (Bader et al. 1939). The permeability of Fairbanks snow (ground) is 2 to 3 times greater than previously measured for depth hoar and 5 to 7 times more permeable than for snow not subjected to strong temperature gradients because it was deposited on a table.

metamorphoses into depth hoar during the winter. As this metamorphism proceeds, the air permeability increases, becoming two to three times more permeable than any previously measured snow (Fig. 2 and Appendix A), thus increasing the likelihood of convection. In addition, a large body of snow texture observations made by Benson (unpublished), Trabant (1970), Benson and Trabant (1972), and Trabant and Benson (1972) at the same experimental site used in the present study suggested that convection occurred in the Fairbanks snow cover.

Intensive measurements were made in the Fairbanks snow during the winters of 1984–1985, 1985–1986, and 1986–1987. Because the movement of air could not be measured directly, natural thermal convection was identified by its perturbation of the three-dimensional temperature field in the snow, which was measured using an array of thermistors. To evaluate the role of convection in mass transport, precise density and grain-size measurements were made to determine the movement of water vapor and the metamorphic changes in the snow.

The vapor movement could not be ignored because heat and mass transport are inextricably linked in the snow cover. Ice, which is generally near its melting point, has a vapor pressure that is several orders of magnitude higher than that of most other geologic materials. The vapor pressure is also an exponential function of temperature (Fig. 4; Section 5, Convective Flow Velocity). Consequently, the strong temperature gradients in the Fairbanks snow cover produce vapor pressure gradients that cause sublimation from warm grains and deposition on cold grains, transferring both latent heat and mass. The temperature gradients

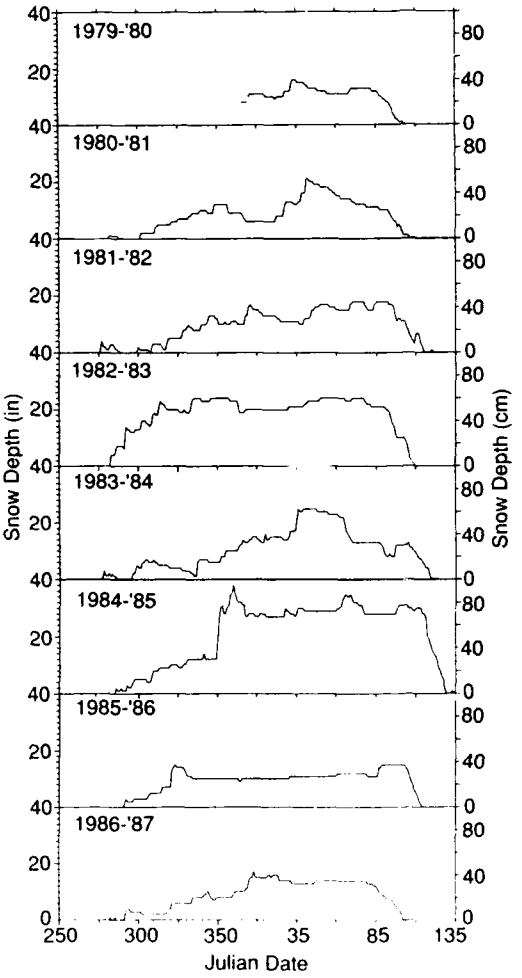

Figure 3. Snow depth in Fairbanks, 1980 to 1987. Data from the Fairbanks International Airport collected by the National Weather Service.

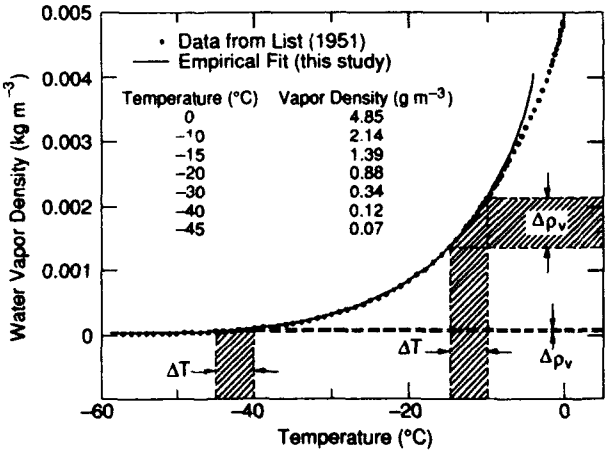

Figure 4. Saturation water vapor density over ice. The data (•) have been fitted with an exponential curve (—) $\rho_v = A e^{BT}$, where A = 0.005789, B = 0.09658 for T in °C. Temperature increments of 5°C between –10 and –15°C and –40 and –45°C produce vapor density changes that differ by a factor of 17 (striped areas labeled $\Delta\rho_v$).

in the Fairbanks snow are not only stronger (Fig. 1), but also include higher temperatures than many other snow covers. Thus, the absolute values of the vapor pressure are higner. For example, with a snow surface temperature of –45°C, the temperature of the base of the Fairbanks snow cover might be about –10°C. At equal depth below the surface on the Greenland Ice Sheet, the temperature would be about –40°C. An increment of 5° between –10 and –15°C corresponds with a change in water vapor density of 0.75×10^{-3} kg m^{-3}; a 5° increment between –40 and –45°C corresponds with a water vapor density change of 0.05×10^{-3} kg m^{-3}. These differ by a factor of 17 (Fig. 4). (Vapor density rather than vapor pressure is used in this report because it is more convenient in calculations. It can be converted to the vapor pressure using the ideal gas law.) In Fairbanks, the 5°C increment would occur over a vertical distance of 0.07 m, but would require a distance of about 0.5 m in the deep snow cover on the Greenland ice sheet, so the vapor density gradient in the Fairbanks snow would be 100 times stronger.

It is the mass transport due to vapor movement that causes snow metamorphism. In Fairbanks, the end result of the metamorphism is the transformation of the entire snow cover into depth hoar. It was this distinctive textural development that led Benson and Trabant (1972) to investigate the mass flux in the first place. One goal of the present investigation was to determine if convection played an important role in the development of the depth hoar texture, and conversely, the role played by depth hoar in establishing and maintaining convection. Depth hoar has been the subject of scientific and engineering interest for many years because of its role in providing a failure plane for avalanches.

There are several reasons why it is important to know if air convects in the snow. Convection can increase the effective thermal conductivity of snow, which in turn means that the ground under snow in which air is convecting would freeze deeper during the winter than ground under snow in which there was no convection. This is important to agriculture. The survival of under-snow biota also depends on how well the snow insulates them from ambient air temperature (Pruitt 1984). Convection may move contaminants into the snow (Gjessing 1977) and affect the mixing of isotopes (Friedman et al., in press). Environmental concerns make the former important, and the latter has a direct impact on the interpretation of snow pits and ice cores in polar regions, where depth hoar layers form the primary annual stratigraphic marker in ice sheets and glaciers.

Though the goal of this study was to determine if convection occurred in the snow, several related questions were of interest:

1) If convection occurs, what flow pattern develops?
2) What are the relative contributions of conduction, vapor movement with latent heat transfer, and convection of air to the overall heat transfer in snow?
3) Can specific metamorphic changes in the snow be attributed to convection?
4) Do existing theories adequately describe vapor transport in snow?

Background

Key points from the literature in heat and mass transport in snow are summarized below. Several relevant studies on convection in porous media other than snow are discussed in Section 5.

Diffusive mass transport in snow

Paulke (1934a, 1934b) and Seligman (1936) determined from their field observations that temperature gradients in the snow resulted in water vapor density gradients that drove vapor diffusion. Subsequently, at least 7 one-dimensional mathematical models of mass transport by water vapor diffusion have been developed (Bader et al. 1939, Yosida et al. 1955, Giddings and LaChapelle 1962, Yen 1963, de Quervain 1972, Palm and Tveitereid 1979, Fedoseeva and Fedoseev 1988). The diffusive mass transport predicted by the model of Bader et al. (1939) was so much smaller than observed mass transport that it led the authors to conclude that convection was transporting considerable mass. When their model results and observations did not agree, other authors (Yosida et al. 1955, Yen 1963, de Quervain 1972, Palm and Tveitereid 1979, Fedoseeva and Fedoseev 1988) concluded that the diffusion coefficient of water vapor was enhanced in the snow cover.

Yosida et al. (1955) used an experimental apparatus to measure the actual vapor flux gradient in a snow layer. Comparing model results to measurements, they determined that an enhancement factor (F) of approximately 5 was necessary for the diffusion model to produce the measured mass transport. Yen (1963), de Quervain (1972), Palm and Tveitereid (1979), and Fedoseeva and Fedoseev (1988), in comparing theoretical and experimental results, also found that they needed enhancement factors of approximately 5 to bring their calculated results into agreement with measurements.

By assuming the diffusion coefficient was enhanced (or the temperature gradients were enhanced) to bring model results in line with measured values of mass transport, the authors obscured the issue of why the models failed. It may have been because the models neglected convection, or because they were one-dimensional. These one-dimensional models required vapor flux to condense at the bottom of each ice layer and sublime from the top. Essentially, the snow was modeled as a series of horizontal ice plates and intervening air spaces—not realistic snow geometry. All the enhancement factors (with the exception of the work by Fedoseeva and Fedoseev [1988], who do not indicate the source nor method of measurement of their flux determinations) were determined by comparing the model results to only two measured values of mass transport. Thus, Trabant and Benson (1972) interpreted their mass transport measurements, which were nearly an order of magnitude greater than predicted by the models even with the enhancement factors, to indicate the presence of convection in the snow. However, the mismatch between the measured value of Trabant and Benson and values predicted by the models may have been the result of inherent problems with the one-dimensional models.

The failure of the one-dimensional diffusion models to predict the correct mass transport, or to predict it only with heuristic diffusion coefficients, led to the development of two- and three-dimensional models with more realistic snow geometry (Adams and Brown 1983, Sommerfeld 1983, Colbeck 1983a, Gubler 1985, Christon et al. 1987). But, unlike the older one-dimensional models, which predicted mass transport between snow layers (i.e. layer-to-layer flux gradients), the multidimensional models were microscopic in scale. They predicted the local growth rate of snow grains. To simplify the mathematics of these multidimensional models, all of the authors assumed that the flux gradients between snow layers were zero, making the one- and multidimensional models contradictory. This assumption was justified by citing the experiments of Marbouty (1980) and the observations of Armstrong (1985), both of whom found that the mass of a snow layer in which there was active grain growth (or shrinkage) remained constant. The work presented in this investigation, and that of Trabant and Benson (1972), clearly indicates that there is mass flux from one layer to another.

The existing multidimensional models are untested. Some incorporate undetermined enhancement factors. The models require detailed geometric measurements of snow grain clusters that are not available, and they predict growth rates, of which there are few reliable measurements. As a result, the models are not yet useful for determining whether observations of mass transport or grain growth in snow can be explained solely by diffusion with realistic snow geometry, or if transport by convection must be included.

The fundamental problem is that none of the models can be adequately tested because there are so few measurements of mass transport or grain growth in snow. The measurements that do exist (Table 1) are difficult to compare because they were made using various experimental techniques on different types of snow subjected to different temperatures and temperature gradients. The measurements listed in Table 1 have been separated into a) flux gradients between snow layers and b) grain growth rates. The results span more than an order of magnitude for both types of measurements. Among the layer-to-layer flux determinations (Table 1a), one value (Giddings and LaChapelle 1962) was based on measured changes in snow density, but failed to account for compaction. Another value (Yen 1963) cannot be verified because the data have not been published. Still another value (de Quervain 1958) is puzzling because the flux gradient was the same for blocks of snow both with and without imposed temperature gradients. The snow grain growth rates were calculated from published values of changes in grain size by assuming spherical grains (except for this study, see Section 4). More accurate

Table 1. Layer-to-layer mass flux gradients and grain growth rates for snow.

Source	*Experiment*	*Comments*	*Flux gradient* ($kg\ m^{-2}\ s^{-1} m^{-1}$)	*Temp.* (°C)	*Temp. gradient* ($°C\ m^{-1}$)
Measured values of layer-to-layer flux gradients					
Kondrat'eva (1954)	Calculated from change in thermal diffusivity.	Indirect calculation subject to large errors.	190×10^{-6}	–1 to –10	–20
Yosida (1955)	Mass change of snow in wire cages in snow cover.	Wire cages may have enhanced temperature gradients.	1×10^{-6}	0 to –6	–4
de Quervain (1958)	Mass change of block of snow in controlled environment.	Got similar values for tests with no temperature gradients as with strong gradients.	10×10^{-6}	–5	0 to –70
Giddings & La-Chapelle (1962)	Observed change in density of natural snow layers.	Did not account for effects of snow compaction.	----	–3 to –8	–30 to –50
Yen (1963)	Change in density of ventilated snow. Results extrapolated to 0 flow.	Data not presented in paper, but confirms Yosida's (1955) results.	1×10^{-6}	–7 to –17	–70
Trabant & Benson (1972)	Comparison of observed change in density of natural snow to snow not subjected to temperature gradient.	Value may be too high due to differences in compaction rate of different snow types.	9×10^{-6}	Varied	Max. –200
This study	Measured mass and thickness change of marked natural strata.	See Section 4 and Appendix F.	3×10^{-6}	Varied	Max. –200
			Growth rate ($kg\ s^{-1}$)		
Measured values of snow grain growth rates					
de Quervain (1958)	Samples subjected to known gradients. Grain size est. by sieving and photos.	Grain size increases from 1 to 5 mm in 40 days.	1.6×10^{-11}*	–5	–70
Pahaut & Marbouty (1981)	Measured from photographs of disaggregated grains (?)	Grain size increases from 0.4 to 6 mm in 30 days.	4.6×10^{-11}*	–4	–40
Sommerfeld (1983)	Samples in plastic subjected to known gradient. Grain size by stereology.	Grain size increases from 2 to 3 mm in 28 days.	0.4×10^{-11}*	–4	–30
This study	Natural samples. Grain mass determined by sieving and stereology.	Grain size increases from 5 to 50 mm in 120 days.	0.8×10^{-11}**		Varied

* Growth rate calculated assuming spherical ice grains with diameter equal to grain size.

** Growth rate calculated by methods indicated in Section 4.

calculations would have required knowledge of grain shape as well as size, but these data were not available.

Diffusive heat transport in snow

In the absence of convection, heat

1) is conducted through the network of ice grains,
2) is conducted through the air spaces in the pores, and
3) moves as latent heat when vapor diffuses from one grain to another.

The effective thermal conductivity of the snow combines all three mechanisms. The thermal conductivity of air and ice are well known, and the effective thermal conductivity of the snow can be measured, but the component of the effective thermal conductivity due to latent heat transport has yet to be calculated from the other components. The reason is that the complex geometry of pore spaces and ice grains produce unknown local temperature and vapor pressure gradients. In addition, all three heat-transfer mechanisms are poorly known functions of temperature. Only three studies have measured the effective thermal conductivity over a range of temperature including low temperatures ($\leq -40°C$) where vapor transport is negligible (Pitman and Zuckerman 1967; Voitkovsky et al. 1975; this study, Section 3).

Several authors have attempted to evaluate the latent heat transported by the vapor flux using theoretical models. Yosida et al. (1955) predicted that about 40% of the total nonconvective heat transport should be due to the vapor. Using the measured vapor transport, however, they found the obvious contradiction that more than 100% heat transport could be accounted for by the latent heat. Yen (1963) concluded that only 8% of the heat moved as latent heat, even at relatively high temperatures, whereas Woodside (1958), modeling ice spheres and air spaces, concluded that up to 48% of the heat was transferred with the vapor. De Quervain (1972) calculated latent heat transport as a function of temperature, snow density, and texture. He found that the percentage of the total heat transferred as latent heat increased with porosity, and that for low-density depth hoar it reached values up to 45%.

Natural thermal convection in snow

In addition to the studies of natural thermal convection in snow discussed at the beginning of this section, Bories and Combarnous (1973) examined the theoretical likelihood of convection in snow on a sloping surface and concluded that there would be a general up-slope flow of air in the snow. Forced convection due to wind-pumping has also been shown to be possible on theoretical grounds (Clarke et al. 1987; Colbeck, 1989). Data presented in Section 3 suggest that wind-pumping occurs. Johnson et al. (1987), reporting results from the first year of this study, found natural thermal convection during a brief period of the winter of 1984–1985. The prevalence of convection in other snow covers is not known.

General characteristics of the Fairbanks snow cover

The Fairbanks snow cover is similar to that found in Siberia, Canada, and the rest of central Alaska, coinciding with the taiga vegetation zone. These snow covers are colder, thinner, less dense, more permeable, of lower conductivity, and subject to more extreme temperature and vapor pressure gradients than snow covers in temperate latitudes and have been called taiga snow (Pruitt 1970, 1984; Benson 1982). They evolve as winter progresses until they consist almost entirely of large depth hoar crystals (see the cover for an example of a depth hoar crystal).

The climate of Fairbanks

Fairbanks, Alaska (64°49' N, 147°52' W, elevation 130 m) has a dry, continental, subarctic climate that is often windless (Searby and Branton 1973). Below-freezing temperatures usually last from October to April, and the seasonal snow cover can form any time after the beginning of October and

Table 2. Maximum snow depth for Fairbanks, Alaska, 1950 to 1987. Note extreme values in adjacent years 1970 and 1971.

Date	Depth (m)	Month	Date	Depth (m)	Month	Date	Depth (m)	Month
1950	1.09	Feb	1963	0.89	Mar	1976	0.46	Mar
1951	0.86	Mar	1964	0.41	Mar	1977	0.74	Feb
1952	0.84	Feb	1965	0.43	Mar	1978	0.48	Feb
1953	0.23	Mar	1966	1.32	Feb	1979	0.64	Feb
1954	0.48	Feb	1967	0.94	Apr	1980	0.41	Feb
1955	0.56	Mar	1968	0.84	Jan	1981	0.53	Feb
1956	0.97	Mar	1969	0.74	Mar	1982	0.46	Apr
1957	0.94	Jan	1970	0.30	Feb	1983	0.61	Mar
1958	0.36	Feb	1971	1.09	Mar	1984	0.65	Feb
1959	0.91	Feb	1972	0.74	Feb	1985	0.88	Jan
1960	0.91	Jan	1973	0.56	Mar	1986	0.40	Apr
1961	0.38	Jan	1974	0.56	Mar	1987	0.42	Jan
1962	0.94	Feb	1975	0.79	Jan			

Based on data supplied by the Arctic Environmental Information and Data Center, University of Alaska.

persist until May (Fig. 3) (see also Bryson and Hare 1974). Thaws occur rarely in winter, so the snow cover is usually free of ice lenses or melt features. The mean wind speed during the winter is less than 3 m s^{-1}.

Depth, density, and texture

The snow cover in Fairbanks reaches its maximum thickness by March; it averages 0.6 m with significant variation from year to year (Fig. 3 and Table 2). Typically, the snow cover is composed of a dozen or more individual snowfalls, many less than 0.1 m thick. Due to the windless conditions, most snowfalls are deposited with initial densities of less than 50 kg m^{-3}. These low-density accumulations often consist of unbroken stellar snowflakes, sector plates, and spatial dendrites (Magono and Lee 1966, Types: P1e, P1f, R1d, R2b, P6a, P1c, P6c). The snowflakes quickly lose their points and become rounded grains as they settle and compact (Bader et al. 1939). Kinetic metamorphism (Colbeck 1986), also called TG metamorphism (Sommerfeld and LaChapelle 1970), quickly turns the grains into depth hoar, which has an average density between 180 and 250 kg m^{-3} throughout the winter.

Observations of natural snow covers (Akitaya 1974) and experimental work (Marbouty 1980, Colbeck 1983b) suggest that the temperature gradient must exceed 10 to 25°C m^{-1} for depth hoar to develop. When temperature gradients are less than these values, snow crystals become rounded, approaching an equilibrium shape that minimizes the surface free energy (Frank 1982; Sommerfeld and LaChapelle 1970; Colbeck 1982a, 1982b). Above the critical gradient, crystal growth dynamics, rather than vapor supply, apparently control the crystal growth process, and ornate depth hoar crystals develop with striated and stepped faces (Frank 1982).

Temperature gradients in the Fairbanks snow cover often exceed the critical gradient by an order of magnitude or more for up to 150 days (Fig. 1). Temperature gradients can be as high as 500°C m^{-1}, particularly in early season when winter ground temperatures are the highest and the snow cover is the thinnest. At that time, the formation of depth hoar can be extremely rapid.

The extreme temperature gradients are the result of the low winter air temperatures and the relatively high snow/soil interface temperatures. The interface temperatures remain high because latent heat is released as moisture in the soil freezes. Interface temperatures rarely drop below –8°C, even when air temperatures are as low as –40°C.

Observations by Akitaya (1974) suggested that depth hoar does not form, regardless of the temperature gradient, if the initial snow density exceeds 350 kg m^{-3}. Because the snow depth in

Fairbanks is usually less than a meter (Table 2), compaction of snow layers at the base of the snow cover resulting from the weight of the overlying snow is minimal and this critical density is rarely exceeded.

Organization of this report

This was primarily an observational investigation. The experimental methods used are described in Section 2. Observations of density, grain size, and temperature used to calculate the mass and heat transport are presented in Section 3. From the density observations it was possible to determine the layer-to-layer mass flux gradients; from the grain size data it was possible to estimate grain growth rates. These are discussed in Section 4 and then used in Section 5, where the evidence for convection is presented and its importance is discussed. Section 6 is a summary of results and recommendations for future work.

2. METHODS

This study was conducted in a natural (as opposed to a laboratory) setting because its purpose was to determine if convection occurred in a natural snow cover. Severe arctic weather and unusual natural events (e.g., a moose treading perilously close to the instrumented snow site) had to be dealt with, and measurement techniques with minimal thermal and structural impact on the snow had to be devised.

Convection was detected primarily by its perturbation of the temperature field in the snow, and secondarily by changes in heat flow at the snow/soil interface. Temperature and heat flow were measured more than 3,000,000 times over three winters using thermistor arrays in the snow, soil, and air, and heat flow meters at the snow/soil interface. Thermistors and heat flow meters were installed at the end of summer and allowed to be buried by the winter snowfall, thus assuring that the snow in which the instruments were buried was representative of the undisturbed snow cover.

Mass transport and snow metamorphism were studied by making measurements of density, stratigraphy, and grain size. Over a period of three years, 55 snow pits were dug and over 600 density measurements were made. Samples from each snow pit were sieved and photographed to determine grain size. Other measurements, such as soil moisture profiles and thermal conductivity of the snow, were made to complete the description of the snow and its environment.

Julian dates were used during the course of the study and appear on several graphs. Table 3 is a Julian-to-conventional date conversion chart.

Experimental setting

Observations were made at the University of Alaska Agricultural Experiment Station, the same site used by Trabant and Benson (1972) for their work. The site is a level, cultivated field with silty soil.

Measurements of the physical characteristics of the snow

Density, stratigraphy, depth, and compaction

Snowfall accumulated on six white tables (1 m × 2 m) 1.5 m above the ground, and on a 20 × 20-m area of level, bare ground. Once a month throughout the winter snow pits were dug in the snow on the ground and the tables. This setup, which was similar to that used by Kojima (1959), Trabant and Benson (1972), and Armstrong (1985), allowed a comparison to be made between the snow on the ground, which was subjected to strong temperature gradients, and the snow on the tables, which was subjected to only weak temperature gradients that had no preferred direction.

Density, snow depth, and stratigraphy were measured in each snow pit using procedures described in NRC Canada Memorandum No. 31 (1954), SIPRE Instruction Manual 1 (1962), and by Benson (1962). Metal tubes (0.5-liter volume) were inserted horizontally into the wall of a snow pit from which

Table 3. Conversion chart for conventional and Julian dates (perpetual).

Day	*Jan*	*Feb*	*Mar*	*Apr*	*May*	*June*	*July*	*Aug*	*Sep*	*Oct*	*Nov*	*Dec*	*Day*
1	001	032	060	091	121	152	182	213	244	274	305	335	1
2	002	033	061	092	122	153	183	214	245	275	306	336	2
3	003	034	062	093	123	154	184	215	246	276	307	337	3
4	004	035	063	094	124	155	185	216	247	277	308	338	4
5	005	036	064	095	125	156	186	217	248	278	309	339	5
6	006	037	065	096	126	157	187	218	249	279	310	340	6
7	007	038	066	097	127	158	188	219	250	280	311	341	7
8	008	039	067	098	128	159	189	220	251	281	312	342	8
9	009	040	068	099	129	160	190	221	252	282	313	343	9
10	010	041	069	100	130	161	191	222	253	283	314	344	10
11	011	042	070	101	131	162	192	223	254	284	315	345	11
12	012	043	071	102	132	163	193	224	255	285	316	346	12
13	013	044	072	103	133	164	194	225	256	286	317	347	13
14	014	045	073	104	134	165	195	226	257	287	318	348	14
15	015	046	074	105	135	166	196	227	258	288	319	349	15
16	016	047	075	106	136	167	197	228	259	289	320	350	16
17	017	048	076	107	137	168	198	229	260	290	321	351	17
18	018	049	077	108	138	169	199	230	261	291	322	352	18
19	019	050	078	109	139	170	200	231	262	292	323	353	19
20	020	051	079	110	140	171	201	232	263	293	324	354	20
21	021	052	080	111	141	172	202	233	264	294	325	355	21
22	022	053	081	112	142	173	203	234	265	295	326	356	22
23	023	054	082	113	143	174	204	235	266	296	327	357	23
24	024	055	083	114	144	175	205	236	267	297	328	358	24
25	025	056	084	115	145	176	206	237	268	298	329	359	25
26	026	057	085	116	146	177	207	238	269	299	330	360	26
27	027	058	086	117	147	178	208	239	270	300	331	361	27
28	028	059	087	118	148	179	209	240	271	301	332	362	28
29	029	(060)*	088	119	149	180	210	241	272	302	333	363	29
30	030		089	120	150	181	211	242	273	303	334	364	30
31	031		090		151		212	243		304		365	31

* For leap years, add 1 day to all dates after February 28.

a core of snow was removed and weighed. The tubes, which were 60 mm in diameter, often sampled across several snow layers. This was undesirable because the density of individual layers often differed. Therefore, in 1985–1986 and 1986–1987 a 30-mm high, 0.1-liter box sampler, similar to the Hydro-Tech/Institute of Low Temperature Science sampler, * was used. Despite its smaller volume, the box sampler measured density to the same accuracy as the larger tubes (Carroll 1977), and the problem of sampling across multiple snow layers was avoided.

It became apparent in 1985 that measuring the snow density more frequently than once a month would improve the resolution of the mass transport calculations. Single density measurements were reproducible to ±5% for a density of 200 kg m^{-3}. This was comparable to the reproducibility determined by Benson (1962) for Greenland snow. Unfortunately, with a 5% reproducibility, the measurements were not accurate enough to differentiate the small changes in density that would occur over intervals of time shorter than a month. To improve the accuracy, multiple snow pits were measured at each site and the average density was determined from several measurements for the same layer. This required processing more samples, so the efficiency of the process was improved by using standardized tare weight containers and an electronic balance.

The accuracy of the average density measurements was a function of the snow texture. In older snow that had not been subjected to strong temperature gradients (i.e. snow on tables), and in fine-grained

* Personal communication from P. Taylor, 1986 (Hydro-Tech, Seattle, Washington).

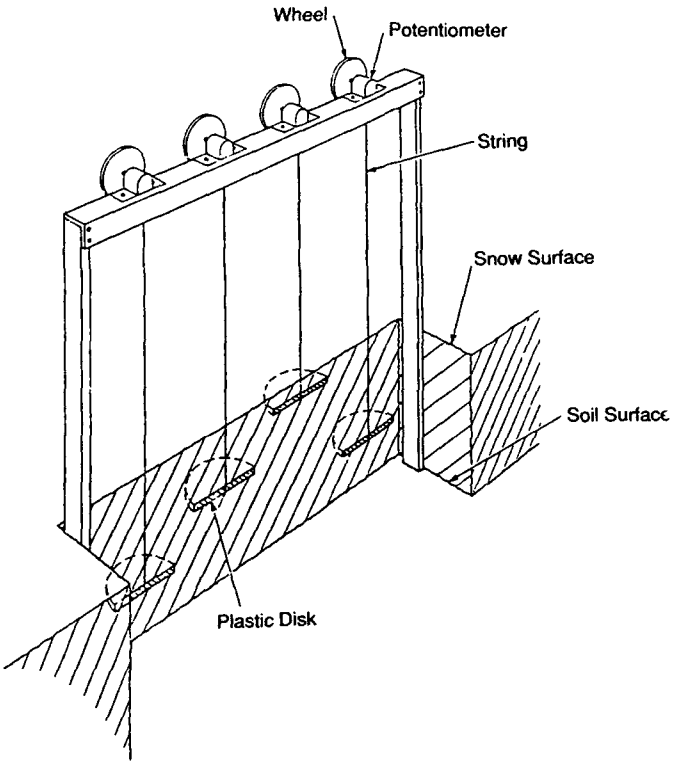

Figure 5. Apparatus for measuring snow settlement. Four plastic disks were placed on the snow surface after significant snowfalls. They were connected by strings to potentiometers turned by pulley wheels. The resistance of each potentiometer was calibrated with the height of the disk and read hourly by the data logger.

new snow, average density measurements were estimated to be accurate to ±1% for a density of 200 kg m^{-3}. For depth hoar, which was difficult to sample, the accuracy was estimated to be ±2.5%. Lateral density variations, particularly in depth hoar, probably produced further uncertainty on the order of ±2.5%, giving a total accuracy of about ±4% for depth hoar.

The metamorphism of the original snow into depth hoar obliterated all primary natural stratigraphic markers by midwinter, so it was necessary to introduce artificial markers into the snow to monitor the compaction of snow layers. In 1985–1986 this was done by laying colored yarn on the snow surface after major snowfalls. This was unsuccessful. In 1986–1987, powdered paint was spread on the snow surface after major snowfalls with a flour sifter, producing a layered effect. The paint was an inert dust that could be spread in thin layers that had little or no effect on the snow permeability; it was unlikely to have had any effect on vapor flow through the snow.

Snow compaction was computed from measured changes in thickness of the layers defined by the paint horizons. These could be measured accurately to ±3 mm. In 1986–1987, cumulative compaction of snow layers was also measured hourly using a data logger and the snow settlement device shown in Figure 5 (see Section 3, Snow Density).

Grain descriptions and photography

Snow crystals and grains were examined in situ using a hand lens. The entire snow cover was often photographed in "thin section" by cutting two adjacent pits and shaving the intervening wall until it was translucent (Benson 1962). Under these conditions, the texture of the snow was highlighted.

Grains from disaggregated snow samples were photographed in a coldroom using an Olympus OM-4 35 mm camera mounted on an American Optical stereo microscope. The best results were achieved by photographing grains on a glass plate illuminated by transmitted light (see Section 3, Depth Hoar Texture).

The photography had two purposes: to make measurements from which grain growth rates could be computed, and to document changes in crystal morphology during depth hoar development. A limited amount of photography was done using polarized light to verify crystal axis orientation, which could usually be determined from both hand lens examination and regular photographs due to the euhedral morphology of most crystals.

Grain size measurements

Sieving and photography were used to determine grain growth rates. Sieving is an old method of measuring grain size that seems to have gone out of favor because it is difficult to determine how much damage is done to the snow grains during the sieving. Several authors (Bader et al. 1939, Benson 1962, Keeler 1969, Fukue 1977, Granberg and Wener 1986) have analyzed sieved snow and most acknowledge that sieving can disaggregate snow grains and break single crystals, potentially biasing the results towards smaller sizes. In this way, sieving snow differs from normal sieve analysis of rock sediments, but as in sieving other sediments, operator error (Folk 1955) and errors due to the sieving process itself (Griffiths 1953, Mizutani 1963, Ludwick and Henderson 1968) also affect the results. Stereological measurements from photographs (Kry 1975, Gubler 1978) have been in use more recently, but they are hard to interpret and are time-consuming and difficult to make on snow composed of large, ornate depth hoar grains.

Despite its shortcomings, sieving is fast and easy to perform in the cold, and, if applied in a consistent manner, is adequate to measure the changes in grain mass necessary to determine grain growth rates. It was used in this study for these reasons. In standard sieve analysis, a particle size distribution is determined from the weight fraction of a sample found in each sieve (Royse 1970, Blatt et al. 1972, Friedman and Sanders 1983). An underlying premise in the standard method is that the size of a grain is related to the size of the sieve mesh opening. This is true for spheres and other simple, regular shapes (Ludwick and Henderson 1968); for highly convoluted shapes like snow grains, no such relationship exists, so the sieving cannot be used to measure snow grain size accurately. However, by sieving a representative sample of depth hoar, then weighing individual grains in each sieve, a direct relationship between sieve mesh opening and the average mass of a grain that remained in the sieve was developed (see Section 3, Grain Size). It was then possible to use sieving to determine the grain mass distribution for a snow layer at several times during the winter. The distributions could be used to determine the number of grains in a snow sample (see Section 3, Grain Size, and Appendix B).

Each time snow pits were dug during the winter of 1986–1987, samples for sieving were taken with a 0.5-liter tube from three fixed heights in the snow cover on both the ground and the tables. Each sample was transferred to the top sieve in a stack of nine sieves, which were at ambient outdoor temperature (usually $< -20°C$). The sample was gently disaggregated by moving it across the sieve mesh with a gloved hand. The sieve stack was then covered and agitated by hand for 30 seconds. The weight fraction in each sieve was weighed using an electronic balance.

Stereological measurements of grain size were made from photographs of disaggregated grains. For each snow layer, two or more photographs showing a grain population of between 50 and 200 grains were digitized (by tracing the grain outlines with a stylus) using a ZeissPlot stereological system. Descriptive statistics for each population (corresponding to a particular snow layer at a particular time) were calculated by the Zeiss software. The results included mean grain size and shape parameters. Sufficient stereological measurements were made to compare the sieving and stereological methods of measuring grain size (see Section 3, Grain Size).

Heat flow and temperature measurements

Heat flow at the snow/soil interface

Heat flow meters (HFMs) (Thermonetics Model H11-18-3-sfh glass phenolic thermopiles) were embedded in the soil surface prior to the first snowfall. Voltage from the HFMs was recorded hourly, and the output was converted to heat flow units using a temperature-compensating factory calibration. The mismatch in the thermal conductivity between the HFMs and the soil produced a "focusing" of heat flow through the meters that was a function of the aspect ratio of the HFMs and the ratio of their thermal conductivity (k_m) to the thermal conductivity of the surroundings (k_s). The correction for this mismatch was made using Schwerdtfeger's (1970) equation:

$$Q_s = Q_m \left\{1 + H\left[\frac{k_m/(k_s - 1)}{k_m/k_s}\right]\right\} \quad (1)$$

where H is a geometric characteristic of the HFMs determined empirically for different aspect ratios, Q_s is the heat flux at the snow/soil interface, and Q_m is the heat flux measured by the meter. For the silt at the experimental site, k_s probably varied between 2.0 and 0.5 W m^{-1} K^{-1} as the winter progressed and the soil moisture froze (Johnston 1981); k_m was 0.17 W m^{-1} K^{-1}. Thus, Q_s was between 2.9 and 1.3 times Q_m. Because k_s was not known precisely, it was decided that an average multiplication factor of 2 should be used.

Corrected readings of the HFMs are reported in this study as the heat flow at the snow/soil interface, but it is unclear if this is exactly what they measured. If the system had been purely conductive with no vapor transport, the measured value would be the vertical heat flow at the interface. However, with air convecting in the snow, and a continuous vapor flux out of the soil, the heat flow should have been a function of location with respect to the air circulation pattern and the soil moisture content. The component of the heat flow due to the the release of latent heat resulting from condensation of vapor on the bottom of the impermeable meters was relatively small and probably did not bias the results. Condensation of about 5 mm of ice beneath the HFMs by the end of each winter released a latent heat flow of less than 1 W m^{-2}, while the measured heat flow varied between 5 and 30 W m^{-2} (see Section 3, Heat Flow). However, the spatial resolution of the small HFMs (6 cm × 6 cm) was a more critical shortcoming. The small HFMs could only measure local heat flow and not the spatial average necessary to identify changes in heat flow due to the onset of convection. It was therefore surprising that the widely spaced HFMs usually gave readings that agreed closely, suggesting that the heat flow may have been relatively constant along the snow/soil interface, despite convection. This point is discussed more fully in Section 3, Measurements Related to Heat Transport in Snow.

Temperature measurements in snow and air

Temperature measurements were made by strings of thermistors that were suspended before the first snowfall of the winter and were allowed to be buried by snow. The number and arrangement of the thermistor strings was improved each year in an effort to optimize coverage of the temperature field in the snow. The thermistor strings were configured as follows:

- *1984–1985* (Fig. 6): Two horizontal strings and one vertical thermistor string with a total of 103 thermistors were set up as described by Johnson et al. (1987).
- *1985–1986 and 1986–1987* (Fig. 7): Six horizontal and five vertical thermistor strings were set up to define a horizontal plane 1.0 m wide by 2.5 m long and a vertical plane 0.8 m wide by 0.7 m high. Each horizontal string incorporated 26 thermistors. They were installed 0.2 m above the ground in 1985–1986, and 0.15 m above the ground in 1986–1987; the smaller height in 1986–1987 was to ensure that the thermistors would be covered earlier in the winter. The vertical strings actually consisted of 12 horizontal strings

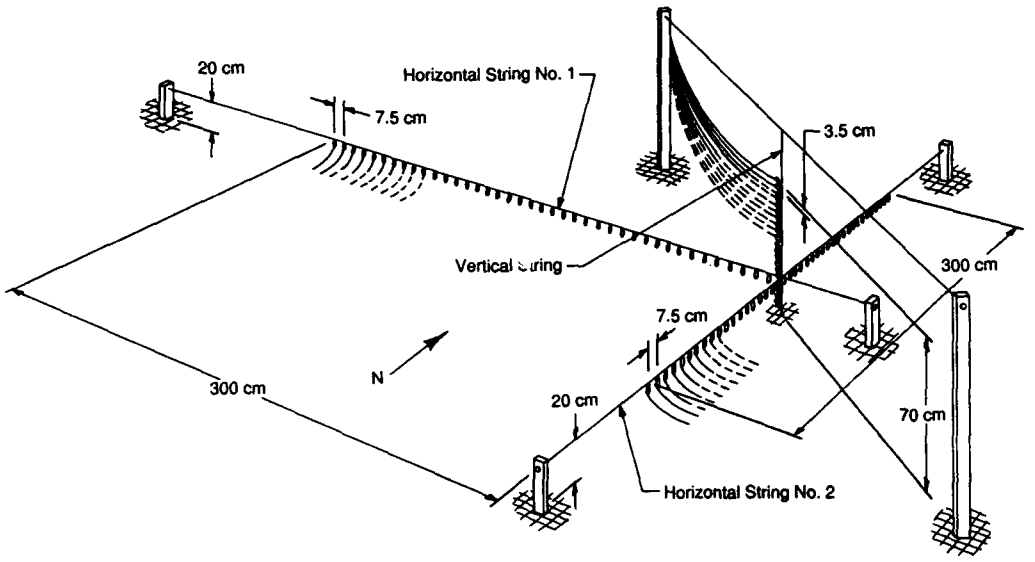

Figure 6. Thermistor array used in 1984–1985. It consisted of two horizontal strings that incorporated 41 thermistors each, and a vertical string that incorporated 21 thermistors.

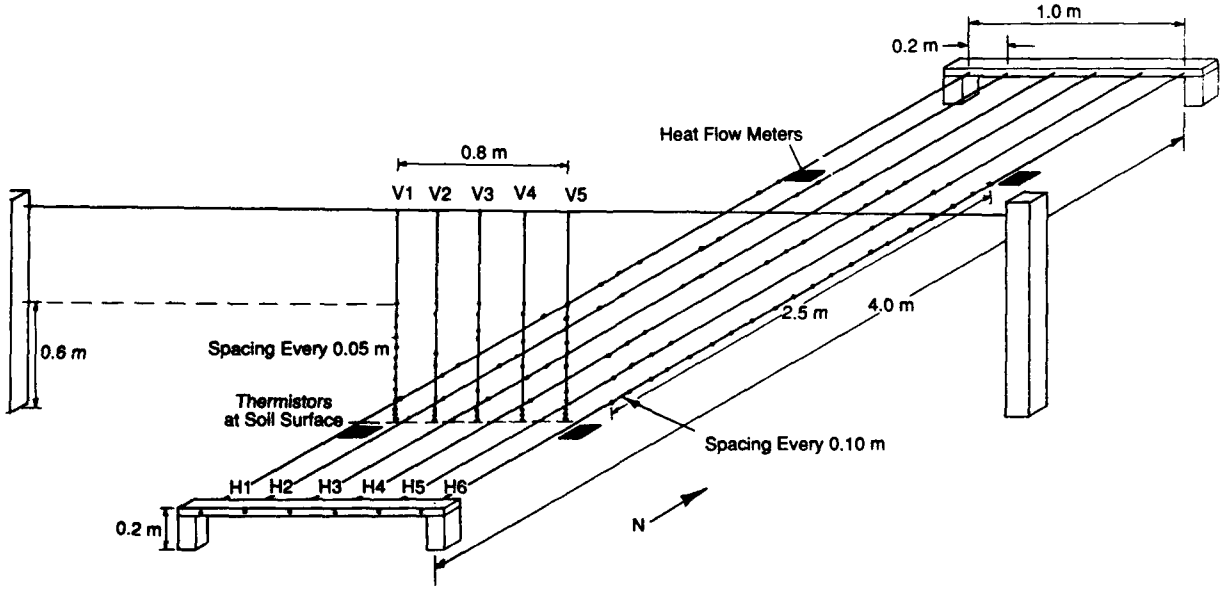

Figure 7. Thermistor array used in 1985–1986 and 1986–1987. It consisted of six horizontal strings, each incorporating 26 thermistors, and five vertical strings (actually made from horizontal strings) incorporating 12 thermistors each. In 1986, the horizontal strings were set 0.20 m above the ground, and in 1987, 0.15 m above the ground. Black squares are heat flow meters (HFMs) at the soil surface.

installed one above the other to create a vertical plane. In 1986–1987, five thermistors were installed at the soil surface to measure the temperature of the snow/soil interface. These were partially embedded in the soil, so that when covered by snow they were half in the snow and half in the soil.

Once the thermistor strings were covered by snow, they were cut free of their supports, so that they could settle with the snow cover. This was preferable to having them settle in catenary curves, which would have resulted had they not been cut free. An exception was the vertical thermistor string used in 1984–1985, which remained fixed to its supports. At the end of the season, the thermistors were excavated from the snow, and their positions were carefully measured with respect to the ground, snow surface, and neighboring thermistors. In 1986–1987, thermistor heights could be determined to ±3 mm throughout the winter by using the snow settlement data, but insufficient settlement measurements were made in 1985–1986, so the vertical positions of the thermistors were not known with enough accuracy to allow extensive analysis.

The thermistors were small glass beads 10 mm long and 3 mm in diameter (Veco Engineering Model T32A11/21). Each thermistor was factory calibrated at 25, 0, and –40°C. From this calibration, the Steinhart-Hart equation (YSI 1984) was used to convert resistance to temperature with an accuracy of ±0.01°C. At the end of each winter, the ice point calibration of each thermistor was checked in an ice bath. Ice point calibrations generally agreed with the factory calibration within 3 to 5 ohms out of 6000 ohms, indicating that loss of calibration through time was less than 0.1%, corresponding with an uncertainty of ±0.02°C at 0°C and less for lower temperatures. Instrument error and Joule heating (Appendix C) resulted in a further uncertainty of ±0.02°C. A conservative estimate of the total uncertainty is ±0.03°C.

There was no discernible effect on the snow cover, or processes occurring within it, due to the presence of the thermistor strings. The thermistors were small, and the thinnest possible wire leads were used so that minimal snow was intercepted during snowfalls, ensuring a natural snow cover surrounding the thermistors. Leads were installed horizontally to eliminate vertical heat flow along the wires. When excavated, the lead wires were found to have remained nearly horizontal despite settling of the snow. During the excavation, particular attention was paid to the nature of the contact between the thermistor beads and the snow around them. Thermistors were always in contact with the snow and often partially encased by ice crystals.

Data collected in 1984–1985 indicated that it was critical for the ground surface below the horizontal strings to be smooth and level in order to minimize perturbations in the temperature field due to variations in the distance between the thermistors and the ground. In 1984–1985, the substrate was bare soil, raked and rolled smooth, leaving undulations with amplitudes of 20 to 40 mm and wavelengths of about 0.5 m on the soil surface. In 1985–1986, the upper 100 mm of soil was tilled and then raked and hoed. The surface was wetted and allowed to settle, then small depressions were filled, resulting in a surface with undulations less than 20 mm high. In 1986–1987, a leveling frame consisting of boards dug into the ground and leveled to 1 mm was used to smooth and level a 20-mm-thick layer of sand spread over the silt. This was accomplished by running a stiff metal rail across the leveling boards and the surface of the sand, and resulted in an undulating surface with an amplitude less than 4 mm.

The number of thermistors (between 103 and 214) and the need for a continuous temperature record throughout the winter required an automatic data-logging system. The system consisted of a computer (Hewlett Packard [HP] 86C) controlling two data loggers (HP 3421A) and one multiplexer (HP 3497A). The system was contained in an insulated box in an unheated building. Waste heat from the equipment kept the mean temperature in the box at 20° ±5°C. Data were stored on 3.5-in. floppy disks, each of which could hold a 10-day record. The entire system was connected to a battery power supply that maintained power during frequent power outages. Transducers were logged every 15 minutes in 1984–1985 and every hour in 1985–1986 and 1986–1987, producing 16 Mb of data.

The raw data collected by the data-logging system were transferred via disk-to-disk transfer to an HP 200 Series computer for reduction. A data handling and graphics program written at the U.S. Army Cold Regions Research and Engineering Laboratory (USACRREL) (Perkins 1987), which could output the temperature and heat flow data in graphic form, was used for initial data handling.

Air temperature was measured by a thermistor housed in a standard meteorological shelter. Wind speed and direction were measured 200 m from the experimental site by a standard anemometer and wind vane. The wind measurements were part of a separate experiment run by J. Kelley and J. McBeath, who generously shared their data.*

Temperature measurements in the soil

Ground temperatures were measured to a depth of approximately 2 m throughout the study using a string of Fenwal thermistors. The thermistor string was attached to a post installed in an augered hole that was back-filled and compacted. For protection, the thermistors were encased in heavy shrink tubing. The Fenwal thermistors (Model UUA-33J1) were not factory-calibrated. A single ice point calibration and the factory-supplied standard curve for resistance vs temperature was used, giving an accuracy of ±0.2°C.

Measurements of thermal conductivity

The thermal conductivity of the snow was measured using a needle probe in a process described by Jaafar and Picot (1970), Lange (1985), and Sturm and Johnson (1987) (Appendix D). Briefly, a 0.1-m-diameter by 0.3-m-long copper cylinder was used to take a horizontal snow sample. The sample was transported to a laboratory where it was placed in a jacket around which cooling fluid circulated. The sample was brought to the desired temperature and stabilized. A thin steel needle 0.2 m long and 1.5 mm in diameter containing a helical resistance heating wire and a thermocouple was inserted along the axis of the sample. The needle was heated for 5 to 10 minutes while its temperature was monitored. The heater was then shut off and the cooling of the sample was monitored. From the heating and cooling curves, two independent values of the effective thermal conductivity could be determined (Blackwell 1954, Lachenbruch 1957, Jaeger 1958, von Herzen and Maxwell 1959, Pratt 1969, McGaw 1984, Lange 1985).

Three measurements of thermal conductivity were made in 1984–1985 and 14 in 1985–1986. In 1986–1987, samples from heights of 0.07, 0.10, and 0.26 m were measured five times during the winter to determine changes in thermal conductivity resulting from snow metamorphism (see Section 3, Thermal Conductivity). Measurements were made over a range of temperatures to assess temperature dependence. One measurement was made on a sample cooled in liquid nitrogen (–196°C) to determine the thermal conductivity in the absence of latent heat transport due to vapor flux.

Miscellaneous measurements

Soil moisture content

In 1984–1985 and 1985–1986, near-surface soil moisture was monitored by drying samples taken from the top 50 mm of the soil. In 1986–1987, the soil was cored to a depth of 1 m; the core was sectioned and weighed, then dried to determine the moisture content. This was done three times during the winter.

Vapor flux out of the soil

An impermeable sheet (polyethylene plastic, 5 m × 5 m) was laid on the soil surface just after the last rain of autumn and at the start of freezeup. Moisture trapped under the sheet was used to determine the moisture flux from the soil to the snow. Periodically through the winter, a 0.3 m × 0.3 m square

*Personal communication from J. Kelley, 1988 (University of Alaska, PICO).

of the sheet was cut away, and the ice under the sheet collected and weighed. The upward flux of vapor from the soil could be determined from this weight.

Air permeability

Air permeability of the snow was measured several times in 1984–1985 and 1985–1986 using an air permeameter similar to the one described by Bender (1957). In 1986–1987, a series of measurements were taken using a newly designed air permeameter that used solid-state pressure transducers, low laminar air flow, and a double-walled sample holder to minimize edge effects. The preliminary results have been reported by Chacho and Johnson (1987) and are summarized in Appendix A.

3. OBSERVATIONS

The observations fall into two categories: 1) observations of the physical characteristics of the snow and 2) measurements related to heat transport in the snow. The first category includes measurements of snow density, stratigraphy, grain size, and observations of the snow texture. These were made to calculate the mass transport in snow, to determine snow grain growth rates, and to document the snow metamorphism and relate it to convection, if possible. The second category includes measurements of heat flow, thermal conductivity, and snow temperature. Temperature measurements made using the horizontal thermistor strings provided the primary evidence from which the presence of convection was inferred. The curvature of the vertical temperature profiles, measured using the vertical thermistor strings, proved useful for differentiating between two types of convection. Heat flow, usually a good indicator of convection, proved difficult to measure in a meaningful manner, but the measurements are included for completeness.

Physical characteristics of the snow

Snow density

Snow on the ground in Fairbanks develops a density profile in which the density decreases (or is constant) with depth. In contrast, the density increases with depth if the snow is allowed to accumulate on a table that is not subjected to strong temperature gradients. The difference is due to depth hoar metamorphism (Fig. 8, 9). During every winter for which there are data from this and other studies (Trabant 1970, Trabant and Benson 1972), comparable snow layers on the ground and table rarely have had the same density. The data show that the basal snow layers on the ground were always less dense than the basal layers on the tables, and the top layers of snow on the ground were denser than the comparable layers on the tables (Fig. 9). These density contrasts increased through the winter, reaching a maximum in March or April.

The striking difference between the two density profiles was interpreted by Trabant and Benson (1972) to be the result of a net transfer of mass from the base to the top of the ground snow cover by an upward-directed vapor flux. The present investigation supports this interpretation (see Section 4).

The upward-directed vapor flux could be measured directly only at the snow/soil interface. There the flux, measured by trapping and weighing the moisture that accumulated under an impermeable sheet (see Section 2, Miscellaneous Measurements), averaged 2.6×10^{-7} kg m^{-2} s^{-1} (Table 4). This average was confirmed by measuring

Table 4. Upward-directed vapor flux at snow/soil interface.

Year	Flux (kg m^{-2} s^{-1})
1967–68*	3.2×10^{-7}
1968–69*	2.8×10^{-7}
1969–70*	3.5×10^{-7}
1973–74**	1.7×10^{-7}
1985–86	1.8×10^{-7}
1986–87	2.6×10^{-7}

* Trabant and Benson (1972)
** Benson, unpublished

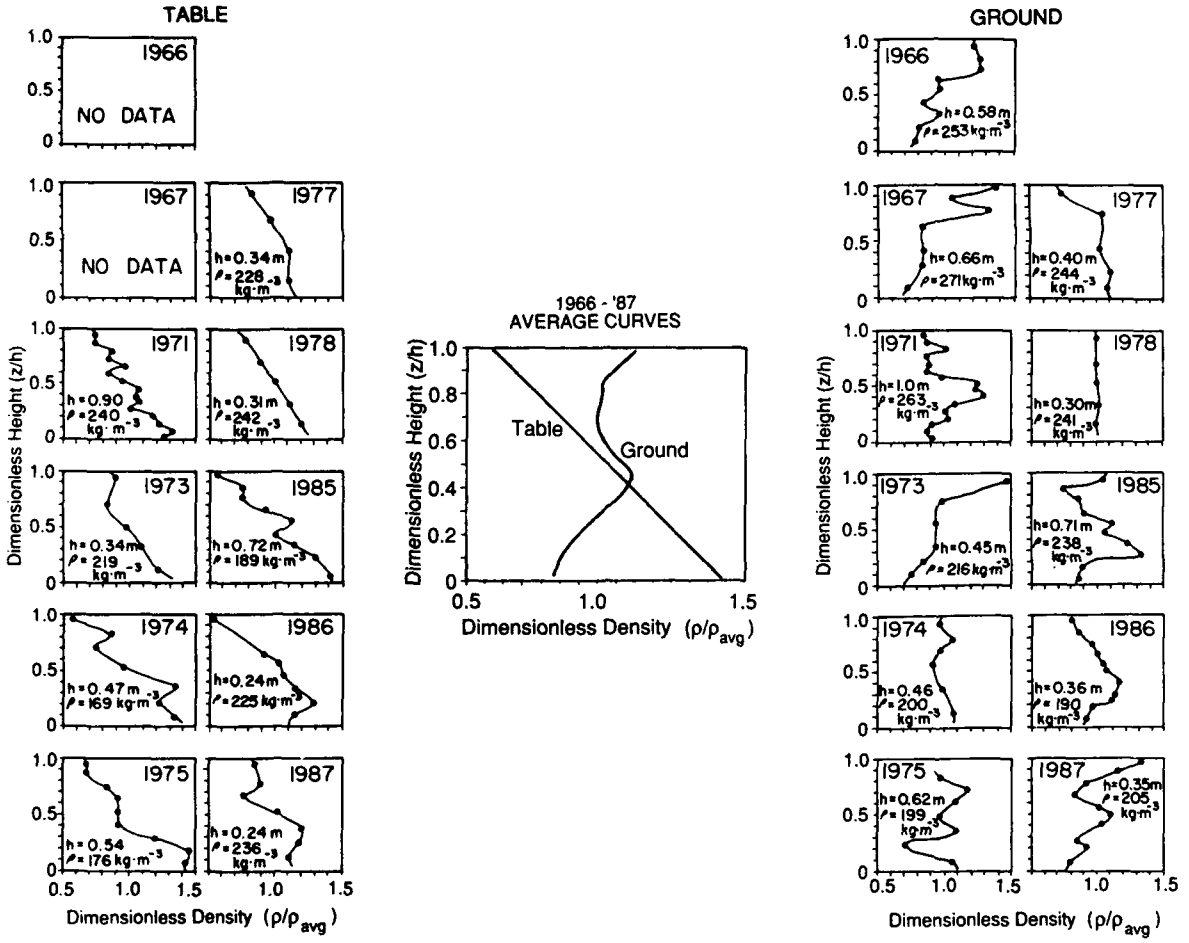

Figure 8. End-of-winter density profiles for Fairbanks snow cover, 1966–1987. Snow on tables not subjected to strong temperature gradients did not metamorphose into depth hoar as did snow on the ground. Average density curves show distinct differences between ground and table profiles. The total snow depth (h) *and average density* (ρ) *is listed for each snow pit.*

the change in the water content of the soil under snow where there was no impermeable sheet. During each of four winters, little or no change in the moisture content of the top meter of the soil was observed, with the exception of a surface layer, 20 to 30 mm thick, that became desiccated and dusty. This layer dried from 40% to less than 10% moisture by dry weight, releasing an average upward-directed vapor flux of 3×10^{-7} kg m^{-2} s^{-1}.

Individual snow layers on the ground and on the tables densified rapidly during the initial 3 to 4 weeks after they were deposited. This was followed by a second, longer period during which their rate of densification decreased (Fig. 10). In 1986–1987, 10 snow layers on the ground (Table 5) and the equivalent 10 layers on the tables were marked with powdered paint, and the density and thickness of the layers were measured up to 12 times during the winter. For all layers, snow on the ground densified at a slower rate than the equivalent layer of snow on the tables during both the initial period of rapid densification and the secondary period of slower densification. Several snow layers on the ground experienced little or no change in density after the initial period was over. In these cases, the density of the snow layers remained constant for nearly 80 days (Fig. 10).

The snow layers compacted and settled as they densified. The compaction (change in thickness) of individual snow layers was determined by measuring the distance between paint layers. The layers changed thickness at a rate of 0.5 to 1.0 mm day^{-1} at first, but the rate of change decreased to less than

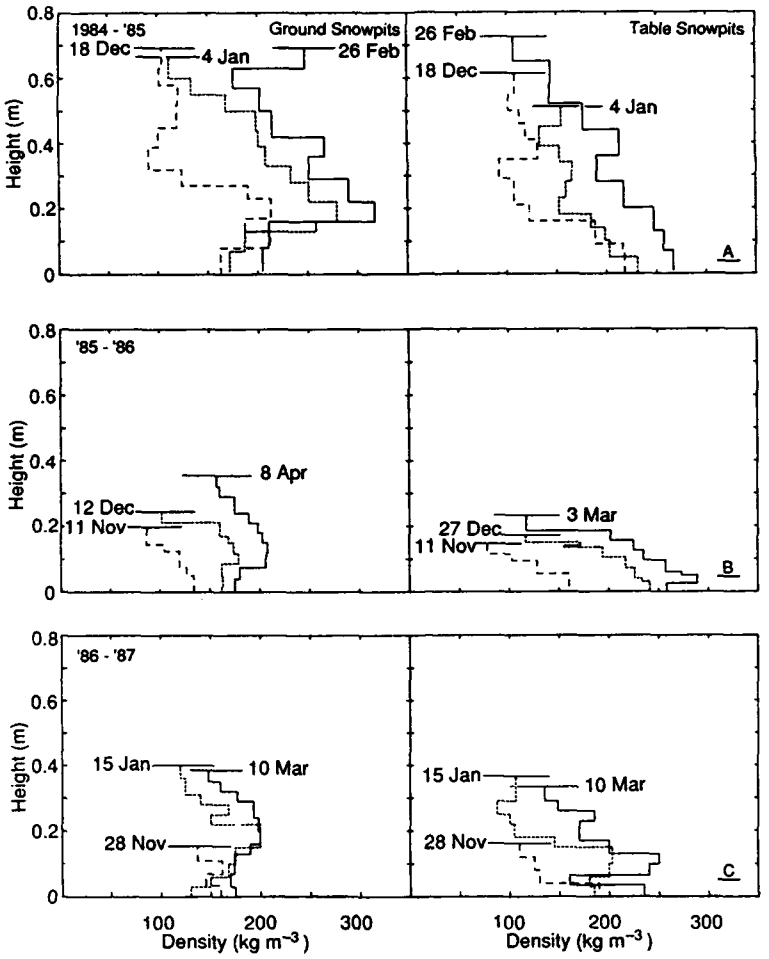

Figure 9. Fairbanks snow density profiles, 1984–1987. Early-, mid-, and late-winter density profiles are shown for the snow cover on the ground and on the tables.

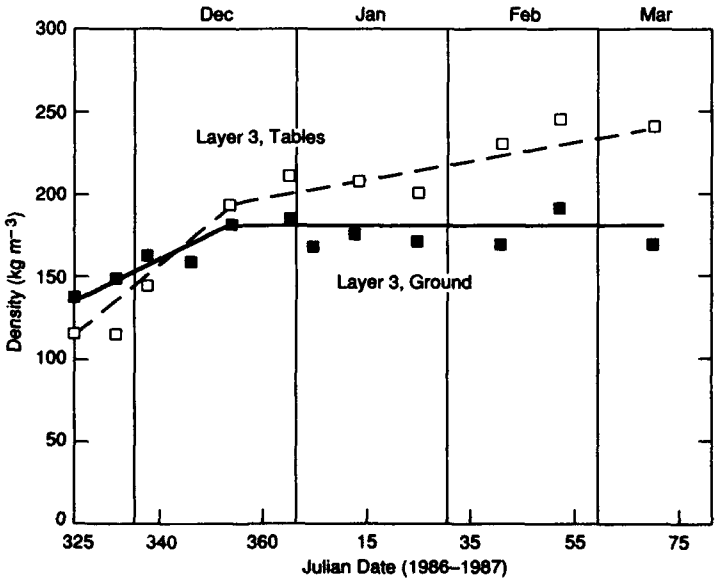

Figure 10. Densification of snow on the ground and on the tables. Snow layer 3 (height 0.10 m) was typical of the 10 layers measured. Both table and ground layers densified rapidly at first, followed by a period of less rapid densification.

Table 5. Density of 10 snow layers, 1986–1987. Layer heights are given in Table 6.

Julian date	*325*	*332*	*337*	*346*	*354*	*365*	*6*	*14*	*26*	*41*	*52*	*69*
Date	*21 Nov*	*28 Nov*	*3 Dec*	*12 Dec*	*20 Dec*	*31 Dec*	*6 Jan*	*14 Jan*	*26 Jan*	*10 Feb*	*21 Feb*	*10 Mar*
Elapsed days	*0*	*7*	*12*	*21*	*29*	*40*	*46*	*54*	*66*	*81*	*92*	*109*
Layer 10									119	116	115	145
Layer 9								125	170	168	175	164
Layer 8							072	150	178	171	196	191
Layer 7						120	111	151	161	192	200	183
Layer 6					200	195	185	191	200	196	185	198
Layer 5					194	187	182	200	201	202	218	192
Layer 4			110	167	191	190	191	198	191	200	200	179
Layer 3	137	150	163	160	180	186	169	175	170	170	189	170
Layer 2	158	145	161	155	168	160	170	155	175	168	168	162
Layer 1	172	155	183	160	151	173	162	145	168	172	157	171
////////////////////////						Ground						////////////////////////

All densities: kg m^{-3}

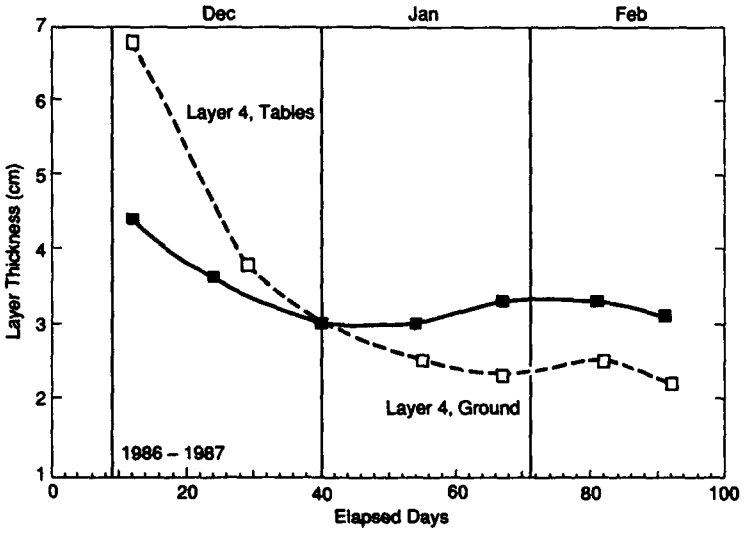

Figure 11. Compaction of snow on the ground and on the tables. Snow layer 4 (height 0.14 m) was typical of the 10 layers measured in 1986–1987. Initial thickness of the snow layer on the table was greater than that on the ground, but the layer on the table compacted more rapidly due to differences in snow texture (see text). Time is measured from the day the snow was deposited (22 Nov).

Table 6. Snow layer thicknesses and heights, 1986–1987.

Date	*21 Nov*	*28 Nov*	*3 Dec*	*15 Dec*	*31 Dec*	*14 Jan*	*27 Jan*	*10 Feb*	*21 Feb*	*11 Mar*
Elapsed days	*0*	*7*	*12*	*24*	*40*	*54*	*67*	*81*	*91*	*110*
Layer 10							36.5 [2.1]	36.3 [1.1]	34.0 [0.9]	34.0 [1.0]
Layer 9						37.8 [5.3]	34.4 [5.4]	35.2 [4.5]	33.1 [4.8]	33.0 [5.2]
Layer 8						32.5 [8.5]	29.0 [6.8]	30.7 [7.3]	28.3 [6.1]	27.8 [6.1]
Layer 7					25.8 [4.8]	24.0 [3.5]	22.2 [2.4]	23.4 [3.2]	22.2 [2.5]	21.7 [2.4]
Layer 6				22.0 [2.0]	21.0 [2.5]	20.5 [2.3]	19.8 [2.3]	20.2 [2.0]	19.7 [2.2]	19.3 [1.5]
Layer 5				20.0 [3.2]	18.5 [2.5]	18.2 [2.2]	17.5 [2.1]	18.2 [2.3]	17.5 [2.0]	17.8 [2.8]
Layer 4			20.0 [4.4]	16.8 [3.6]	16.0 [3.0]	16.0 [3.0]	15.4 [—]	15.9 [3.5]	15.5 [3.0]	15.0 [2.7]
Layer 3	15.0 [6.7]	15.5 [7.5]	15.6 [6.8]	13.2 [5.0]	13.0 [5.0]	13.0 [5.5]	12.1 [4.3]	12.4 [4.9]	12.5 [4.6]	12.3 [5.3]
Layer 2	8.3 [2.3]	8.0 [2.0]	8.8 [1.8]	8.2 [2.3]	8 [2.0]	7.5 [—]	7.8 [—]	7.5 [1.5]	7.9 [2.1]	7.0 [2.4]
Layer 1	6.0 [6.0]	6.0 [6.0]	7.0 [7.0]	5.9 [5.9]	6 [6.0]	? [?]	? [?]	6.0 [6.0]	5.8 [5.8]	4.6 [4.6]
	0.0	0.0	0.0	0.0	0.0	0.0	0.0	0.0	0.0	0.0
//////////////////////////					Ground		//////////////////////////			

All measurements are in centimeters.
Bracketed values indicate layer thickness.
Unbracketed values indicate the height of the top of each layer.

than 0.1 mm day^{-1} several weeks after the snow was deposited (Fig. 11). For several snow layers on the ground, layer thickness remained constant (within the measurement error) following the initial period of rapid compaction (Table 6). Layers of snow on the tables compacted twice as fast as the equivalent layer of snow on the ground during the initial period of rapid compaction (Fig. 11). The difference in compaction rates was the result of differences in the texture of the snow on the tables and on the ground. The snow on the tables was composed of small (about 1 mm), rounded grains that were well-bonded, compared to the large (5 to 20 mm), ornate, poorly bonded depth hoar grains found on the ground. Kojima (1959, 1966), Bergen (1978), and Armstrong (1985) have reported that depth hoar, although brittle and weak in shear, is more resistant to compaction than snow of other textures with the same density.

Snow settlement was measured automatically by the movement of plastic disks embedded in the snow. The settling of the disks, the paint layers, and measurements of the total snow depth, compiled in Figure 12, agree closely.

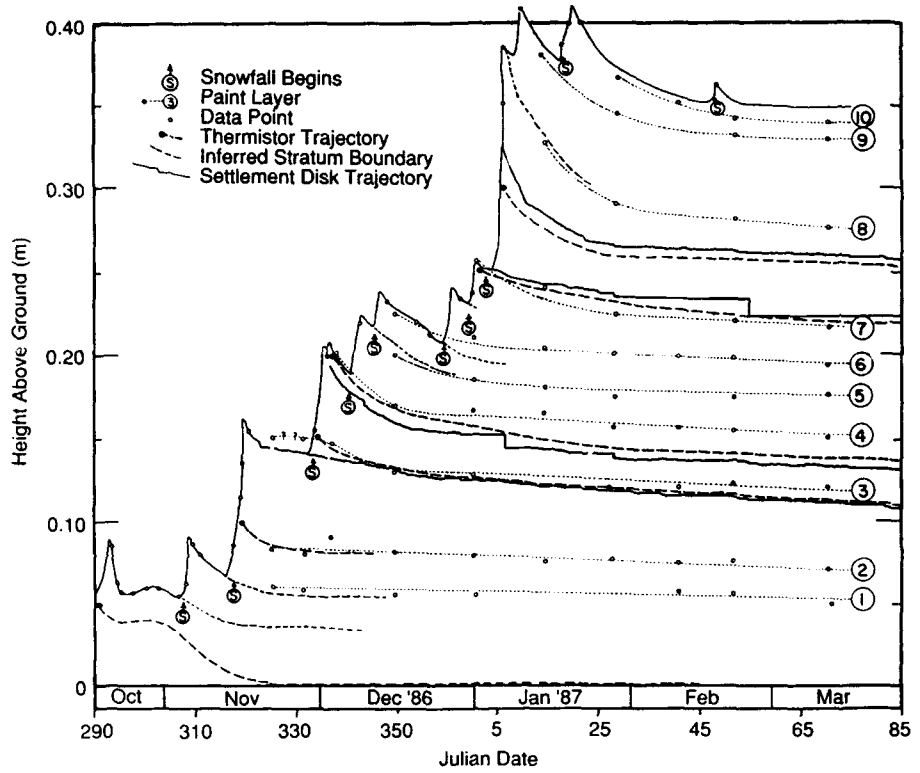

Figure 12. Stratigraphic record of the snow cover of 1986–1987. The solid lines were measured by plastic disks attached to potentiometers that sometimes "stuck," then released, giving the record characteristic steps. The settling trajectories of thermistors (bold dashed lines) have been interpolated from the trajectories of the disks. Dotted lines show the settling trajectories of stratigraphic horizons marked by powdered paint. The snow surface position (open circles) was determined from data collected at the experimental site and augmented by data reported by the National Weather Service data for Fairbanks International Airport. Significant snowfalls are indicated by (S).

Grain size

Snow grain size is difficult to measure and varies with the method of measurement because 1) there is no standard definition of a snow grain, and 2) snow grains have irregular shapes. The second point is particularly true for depth hoar grains. Bader et al. (1939) and Sommerfeld and LaChapelle (1970) have proposed definitions of snow grains. Using the latter authors' definition, snow grains are considered to be the fundamental unit of the snow cover. They are either single ice crystals or aggregates of well-bonded ice crystals separated from the rest of the snow by weaker and fewer bonds than in the aggregate itself. Thus, sieving or disaggregation for photography generally breaks the snow into grains, as opposed to breaking the grains apart. This propensity to break into grains is particularly prevalent in depth hoar because of the fragile nature of the connections between grains. Because the Fairbanks snow cover was composed predominantly of depth hoar, sieving and stereological measurements made on photographs of disaggregated snow grains were acceptable methods of determining grain size and grain growth rates.

The results of the sieving are presented first in standard form to highlight the nature of the depth hoar as a geologic material. Figure 13 shows cumulative curves of the grain size distribution (in terms of ϕ-size, where $\phi = -\log_2$ [sieve mesh size (mm)]/$\log_2$ [1.0 mm] [Royse 1970]) for three layers of snow on the ground and two layers on the tables. At a height of 0.04 m above the ground, the snow was already depth hoar on 28 November when it was first sieved, so there was little further change in the

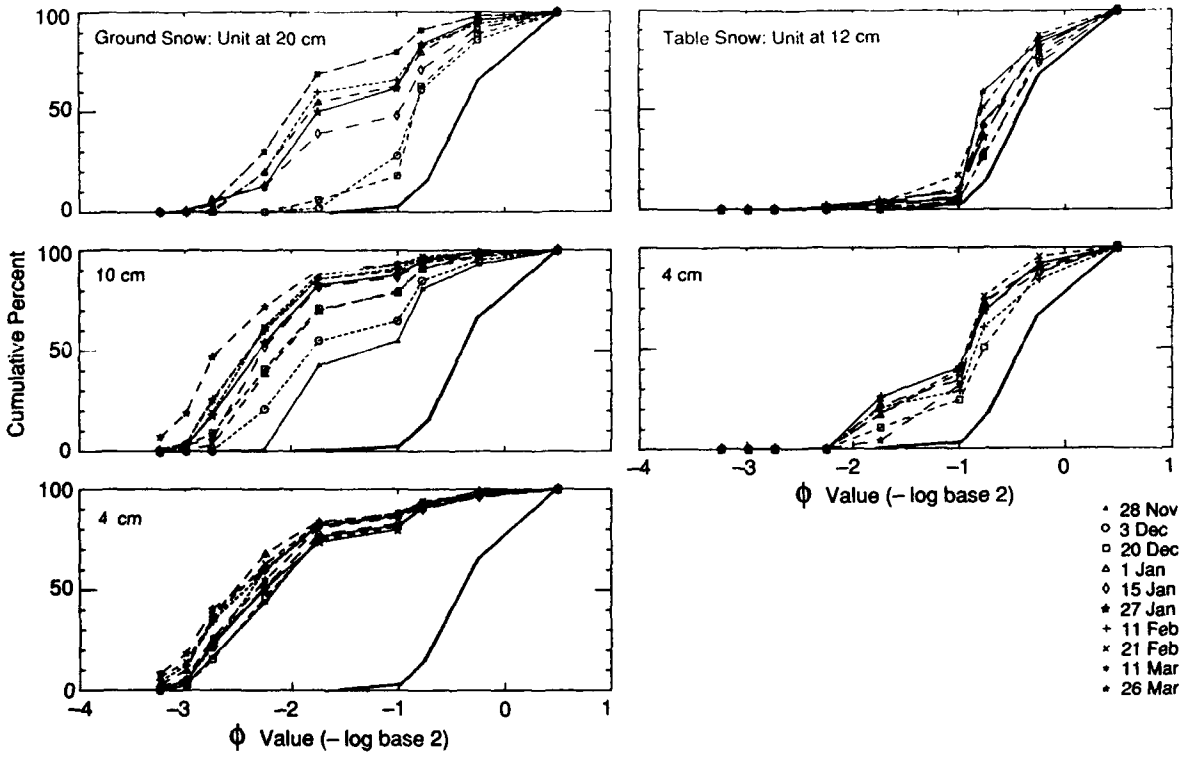

Figure 13. Cumulative size distribution curves for snow grains, 1986–1987. ϕ value = $-\log_2$ [sieve mesh size (mm)]/ $\log_2$ (1.0 mm). Cumulative curve for new snow is shown by a heavy line.

grain size distribution during the winter. Higher (at 0.1 m and 0.2 m), large shifts in ϕ-size occurred as the snow coarsened, and the distribution changed from fine-grained and bimodal to coarse-grained and nearly unimodal. A distribution curve from 15 January 1987 at 0.3 m height for snow less than 3 days old represents the approximate starting configuration for the each layer and has been added to each set of curves for reference. Distribution curves for samples of snow on the tables, unlike snow on the ground, showed no systematic change, and throughout the winter maintained essentially the same distribution as new snow.

Following standard practice in sieve analysis, grain size can be calculated from (Friedman and Sanders 1983):

$$\bar{d} = \frac{\sum_{j=1}^{L} M_j \bar{D}_{j,j+1}}{100} \qquad (2)$$

where $\bar{d}$ is the mean grain size of the sample, L is the number of sieves, M_j is the weight fraction in the jth sieve, and $D_{j,j+1}$ is defined as the arithmetic mean of the diagonal of the sieve mesh through which the grain passed (sieve j+1) and the diagonal of the sieve mesh on which it was trapped (sieve j). The uppercase D is used to clearly differentiate the size of the sieve mesh from the size of the grains measured by the sieves (lowercase d). Results calculated from eq 2 are plotted in Figure 14.

Grain size was also measured from photographs using stereological techniques, as described in Section 2. In this case, the grain size plotted (Fig. 14) is the diameter of a circle with the same area as the mean cross-sectional area of the grain population (equivalent circle). The stereological and sieving values do not agree. The maximum difference occurs for snow that has metamorphosed into the largest,

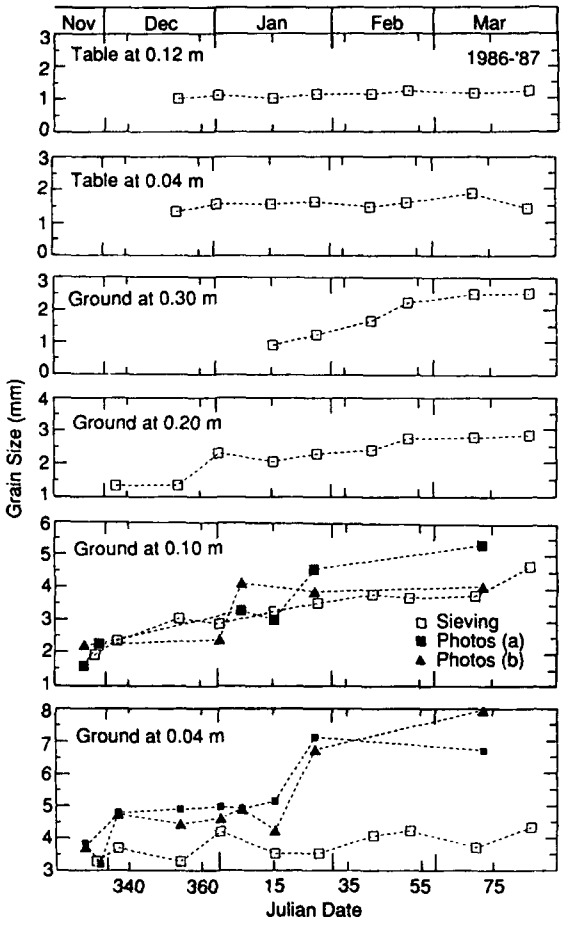

Figure 14. Snow grain size determined by sieving (open symbols) and stereology (solid symbols). The two methods differed most for snow grains that had metamorphosed the longest (sample from 0.04 m) and that had the most complex shapes. Two separate loose-grain samples (a and b) were photographed and measured by stereology.

most ornate depth hoar grains, because these grains were least suited to characterization by an equivalent circle. For weakly metamorphosed snow (i.e. higher in the snow cover), the agreement is better. Both methods indicate that grain size increased as new snow metamorphosed into depth hoar.

Grain growth rates were easier to calculate and more accurately determined if grain mass rather than grain size was determined directly from the sieving. To do this, it was necessary to establish a relationship between sieve mesh size and the average mass of a grain trapped in that sieve. A sample of depth hoar was sieved and each grain contained in each sieve was weighed. For sieves with finer mesh, only a fraction of the total grains could be weighed and it was necessary to weigh 10 grains at a time, due to the resolution limits of the electronic balance. From the distribution of individual grain masses in a sieve, the mean grain mass was determined. Within each sieve, the grain masses were generally normally distributed. These data and similar data reported by Bader et al. (1939) are plotted (Fig. 15). There is close agreement between the two data sets at the finer mesh sizes, but Bader's average grains weighed more for coarser meshes. This discrepancy probably results from differences in the way the sieves were shaken. Bader agitated his sieves for 40–60 minutes, vs 30 seconds in this study. As a result, in Bader's case lighter grains were driven through the sieve mesh, producing a heavier mean grain in the residual.

The grain mass vs sieve size data were fit with a cubic polynomial (Fig. 15):

$$\overline{m}_j = a_2\left(\overline{D}\right)^2 + a_3\left(\overline{D}\right)^3 \qquad (3)$$

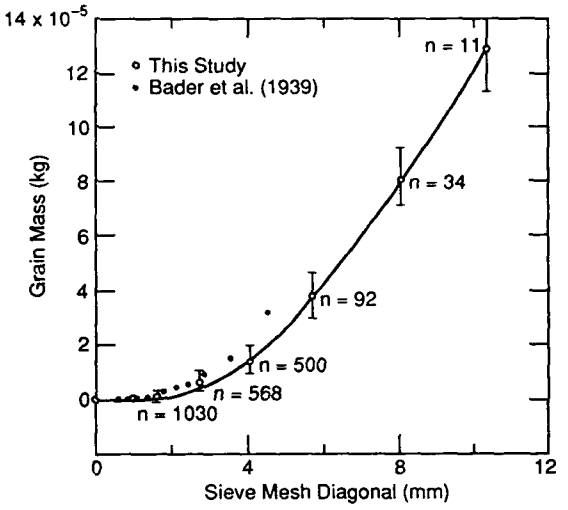

Figure 15. Snow grain mass as a function of sieve size. The number of grains sampled at each sieve size (n) is shown. A cubic polynomial was fit to the data ($r^2 = 0.998$). Data from Bader et al. (1939) agree with the results of this study for the smaller sieve sizes, but diverge for the larger sizes due to differences in the length of time the sieves were agitated. Standard error of the mean is shown.

where $\overline{m}_j$ is the average mass of an individual grain (kg) in the jth sieve, $\overline{D}$ (equals $\overline{D}_{j,j+j}$ of eq 2) is the diagonal of the sieve mesh opening in mm, $a_2 = 1.149 \times 10^{-6}$ kg mm^{-2}, and $a_3 = 4.495 \times 10^{-9}$ kg mm^{-3} ($r^2 = 0.998$).

Using the polynomial fit, the average mass of a grain caught in a particular sieve could be determined from the sieve size. Since the total weight fraction of snow in the sieve was measured, the total number of grains in the sieve could be estimated. Summing for all sieves permitted the total number of grains in a sample to be estimated. The formulae and error estimates associated with these calculations are presented in Appendix B.

There was an order-of-magnitude decrease in the number of grains per unit volume as the snow on the ground metamorphosed into depth hoar (Fig. 16). Most of the reduction in number of grains

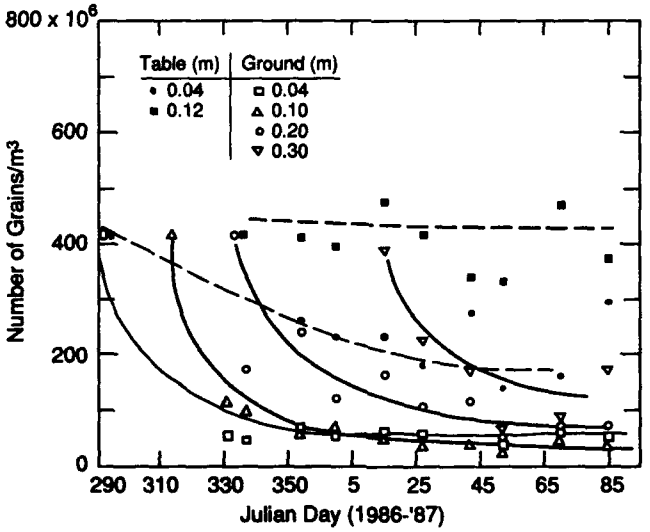

Figure 16. Number of snow grains per cubic meter, 1986–1987. Trajectories of grain number vs time have been drawn in by assuming that all samples had 400×10^6 grains per cubic meter when deposited, a value determined from snow samples at 0.2 and 0.3 m immediately after they were deposited. Trajectories for all snow layers on the ground (solid lines) were similar, but differed from those of snow on the tables (dashed lines).

Table 7. Number of grains (thousands) per cubic meter by sieve size, 1986–1987.

Julian date	*Sieve size*									
	8.7mm	*7.3mm*	*5.7mm*	*4.2mm*	*2.8mm*	*1.9mm*	*1.4mm*	*0.9mm*	*0.3mm*	*Total*
Snow on tables at 0.12 m										
354	0	0	0	0	0	1941	16581	90079	305421	414021
365	0	0	0	0	341	2153	31361	71937	289800	395592
15	0	0	0	0	249	1224	20242	90214	367779	479708
27	0	0	0	228	515	1162	28810	102718	285517	418950
42	0	0	0	0	1233	2102	26399	107694	203276	340704
52	0	0	0	0	822	8662	34781	88010	202759	335033
70	0	0	0	0	1136	3848	32877	101107	332828	471796
85	0	0	0	130	506	1322	53165	58460	262621	376204
Snow on tables at 0.04 m										
354	0	0	0	0	2217	6469	20301	68446	166366	263798
365	0	0	0	0	4271	11492	32628	37934	146979	233305
15	0	0	0	0	4572	6270	28311	33008	163338	235499
27	0	0	0	0	5550	7084	22527	43992	104143	183296
42	0	0	0	0	4286	3852	24619	42979	201393	277128
52	0	0	0	0	3859	10889	29707	37678	59476	141608
70	0	0	0	0	10148	3818	13415	33029	104276	164686
85	0	0	0	0	1238	18886	47236	42466	188069	297896
Snow on ground at 0.30 m										
15	0	0	0	0	45	409	6539	69466	315621	392080
27	0	0	0	0	0	5833	31691	41650	147931	227106
42	0	0	0	18	5953	4495	22445	37501	99434	169846
52	0	0	0	858	9664	7758	16033	16777	13241	64331
70	0	0	55	1480	13104	4841	10672	12408	44069	86629
85	0	13	459	2010	10444	6376	18339	24257	110641	172538
Snow on ground at 0.20 m										
337	0	0	0	0	336	8081	16962	31189	119828	176396
354	0	0	0	0	1268	5727	35511	47525	152503	242536
365	0	0	0	2103	8426	4323	15547	31996	60510	122906
15	0	0	266	631	5246	3887	17489	35800	103697	167015
27	0	31	201	766	7988	5848	17729	22485	53241	108289
42	0	0	58	1754	8257	2896	12668	20835	70172	116640
52	0	0	206	2555	8638	5500	9094	13456	13655	53104
70	0	0	223	2443	11490	4323	8935	10388	29517	67320
85	18	35	361	1796	10028	4061	9735	12294	36041	74369
Snow on ground at 0.10 m										
331	0	0	0	58	6828	4284	16225	15908	74000	117303
337	0	0	0	1712	6052	4255	13122	15885	59214	100241
354	0	59	268	2322	5033	2897	7403	11139	27745	56866
365	0	23	101	3306	6442	4321	8605	11612	34262	68671
15	0	79	122	3788	5604	2319	4532	6972	25338	48754
27	0	81	668	3055	5547	2159	4998	6641	11793	34942
42	14	92	998	2935	5187	1989	3507	5097	19310	39129
52	0	63	876	4225	5758	2500	3307	3845	4097	24671
70	22	92	1055	3448	5397	1949	3223	5621	26621	47429
85	141	363	1334	2207	3644	1479	2674	4086	18931	34859

Table 7 (cont'd).

Julian date	Sieve size 8.7mm	7.3mm	5.7mm	4.2mm	2.8mm	1.9mm	1.4mm	0.9mm	0.3mm	Total
Snow on ground at 0.04 m										
331	0	62	481	1842	4893	1943	4735	7995	31655	53607
337	0	112	673	2969	3680	1970	3833	6387	26379	46003
354	0	65	526	2431	5090	2474	6135	9511	44676	70908
365	65	219	1329	2992	3350	1988	4570	7270	31779	53563
15	0	90	756	2022	4213	2028	4389	8363	39269	61131
27	18	100	736	2182	4039	2379	8522	9146	32483	59603
42	87	195	923	2042	4023	1882	3991	7078	33517	53738
52	116	164	847	1983	3311	1869	3708	5748	20414	38160
70	40	112	921	2547	5148	2235	4434	8592	36621	60650
85	159	277	979	1706	4151	1900	4355	7305	33021	53852

occurred in the first few weeks after the snow was deposited. For example, samples from 0.04 m and 0.10 m contained more than 4×10^8 grains per cubic meter at the start of the winter; this was reduced to less than 5×10^7 grains per cubic meter in the first 40 days. During the next 110 days the number of grains hardly changed at all. The similarity of trajectories of number of grains per unit volume vs time suggests that, regardless of when the snow started to metamorphose, the metamorphic process for all samples of snow on the ground was the same. In comparison, the number of grains per unit volume on the tables remained high throughout the winter and followed different trajectories. The reduction in the number of snow grains per unit volume during depth hoar metamorphism has been noted by many observers including Paulke (1934a), Seligman (1936), Bader et al. (1939), Benson (1962), and Akitaya (1974), but has not been quantified before.

The distribution of the number of grains as a function of sieve size listed in Table 7 shows that the decrease in total grain number was accomplished by a decrease in the number of small grains and an increase in the number of large grains. This can be seen most clearly in samples taken from the snow on the ground at a height of 0.2 m. On 3 December 1986 (Julian day 337), there were no grains in the four largest size classes and there were over 10^8 grains per cubic meter in the smallest size class. By the end of the winter, there were over 10^6 grains per cubic meter in the four largest size classes and the number in the smallest size class had been reduced by a factor of 3. This contrasts with snow on the tables, for which there was no systematic change in the distribution of grains.

Depth hoar texture

The extreme temperature gradients found in the Fairbanks snow cover produce several metamorphic textures in the snow by late winter. These textures were observed from 1982 to 1989 and were photographed during the winters of 1985–1986 and 1986–1987 using the techniques explained in Section 2. C. S. Benson,* who has studied snow in Fairbanks since 1962, confirmed that the snow was typical during the years the observations were made.

Five distinct textures, found as a sequence of metamorphic layers (Fig. 17), were identified based on the following criteria:

1) grain size,
2) crystal habit and aspect ratio of a:c axes,
3) c-axis orientation,
4) secondary crystallographic features such as striae, scrolling and eroded crystal edges,
5) qualitative "strength" of the snow.

*Personal communication with C.S. Benson, March 1987 (Geophysical Institute, University of Alaska, Fairbanks).

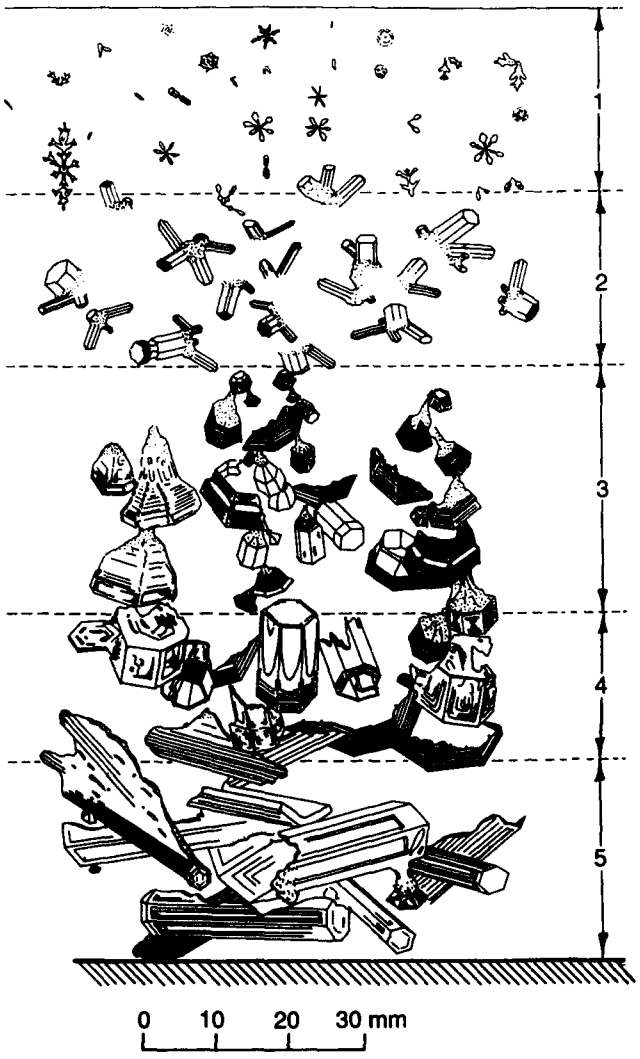

Figure 17. The five metamorphic layers found in Fairbanks snow in late winter. Prominent textural features that define each layer are shown. Grain sizes are to scale, and layer thicknesses are shown in relative proportion.

Each texture was associated with a layer. These are described starting from the top of the snow cover. To facilitate discussing the textures, they have been called metamorphic layers 1 through 5. This was also done to emphasize that the textures developed as a metamorphic sequence that produced a layered structure in the snow. The most intense metamorphism was found in the oldest layers at the base of the snow cover. Layer descriptions are cross-referenced to existing classification systems for snowflakes, and for snow that has been deposited on the ground. ML indicates the snowflake classification system of Magono and Lee (1966), which is similar to the classification system of UNESCO (1970), but uses different code letters. SL indicates the deposited snow classification system of Sommerfeld and LaChapelle (1970), and C indicates the deposited snow classification system devised by Colbeck (1986).

Metamorphic layer 1 (Fig. 18) consists of new snow and snow showing slight cataclasis and some effects resulting from wind or above-freezing air temperatures (SL: III-A-1; C: II-C-1).

Metamorphic layer 2 (Fig. 19) consists of small (≤ 1 mm) grains composed of squat, euhedral, hexagonal prisms with a:c axial ratios of about 1:1. C-axis orientations are random. von Eugster (1950) called this type of snow crystals "*prismatische Vollformen*," and Akitaya (1974) called them "*koshimo-zapame-yuki*" or solid-type depth hoar (SL: III-A-2; C: II-C-2; ML: Cle, Clg).

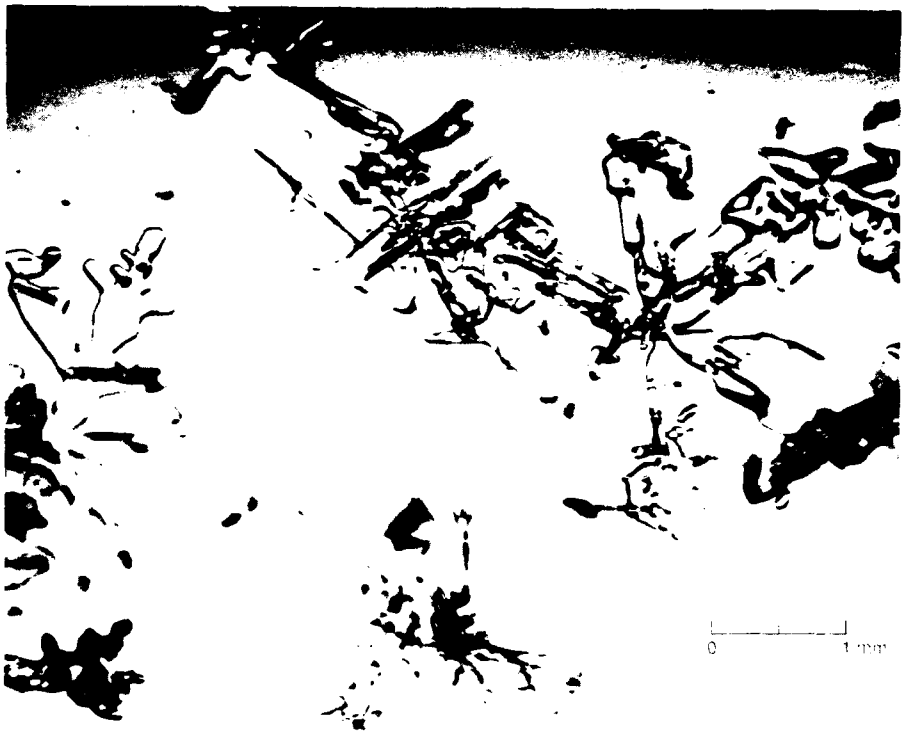

Figure 18. Snow grains from metamorphic layer 1. Partial and nearly complete dendrites and spatial dendrites are present. Crystal edges are smooth and rounded, suggesting that vapor transfer is taking place.

Figure 19. Snow grains from metamorphic layer 2. Crystals are solid, euhedral, hexagonal prisms known as solid-type depth hoar. Crystal edges are sharp and striae are absent. C-axis orientations are random.

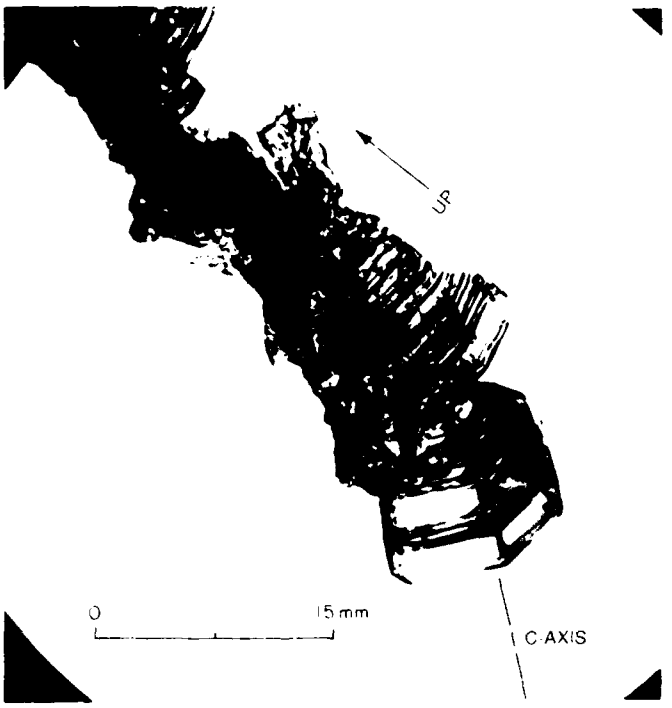

a. A chain of cup crystals.

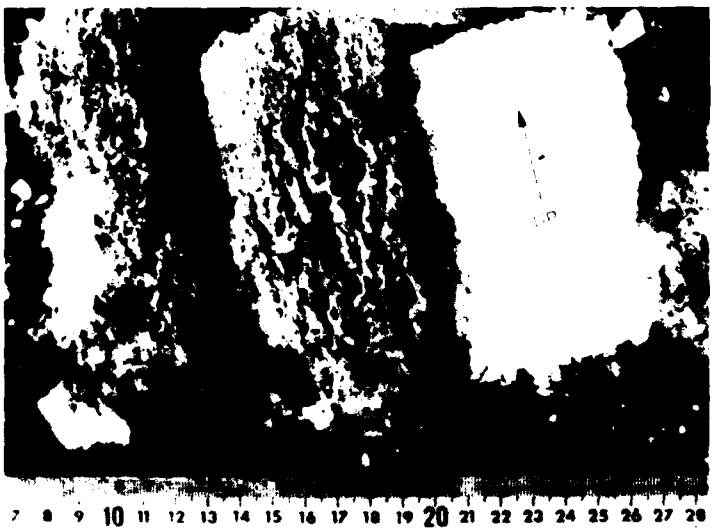

b. Snow samples from the Brooks Range, Alaska, showing the vertical structure of layer 3. Wind incorporated dirt and dust in the snow during its deposition, highlighting the texture.

Figure 20. Snow grains from metamorphic layer 3. (Photos by C. S. Benson)

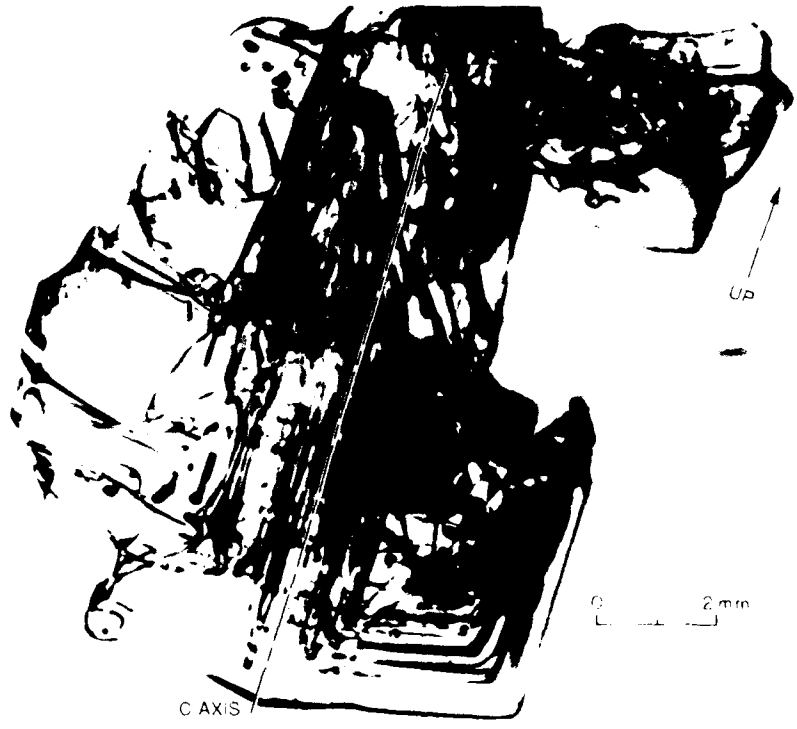

Figure 21. Column crystal from metamorphic layer 4. It exhibits the distinctive erosional features such as rounded upper edges, glassy crystal surfaces, and truncated crystal facets that are typical of this layer. C-axes are usually vertical.

Metamorphic layer 3 (Fig. 20) consists of moderate-sized grains (≤ 10 mm) composed of hexagonal, pyramidal cups that open downward and have a:c axial ratios of 2:1 or greater. The crystals are heavily striated, with sharp downward-facing edges. C-axes of the crystals generally fall within 15° of vertical, and the crystals are bonded into vertical ice columns with intervening, vertically elongated air spaces (Trabant and Benson 1972), or "chains of grains" (Colbeck 1986) (Fig. 20). Bonds between crystals consist of unfaceted ice attached to the crystals like a calyx attaches to a flower. The bonding is weak, making the layer fragile. von Eugster (1950) called the type of crystals found in this layer "*Hohlformen basale Teilbecher*," and Akitaya (1974) called them "*shimo-zarame-yuki*" or skeleton-type depth hoar, but neither author reported the vertical chains of grains (SL: II-B-2; C: II-C-3; ML: clh).

Metamorphic layer 4 (Fig. 21) consists of large (≤ 20 mm) grains that show evidence of erosion by sublimation. The grains are aggregates of several crystals that are either hollow, hexagonal columns with axial ratios (a:c) of about 1:2, or partial crystals whose interfacial angles suggest that they are the remnants of cup-like crystals that were greater than 20 mm across. C-axes of both types of crystals are approximately vertical. Downward-facing crystal edges are sharp and have pronounced striae. Several features found on the upper parts of crystals (rounding, ragged edges, loss of striae, and smooth crystal faces, sometimes with irregular holes) indicate erosion by sublimation (Colbeck 1986). Bonding between grains is poor. In fact, metamorphic layer 4 can be identified because it is the least cohesive layer and it is difficult to sample. The hollow columns found in the layer are similar to ML type Clf, and von Eugster (1950) called similar crystals "*Hohlformen prismatische Becher.*" They are not included in the SL or C classification system.

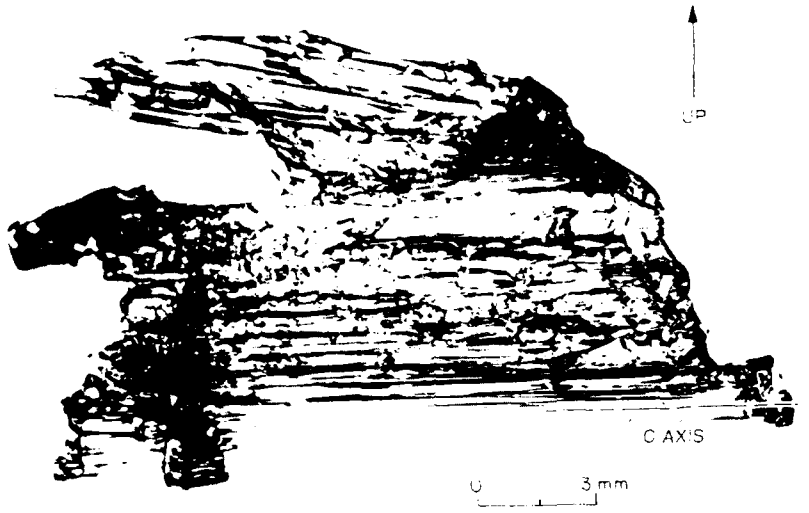

Figure 22. Snow grain from metamorphic layer 5. It consists of several elongated prismatic columns with keel-like growths on their upper surfaces. Lower edges are sharp, indicating active crystal growth. A small "secondary" cup crystal is growing downward from the bottom edge of the largest column. C-axis orientations of most large columnar crystals are horizontal to subhorizontal.

Metamorphic layer 5 (Fig. 22) consists of grains that average 10 to 20 mm in length, though grains longer than 30 mm can be found. Most grains consist of several elongated, hexagonal column crystals with axial ratios (a:c) of approximately 1:5. C-axes of most crystals are close to horizontal. Crystals are euhedral and are generally more complete than those of metamorphic layer 4. Erosion features are not prominent. The majority of crystal faces show skeletal growth (i.e., they step inward towards the c-axes [Knight and DeVries 1985]). Occasionally "secondary" growth features, such as downward-facing cup-crystals, with vertical c-axes, grow like small buds along the bottom edges of large columns. The bonding of the layer is surprisingly strong, particularly in contrast to the overlying layer, producing a felt-like texture of interlocking horizontal crystals. The column crystals are similar to the "needle" and "sheath" crystals photographed by Akitaya (1974), but are not included in the SL or C classification system.

The five metamorphic layers developed every winter during which observations were made, though the relative thicknesses of each layer varied from winter to winter. The thicknesses of metamorphic layers 1, 2, and 3 were difficult to determine because the boundaries between these layers were gradational. The lower boundary of metamorphic layer 3, however, could be located by gently scraping a snow pit wall, because the cohesionless crystals of metamorphic layer 4 were removed, leaving the "chains of grains" in metamorphic layer 3 intact. The boundary between metamorphic layers 4 and 5 was usually distinct because of the change in c-axis orientation. This boundary swept upward through the winter. In December 1987, metamorphic layer 5 was 20 mm thick; by March it was 80 mm thick.

A reconnaissance survey conducted during this study suggests that metamorphic layer 5 develops better (i.e., has larger column crystals) in snow deposited on lake or river ice than over bare soil, and it is often better developed over moss tussocks than other vegetation. A qualitative comparison of two snow pits, one over bare soil and the other over an impermeable tarp, indicated that metamorphic layer 5 was better developed over the bare soil, but was not absent over the tarp.

Metamorphic layers 1 and 2 are common in most snow covers. The cup crystals of metamorphic layer 3 have been described by Paulke (1934a,b), Seligman (1936), von Eugster (1950), Sommerfeld

and LaChapelle (1970), Trabant and Benson (1972), Akitaya (1974), Pahaut and Marbouty (1981), Kolomyts (1984), and Colbeck (1986), but the vertical structure (Fig. 20b) has received less attention. Kojima (1956), working on snow with a texture similar to metamorphic layer 3, found that depth hoar was "stiff" in vertical compression, but subject to brittle failure. Akitaya (1967, 1974) suggested that a "vertical columnar structure" was the cause of this property. Benson and Trabant (1972) and Trabant and Benson (1972) noted "vertically oriented channels" in the Fairbanks snow. Sommerfeld and LaChapelle (1970) observed a texture they called "late-stage advanced temperature gradient metamorphism" or "lattice grains" that is probably equivalent to metamorphic layer 3. Most recently, Colbeck (1986) described one aspect of the texture as "chains of grains".

Metamorphic layers 4 and 5 have not been described before, perhaps because most snow covers do not metamorphose long enough or under strong enough temperature gradients to develop the five-layer sequence. von Eugster (1950) identified a metamorphic sequence in which solid depth hoar crystals developed into skeletal crystals or the reverse. Sommerfeld and LaChapelle (1970) identified a similar sequence of early- and late-stage depth hoar metamorphism, with their late-stage corresponding to metamorphic layer 3. Akitaya (1974) also described a sequence that includes metamorphic layers 1 through 3. Bradley et al. (1977a, 1977b) and Adams and Brown (1982a) associated changes in the strength of snow layers with the development of depth hoar. They found minimum strength in a snow layer consisting of small, anhedral grains, probably equivalent to the transition between metamorphic layers 1 and 2, while in this study, the minimum strength was observed in metamorphic layer 4.

The transitions in crystal habit or form observed in the five metamorphic layers can be explained, in part, by differences in the local temperature and the temperature gradient with height in the snow, since the base of the Fairbanks snow cover is often –2°C while the top is –40°C. In clouds, snow crystal habit is determined by temperature, with secondary features determined by growth rate or the supersaturation at the crystal surface (Nakaya 1954, Kobayashi 1961, Mason et al. 1963, Magono and Lee 1966, Lamb and Hobbs 1971, Lamb and Scott 1972, Frank 1982, Keller and Hallett 1982). Distinct and abrupt transitions between hexagonal plate crystals and hexagonal columns occur at –4, –9, and –22°C. Akitaya (1974; p. 28) found that similar transitions occurred for snow deposited on the ground, though he related the transitions to temperature and temperature gradient. Marbouty (1980) and Adams and Brown (1982b) have reported similar results. However, the c-axis orientations observed in three of the five metamorphic layers cannot be explained by changes in temperature or temperature gradient. A speculative explanation for the c-axis orientation, based on the convective circulation pattern, is discussed at the end of Section 5.

Measurements related to heat transport in snow

Heat flow

Heat flow at the snow/soil interface, measured using thermopile heat flow meters (HFMs), varied between 5 and 30 W m^{-2} during the winters of 1984 to 1987 (Fig. 23). In comparison, the geothermal heat flow is about 0.05 W m^{-2}. The major source of the heat came from latent heat liberated as the soil moisture froze. This can be verified by comparing the latent heat flow released in 1986–1987 to the heat flow measured by the heat flow meters. The latent heat flow, calculated from soil moisture profiles and the rate at which the freezing front moved downward in the soil, varied between 6 and 24 W m^{-2}, which is in broad agreement with the heat flow measured by the HFMs.

There was a marked difference in the heat flow signal between the winter of 1984–1985 and the next two winters. The 1984–1985 signal varied smoothly and regularly. The mean heat flow was approximately 6 W m^{-2}, except during two discrete periods when air convected in the snow (see Section 5). During the next two winters the heat flow showed greater and more rapid fluctuations, and its mean value was about 10 W m^{-2} (Fig. 23).

The interannual differences in heat flow were the result of differences in the snow depth during the three winters (Fig. 24). The thinner snow of 1985–1986 and 1986–1987 gave rise to larger and more

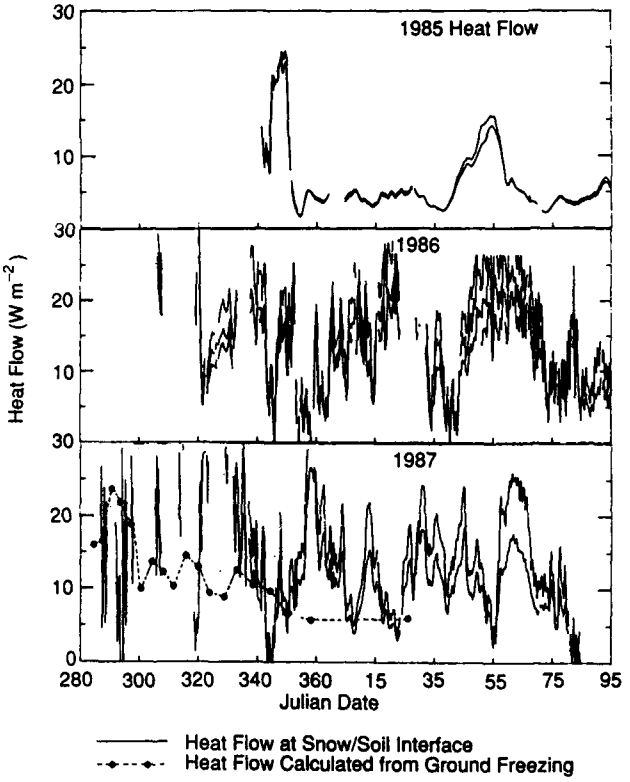

Figure 23. Heat flow at the snow/soil interface, 1984–1987. Heat flow was measured by heat flow meters and computed from soil temperature and moisture data.

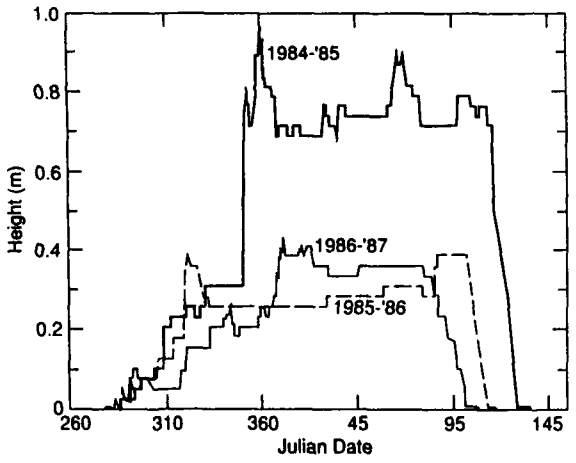

Figure 24. Fairbanks snow depth, 1984–1987. The large snowfall in December 1984 was the single largest snowfall for Fairbanks in 10 years.

rapidly varying temperature gradients than those present in 1984–1985. The larger temperature gradients and fluctuations of the gradients resulted in greater and more rapidly varying heat flow.

Thermal conductivity

The bulk effective thermal conductivity of the snow can be written:

$$k_{\text{bulk}} = Q_s / \left[\overline{\partial T / \partial z}\right] \tag{4}$$

where Q_s is the heat flow at the snow/soil interface, and $\overline{\partial T / \partial z}$ is the average vertical temperature gradient across the snow cover. k_{bulk} showed little difference from one winter to the next, ranging from 0.1 to 0.3 W m^{-1} K^{-1} (Fig. 25).

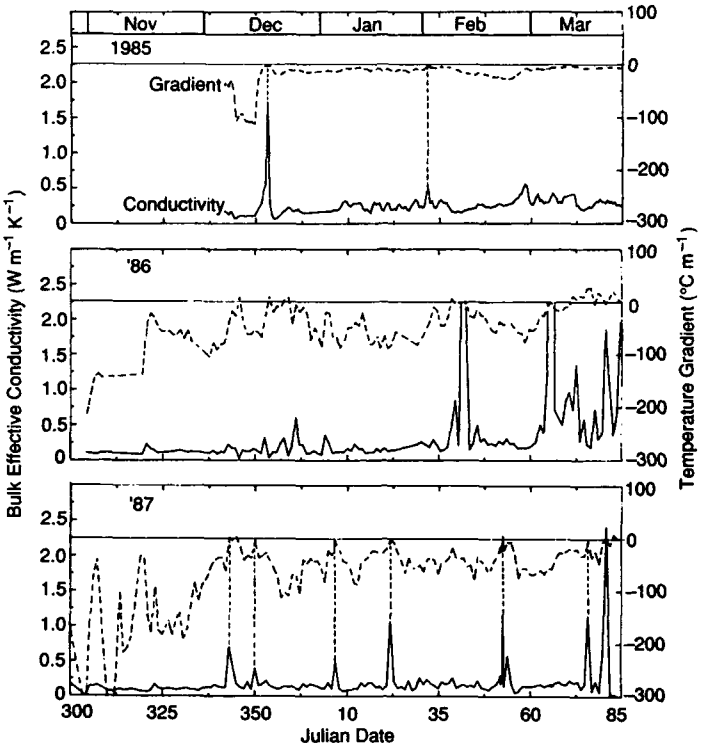

Figure 25. Bulk effective thermal conductivity of Fairbanks snow cover, 1984–1987. Conductivity (solid line) was calculated by dividing the heat flow at the snow/soil interface by the average vertical temperature gradient (dashed line). When the temperature gradient approached zero, the conductivity was undefined, producing large spikes. The mean value of the conductivity was 0.1 to 0.2 W m^{-1} K^{-1} for all three winters.

Needle probe measurements of the effective thermal conductivity of the snow (ke_{ff}) were sporadic in 1984–1985, but became routine in 1985–1986 and 1986–1987. The measurements showed that the thermal conductivity of depth hoar is lower than predicted. Most authors (Hjeltström 1890, Jansson 1901, Okada 1905, Devaux 1933, Kondrat'eva 1954, Yosida and Iwai 1954, Mellor 1977) suggest that for snow with a density of 200 kg m^{-3}, typical for depth hoar, the thermal conductivity (in the absence of convection) should range from 0.10 and 0.20 W m^{-1} K^{-1}, but the measured values ranged from 0.04 to 0.10 W m^{-1} K^{-1} (Appendix D). It is likely that the thermal conductivity values determined in this study were lower than predicted because most predictive equations are based on studies that did not include measurements of depth hoar. However, since few of the studies reported the type of snow or the temperature at which measurements were made, and because thermal conductivity is a function of temperature and snow texture as well as density (de Quervain 1972), the actual cause of the discrepancy cannot be determined. Lange (1985) is the only author who unambiguously states that he measured the thermal conductivity of depth hoar, and obtained values of 0.04 to 0.05 W m^{-1} K^{-1}, which is within the range determined in the present study.

The bulk effective thermal conductivity of the snow (k_{bulk}) (Fig. 25) was higher than the average values of conductivity measured by needle probe (k_{eff}). The disagreement between these two values is discussed in Section 5 as evidence for convection in the snow.

The effective thermal conductivity (k_{eff}) was measured over a range of temperatures to determine its temperature dependence. Unfortunately, available equipment limited normal measurements to –20 to 0°C, and measurements near 0°C were difficult to make without melting the sample. To separate

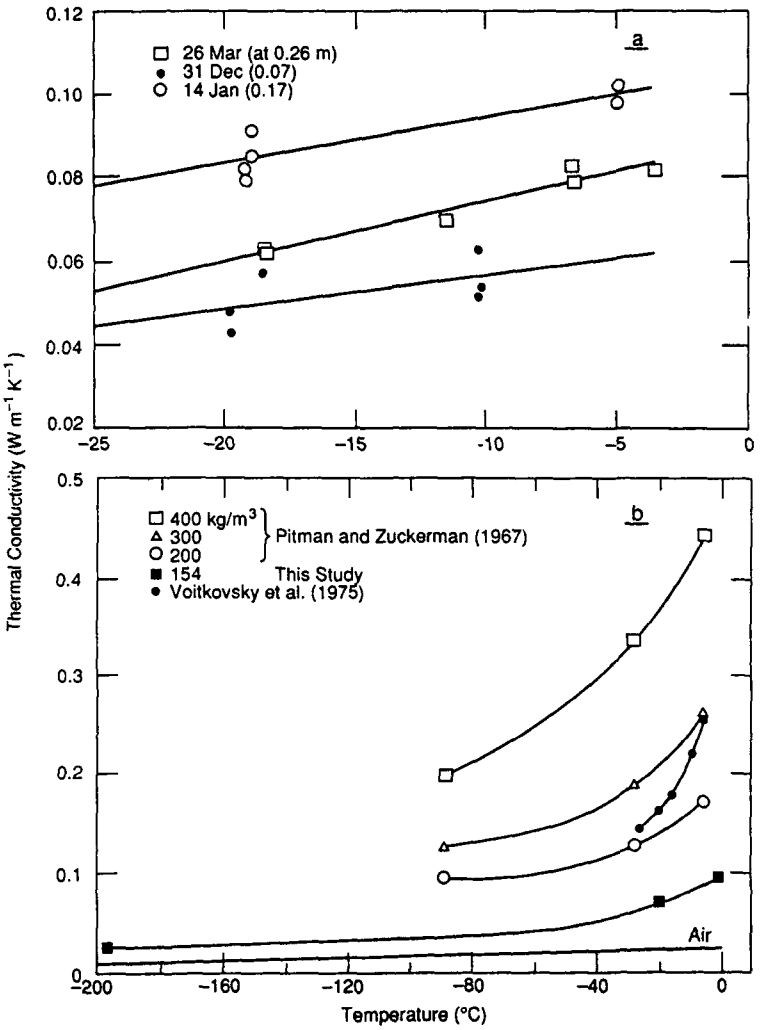

Figure 26. Temperature dependence of the thermal conductivity of depth hoar. (a) 0° to –20°C; different textures are plotted separately. (b) 0° to –196°C; data for dry air (dashed line) and from Pittman and Zuckerman (1967) and Voitkovsky et al. (1975) are included for comparison.

the effects of temperature from those of snow density and texture, measurements for each snow sample were plotted separately (Fig. 26a). Over the range of temperature for which measurements were made, the thermal conductivity was linear and the slopes of the lines were similar, suggesting that $\partial k_{eff}/\partial T$ may be independent of snow texture.

To get a datum at a temperature for which there would be no latent heat transfer, one measurement was made with the sample jacketed and immersed in liquid nitrogen (–196°C). Using measurements made at –5, –20, and –196°C, and with the thermal conductivity of air as a limiting value, a composite curve for the temperature dependence of k_{eff} was plotted (Fig. 26b). Data measured by Pitman and Zuckerman (1967) and Voitkovsky et al. (1975), are plotted for comparison. The methods used in the latter study are not published.

During 1986–1987, the thermal conductivity of three layers was measured throughout the season (Fig. 27). The layer at 0.07 m height in the snow was already completely metamorphosed into the texture described as metamorphic layer 3 when the initial measurement was made. As the layer

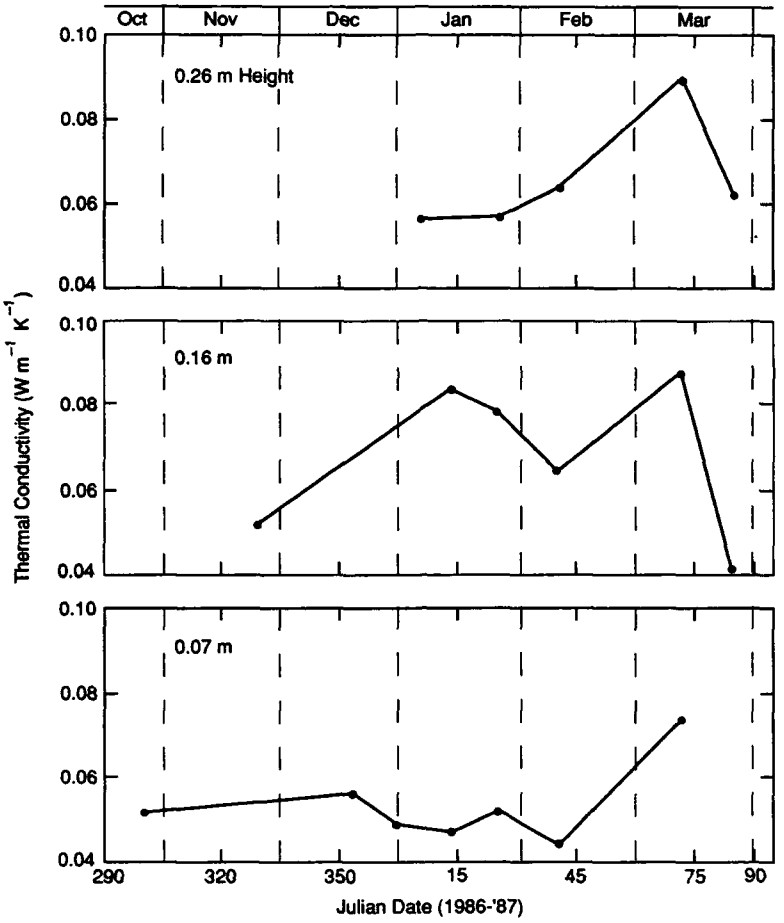

Figure 27. Changes in thermal conductivity of three snow layers, 1986–1987. The layer at 0.07 m was already depth hoar when first measured.

metamorphosed into metamorphic layer 4 and then metamorphic layer 5, its thermal conductivity first decreased, then increased. This is consistent with the observations of the relative strength and cohesiveness of the metamorphic layers. Metamorphic layer 4 is the least cohesive, most poorly bonded layer, which would contribute to the low thermal conductivity. Metamorphic layer 5 is stronger, more cohesive, and has a higher thermal conductivity than metamorphic layer 4.

At 0.16 m height, the initial measurement was in new snow. Compaction of this very light snow caused an increase in thermal conductivity, but as metamorphic layer 3 and 4 textures developed, the thermal conductivity decreased. Results for the layer at 0.26 m were similar, but metamorphism did not progress as completely as in the underlying layers.

Temperature

The fluid in a porous medium heated from below and cooled from above will convect when buoyancy forces overcome the fluid's viscous resistance. When this occurs, regions of upwelling warmer fluid and downwelling cooler fluid will develop. The thermistor arrays used in this study to measure in-situ snow temperatures, described in Section 2, were designed to detect the horizontal temperature gradients resulting from fluid (air) flow in the snow. In the absence of convection, the horizontal plane defined by the thermistor strings was expected to be isothermal because the snow layers were horizontal and nearly homogeneous.

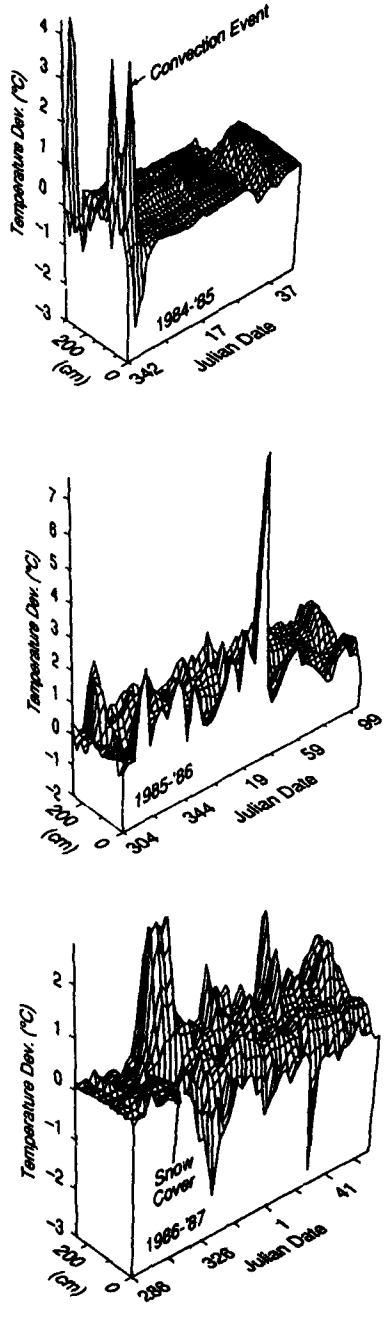

Figure 28. Temperature deviations for horizontal thermistor strings, 1984–1987. The event from 1984–1985 discussed in the text is marked. The flat part of the surface from early winter 1985–1986 and 1986–1987 results from when the thermistors were still in the air.

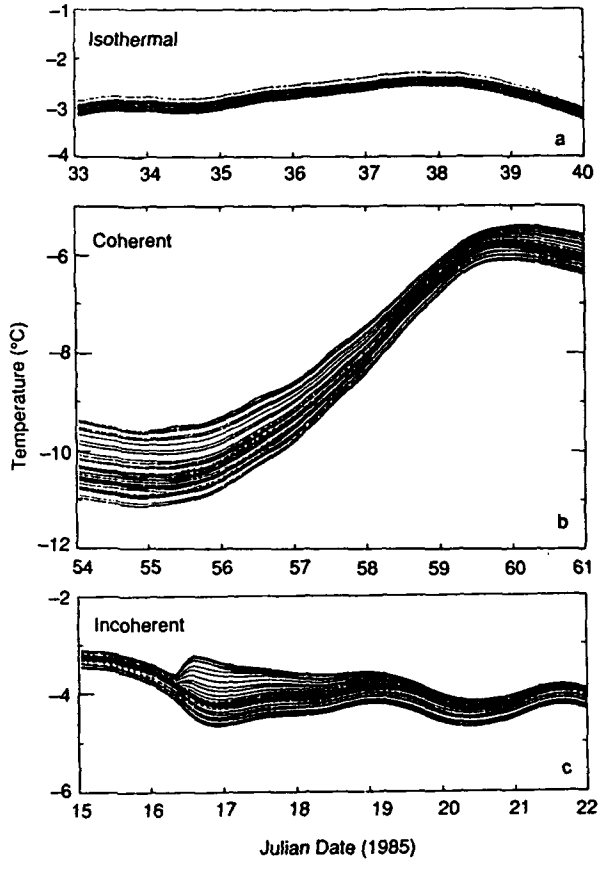

Figure 29. Three types of temperature records.

Isothermal conditions were rare during all three winters. At times the temperature along horizontal thermistor strings varied as much as 16°C over distances of half a meter. To illustrate these large horizontal temperature gradients, the temperature deviation, defined as the difference between the observed thermistor temperature and the mean temperature of the entire string, is plotted in Figure 28 for a selected horizontal thermistor string from each winter.

The large temperature deviations shown in Figure 28a were first reported for the winter of 1984–1985 by Johnson et al. (1987), who were able to show that the deviations could only be accounted for by convection in the snow. Temperature deviations were present more frequently during the next two winters, indicating that convection was present in the snow cover during all three winters that the study was in progress. The two horizontal strings installed in 1984 were insufficient to allow the geometry of the convective flow to be deduced for that winter. The increased number of thermistor strings used in 1985–1986 and 1986–1987 (Fig. 7) made it possible to infer some aspects of the convective circulation, which are discussed in Section 5.

The magnitude and prevalence of temperature deviations differed between 1984–1985 and the next two winters, due largely to differences in the snowfall history (Fig. 24). In 1984–1985, temperature deviations virtually vanished on 17 December 1984 (Julian date 351) when 0.45 m of snow fell in an unusual snow storm. The new snow, accompanied by high air temperatures, reduced the vertical temperature gradient by a factor of 20 and compressed the initial snow layer, which was already depth hoar, to slightly more than half its original thickness, greatly reducing its permeability. During the following two winters there was only half as much snow on the ground and no large snowfalls.

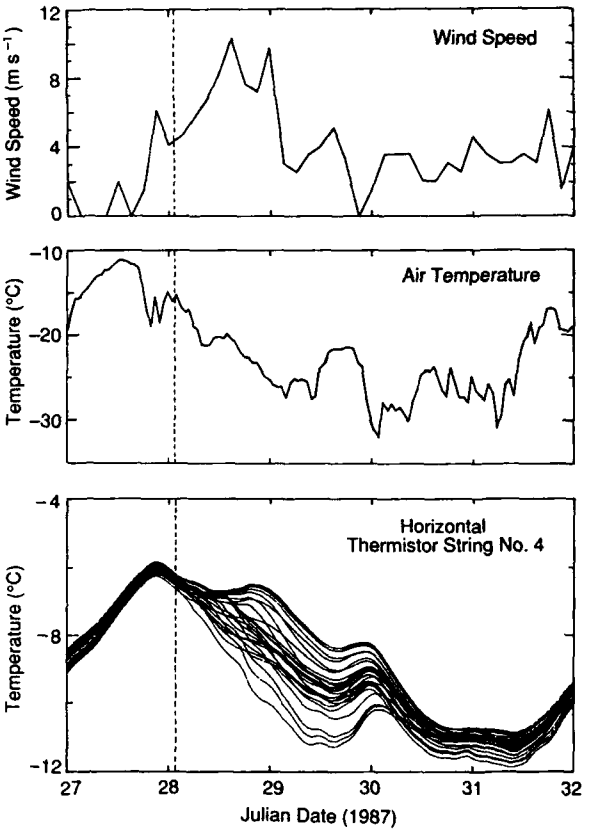

Figure 30. Incoherent temperature record correlated with high wind speed. In this event 45 thermistors were warming and 111 were cooling (for all six horizontal strings).

There were three distinct types of temperature records: 1) isothermal, 2) coherent, or 3) incoherent. The latter two types of records were the result of convection, as discussed in Section 5. Isothermal records resulted when all thermistors on a string registered temperatures within ±0.2°C of the mean (Fig. 29a). Coherent records resulted when the range of temperature about the mean was greater than ±0.2°C. The temperature of all thermistors rose and fell synchronously, producing traces that were parallel and did not cross (Fig. 29b). Incoherent records resulted when the temperature of some thermistors decreased while others increased. This asynchronous behavior resulted in the crossing of thermistor traces (Fig. 29c). The transition between isothermal and coherent records was gradational, based solely on the range of temperature, but the transition from isothermal or coherent records to incoherent records was abrupt (Fig. 29c). In most cases, incoherent records ended when they gradually changed into coherent records. Incoherent records were not due to the spurious behavior of one or two thermistors; they reflect deviations in temperature throughout the entire horizontal thermistor plane. For example, during one period in 1987, 45 thermistors warmed at rates up to 0.05°C hr^{-1}, while 111 thermistors cooled at rates up to 0.10°C hr^{-1} (Fig. 30).

Coherent records were present about 20% of the winter of 1984–1985. In 1985–1986 and 1986–1987, with the snow cover half as thick, they were present virtually throughout the winter except when incoherent records occurred or during the few times the temperature gradient approached zero. Incoherent records were present 15% of the winter of 1986–1987, 16% of the winter of 1985–1986, and 8% of the winter of 1984–1985. During coherent records, the range of temperature on the horizontal strings often exceeded 5°C and occasionally reached 10°C. During incoherent records, the range was greater, exceeding 16°C at one time.

Eleven of the 25 incoherent records identified between 1984 and 1987 correlated with the few periods when the wind exceeded 5 m s^{-1} (Table 8). One example of the correlation between an

incoherent record and high wind is shown in Figure 30. This event, the most conspicuous incoherent record of 1987, began when the wind speed increased rapidly to the highest value recorded during the winter. Observations (Dubrovin 1961, Gjessing 1977) and theoretical studies (Clarke et al. 1987, Colbeck 1989) have suggested that the temperature in the snow could be affected by wind.

The remaining 14 incoherent records occurred during calm conditions. Four of these incoherent records not correlated with wind occurred 10 to 20 hr after the air temperature dropped sharply. If it is assumed that the events were triggered by the air temperature, then the onset of the events occurred 24 to 48 hr before the cold wave could have penetrated to the depth of the thermistors by diffusion. For example, if we define the start of an incoherent record as the onset of rapid divergence in temperature, record B of Figure 31 started 17 hr after the air temperature dropped sharply. At that time, the thermistors were covered by 0.13 m of depth hoar with a thermal diffusivity estimated to be 10^{-7} m^2 s^{-1}. If the drop in temperature propagated into the snow in a purely diffusive manner, the time necessary for it to reach the thermistors would have been 40 to 50 hr (Turcotte and Schubert 1982), rather than the 17 hr that was observed. This point is discussed further in Section 5. The other incoherent record, labeled A in Figure 31, is typical of the events that correlated with neither strong wind nor rapid changes in air temperature.

Table 8. Correlation of wind with incoherent temperature records.

Record number	*Julian date*	*Avg. wind speed (m s^{-1})*	*Peak gust (m s^{-1})*	*Correlated*
1984–1985				
1	345	0.0	0.0	
2	16	4.0	7.0	*
3	45	6.9	10.1	*
4	107	---	9.0	*
1985–1986				
5	320	0.6	3.0	
6	331	1.3	3.5	
7	---	---	---	
8	351	5.0		*
9	357	7.0	11.5	*
10	---	---	---	
11	8	1.6	3.2	
12	11	4.1	6.0	
13	18	3.5	5.5	
14	21	1.9	2.8	
15	28	5.2	6.9	*
16	34	---	13.4	*
1986–1987				
17	323	5.5	---	
18	326	---	---	
19	335	4.5	---	
20	351	5.0	---	*
21	363	5.0	---	*
22	28	10.0	---	*
23	55	6.1	---	*
24	58	2.8	---	
25	63	1.0	---	

--- No reliable data
* Temperature record correlates with onset of strong wind

Analysis of the spatial distribution of temperature during coherent and incoherent records indicates that relatively warm and cold zones developed in the snow and persisted throughout most of the winter, evolving slowly, but never changing location abruptly (Fig. 32). The two horizontal strings used in 1984–1985 were insufficient to determine the presence of these zones, but in both 1985–1986 and 1986–1987 their presence was definite. For example, in 1986–1987 a relatively warm zone developed on the north edge of the thermistor plane and persisted for more than a month (Fig. 32b–d) before it evolved into two warm zones (Fig. 32e). The zones diminished or disappeared only during periods when the air temperature increased and the vertical temperature gradient in the snow approached zero, as can be seen in Figure 32i. The warm and cold zones reappeared in approximately the same locations following the periods of higher air temperatures.

A correlation analysis was used to verify that the relative warm and cold zones stayed in the same location and maintained the same spatial relationship to each other. The analysis was done by selecting an arbitrary reference date for each winter and comparing the locations of the temperature maxima and minima for all other days of the winter to their locations on the reference date. An auto-correlation

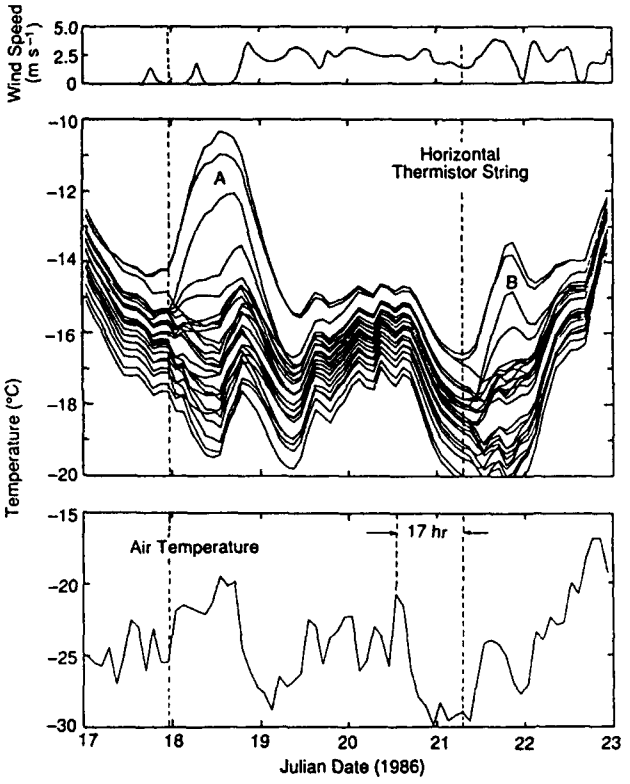

Figure 31. Two incoherent temperature records, one correlated with a sharp drop in air temperature. Record A does not correlate with changes in wind speed or air temperature. Record B began 17 hr after a distinct drop in air temperature. Snow thickness above the thermistors was 0.13 m.

function (Davis 1973) was used; correlation coefficients (r-values) near 1 implied that temperature maxima and minima remained in nearly the same location as on the reference date.

Johnson et al. (1987) performed separate correlation analyses for each horizontal string used in 1985 and found that the warm and cold spots remained in fixed locations during the 10-day event that ended on 17 December 1984 (Julian date 351), but after that, the r-values fell from 0.9 to near 0, implying that through the rest of the winter the location of warm and cold spots was random (Fig. 33a). For 1985–1986 and 1986–1987, all six horizontal thermistor strings were treated as a single composite string consisting of 154 thermistors. The analysis showed that during each winter the warm and cold spots persisted in the same location throughout the winter (Fig. 33b, c). For example, the temperature field from 21 December 1986 (Julian date 355) was chosen as the reference date for 1986–1987. At the beginning of the winter, when the thermistors became buried in snow, there was a rapid rise in the r-values from approximately 0 to greater than 0.7. During the entire period that the strings were covered in snow the r-values were high. The three brief exceptions, when the r-value approached 0, coincided with the three thaws during which the vertical temperature gradient changed sign (Fig. 1).

A second correlation analysis was used to check the possibility that the spatial persistence of warm and cold zones during 1985–1986 and 1986–1987 might have been the result of vertically displaced thermistors or variations in the snow-cover thickness. Before being covered by snow, the thermistors were within ±2 mm of their specified vertical positions. Excavation of the thermistors after they had settled through the winters indicated that the maximum vertical displacements from the mean height were less than 10 mm for all but one thermistor in 1986–1987 (Fig. 34c), which, combined with spatial variations in the snow depth (Fig. 34a), produced variations in the snow thickness above each thermistor of ±10 mm (Fig. 34b). Correlation of the temperature deviations at each thermistor with a) thermistor height, b) the snow layer thickness above each thermistor, and c) the total snow depth at each thermistor were poor. Best correlations were achieved for b), but even in this case r-values averaged less than 0.40.

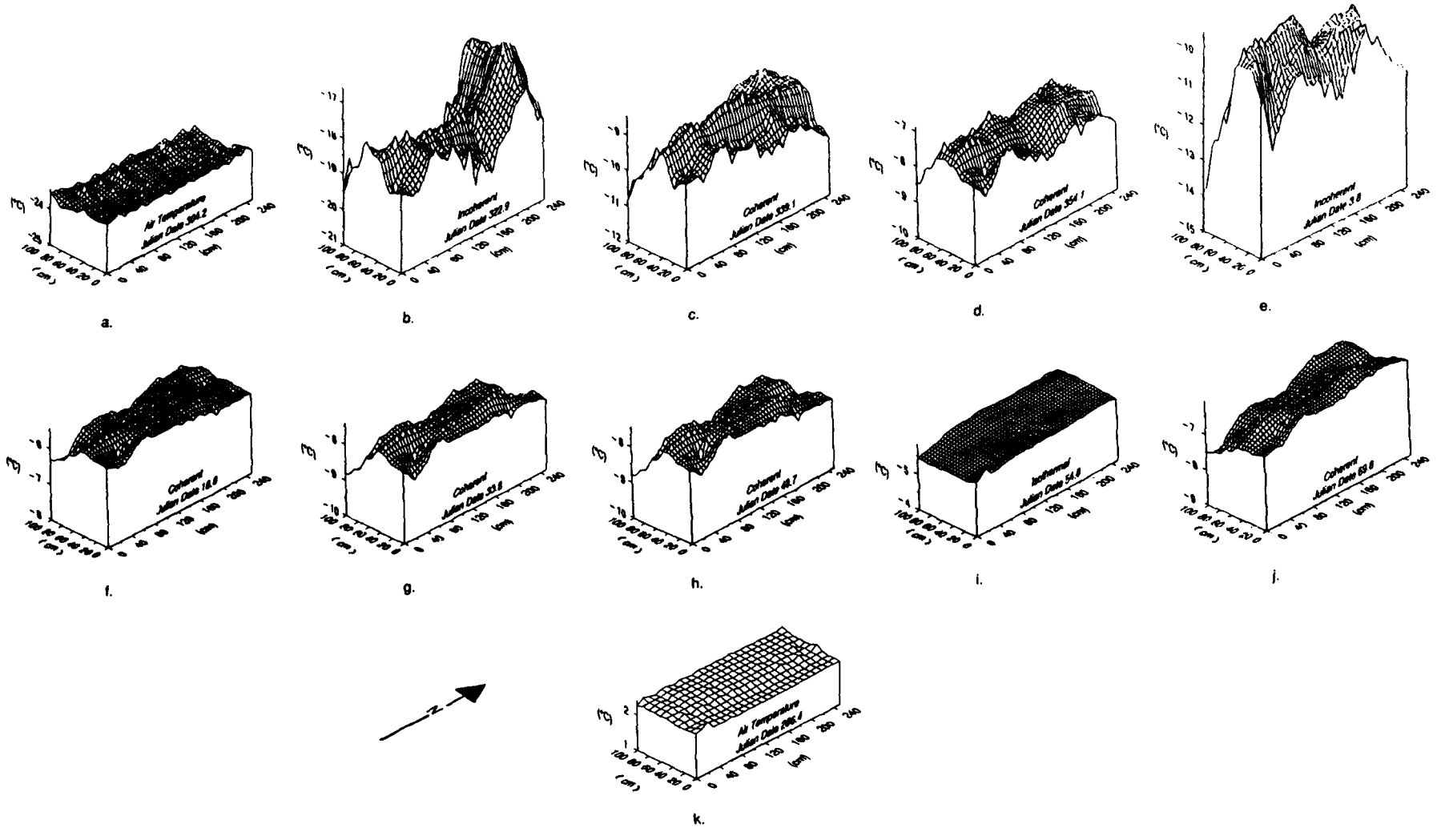

Figure 32. Evolution of relative warm and cold zones in the horizontal temperature field, 1986–1987. Vertical coordinate is temperature (in 1 °C increments). Higher temperatures appear as peaks, lower temperatures as valleys. Surfaces of little relief correspond to when the thermistors were not yet buried in snow or when the vertical temperature gradient approached zero.

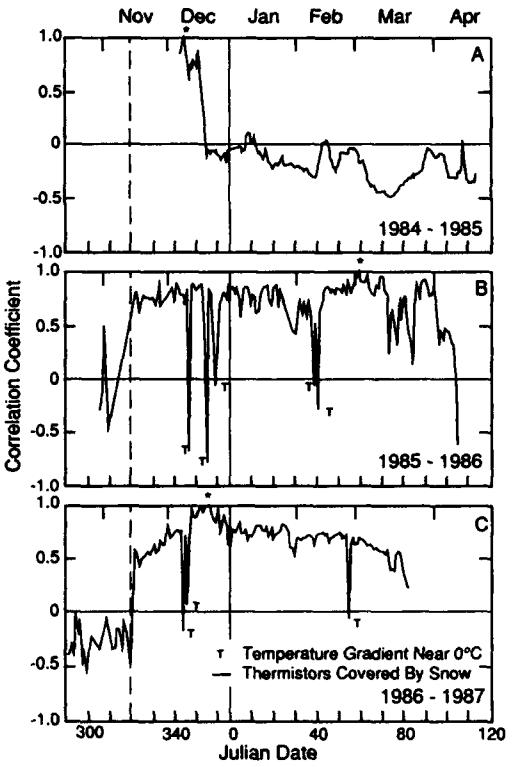

*Figure 33. Correlation between the horizontal temperature field on a reference day and the rest of the winter, 1984–1987. High correlation (≈1) indicates that warm and cold zones stayed in the same location, * indicates the correlation base date.*

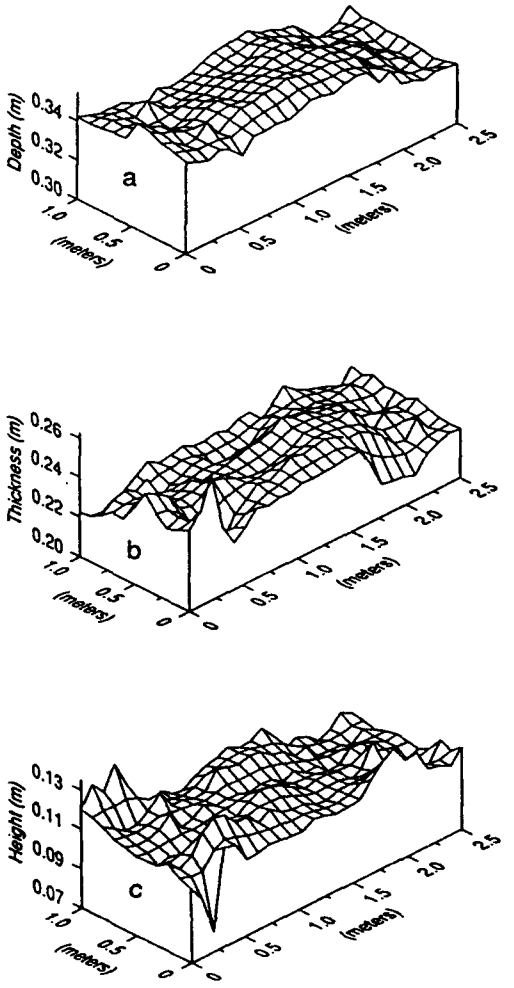

Figure 34. Thermistor heights and snow depth, 1986–1987. Thermistors were excavated on 25 March 1987; one thermistor, located in the southeast corner, was found displaced downward 20 mm from the mean height. (a) Snow depth. (b) Snow thickness above thermistors. (c) Height of thermistors.

The persistence of warm and cold zones in the snow suggested that there were spatial variations in the temperature at the base of the snow, so in 1986–1987 a string of five thermistors was placed at the snow/soil interface. Interface temperatures were never isothermal, with horizontal temperature differences exceeding 4°C early in the winter (Fig. 35). Measurements made by Gosink et al. (1988) in the same field confirm that differences of several degrees exist at the snow/soil interface every winter.

Regions of higher temperature at the snow/soil interface generally coincided with relative warm zones in the snow. This correlation could only be made along the southern edge of the thermistor array where the snow/soil interface thermistors had been placed (Fig. 7), and unfortunately, the most pronounced warm zone in the snow was along the north edge of the array (Fig. 32). However, along the southern edge, higher temperatures in the snow coincided with higher temperatures at the interface throughout the winter.

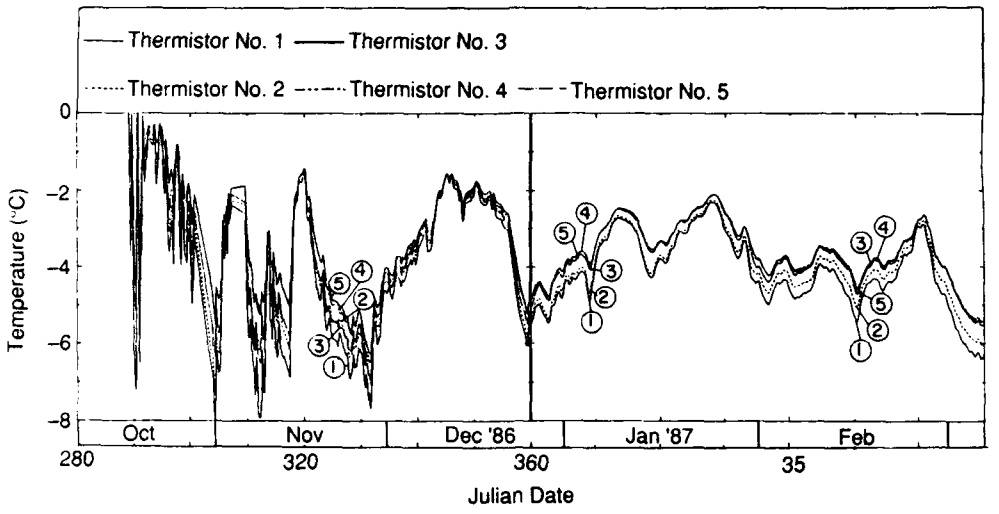

Figure 35. Temperature at the snow/soil interface, 1986–1987.

One possible reason for the variation in temperature at the snow/soil interface was that the soil was not uniformly saturated prior to the onset of freezing, resulting in an unequal release of latent heat. To verify that the soil surface temperature would differ between adjacent wet and dry spots, the Stefan solution (Turcotte and Schubert 1982) was used to calculate the snow/soil interface temperature as a function of time. It was assumed that both wet (50% moisture by dry weight) and dry (10% moisture) soils were silt covered by 0.5 m of snow with air temperature maintained at a constant –20°C. The two soils were initially at 0°C throughout. Results indicate that after 30 days, the wet soil would be 2°C warmer at the surface than the dry soil. For an inexhaustible moisture supply, the temperature of the two adjacent spots would continue to diverge with time, but if all the available moisture froze, the two temperatures would begin to converge.

Temperature differences of more than 1°C persisted at the snow/soil interface through 6 March 1987 (Julian date 65) (Fig. 35), 110 days after latent heat effects should no longer have contributed to maintaining the temperature contrast because all the available moisture would have been frozen. Soil moisture measurements made at the experimental site indicate that below 0.4 m depth, the soil moisture content is negligible (≤ 16%). The freezing front reached this depth by 16 November 1986 (Julian date 320). However, as the ground freezes, wet spots become ice-rich and dry spots become ice-poor. Ice-rich soil has a thermal conductivity four times higher than dry soil (Johnston 1981), which is adequate to maintain the differences in snow/soil interface temperatures.

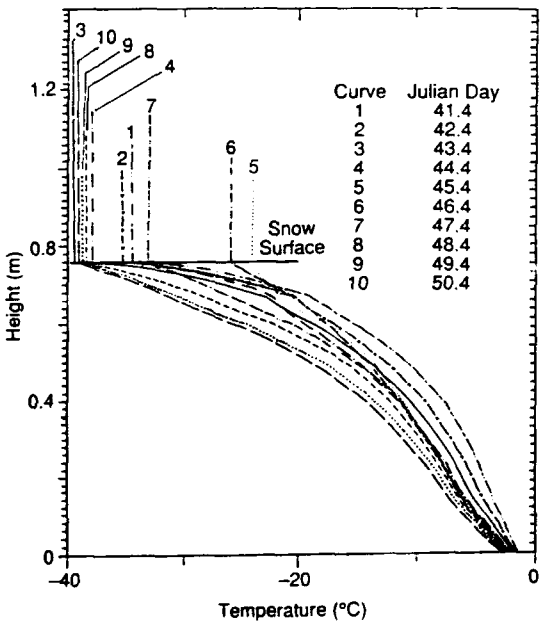

Figure 36. Typical vertical temperature profiles showing negative curvature. Profiles were measured during a period of relatively stable air temperature in 1985.

The vertical thermistor strings yielded data from which the temperature gradient, $\partial T/\partial z$, and curvature, $\partial^2 T/\partial z^2$, could be calculated. Negative curvature (concave-downward) persisted throughout the study, with only a few exceptions. A sequence of typical vertical temperature profiles from 1984–1985 is shown in Figure 36. They represent most of the profiles measured during the study; few profiles were linear or concave-upward.

The negative curvature of the profiles could have been caused by:

1) The response of the snow to rapidly falling air temperatures,
2) Vertical variation of the thermal conductivity,
3) Latent heat liberated as vapor diffuses upward, and
4) Vertical advection of warm air.

By examining only periods of stable air temperature or periods when the air temperature fluctuated closely about a mean value, curvature due to rapidly falling air temperature (possibility 1) can be avoided. For example, the curves in Figure 36 were measured at a time when the air temperature fluctuated less than ±8°C about a mean of –30°C, yet they are still strongly curved. The vertical variation of thermal conductivity (possibility 2) was not the cause of the vertical curvature because there was little variation in conductivity, and it would have given rise to positive rather than negative curvature (because the snow at the base of the snow cover was generally of lower conductivity than the snow at the top) (Fig. 27). Thus, the observed curvature during periods of relatively stable air temperature could only be the result of possibilities 3 or 4 or a combination of both, a point that is discussed at the end of Section 5.

The curvature was greatest during incoherent records, intermediate during coherent records, and least during isothermal records. This was determined in the following manner: periods of stable air temperature were identified, and a determination of the type of record was made from temperature records from the horizontal thermistor strings. Sequential vertical temperature profiles were fit with quadratic curves:

$$T(z) = a_0 + a_1 z + a_2 z^2 \qquad \left(r^2 > 0.99\right) \tag{5}$$

that were differentiated twice to get the curvature. The range of temperature along the horizontal strings was measured and plotted against the curvature (Fig. 37). The results suggest that the curvature (or the range) can be used, in a general manner, to determine if convection is taking place. The four fields drawn on Figure 37 facilitate the determination. This is potentially useful, because it is much easier and requires far simpler instrumentation to measure vertical temperature profiles in snow and determine their curvature than it does to install and monitor horizontal thermistor strings.

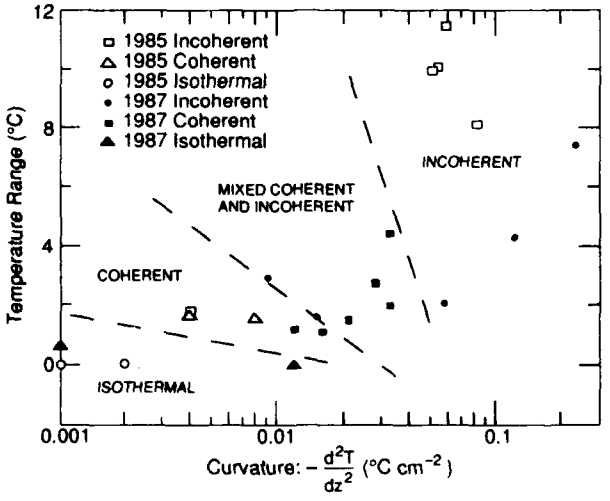

Figure 37. Type of temperature record as a function of magnitude of the curvature of the vertical temperature profiles. Curvature is greatest during incoherent records, least during isothermal records. The range of temperature along horizontal strings is also maximum for incoherent records.

4. ANALYSIS AND DISCUSSION OF MASS TRANSPORT IN THE SNOW COVER

Layer-to-layer mass transport changes the density of snow layers. Within a layer, mass transfer between neighboring grains results in grain growth and shrinkage. (Gubler [1985] referred to the latter case as "interparticle vapor fluxes.") In this section, density measurements are used to calculate mass transport between snow layers, and the maximum grain growth rate is estimated.

The growth of large depth hoar crystals clearly demonstrates the existence of mass flux gradients between snow grains, but the existence of layer-to-layer mass flux gradients has been disputed. Marbouty (1980) and Armstrong (1985) found that the mass of a layer of snow remained constant during the growth of faceted depth hoar grains, suggesting that the net layer-to-layer transport was zero. Using this finding, Adams and Brown (1983), Sommerfeld (1983), Colbeck (1983a), Gubler (1985), and Christon et al. (1987) explicitly assumed no net mass transport between layers in their models of dry snow metamorphism. However, Trabant and Benson (1972), working in snow subjected to stronger temperature gradients for a longer period of time than the snow studied by Marbouty (1980) and Armstrong (1985), found significant layer-to-layer mass flux gradients. An important result of the present study is that it confirmed the work of Trabant and Benson (1972). Though the analysis presented below shows that the values determined by Trabant and Benson (1972) may be slightly high, the essence of their result, i.e., that there are measurable layer-to-layer mass flux gradients in the snow cover, is valid.

The relationship between layer-to-layer mass flux gradients and grain growth is poorly understood. Yosida et al. (1955) postulated that the layer-to-layer flux was the result of innumerable microscopic fluxes between grains in a process they called "hand-to-hand" transfer. In this process, a water molecule accreting to the bottom of an ice grain causes a different water molecule to leave the top of the grain. Repeating the process at successively higher grains results in a net transport of water vapor over a macroscopic distance. The "hand-to-hand" model of vapor transport has become a virtual paradigm in snow science, but it has not been verified nor quantified, and it sheds little light on the relationship between the two scales of mass transport.

Existing theoretical and experimental studies have done little to clarify the relationship between layer-to-layer mass flux gradients and grain growth. Many studies do not explicitly state the scale of the mass transport, and some studies do not even recognize that there are two scales of transport. Yosida et al. (1955), Giddings and LaChapelle (1962), de Quervain (1972), and Trabant and Benson (1972) measured or modeled the layer-to-layer mass flux gradients. Adams and Brown (1983), Sommerfeld (1983), Colbeck (1983a), Gubler (1985), and Christon et al. (1987) developed models of grain growth. Results from both grain- and layer-scale models and measurements have been compared without regard for the differences in scale. There are more models than measurements; there are only 10 measurements of mass transport at either scale (Table 1) and, excluding the present study, only a single work (de Quervain 1958) in which the measurements necessary to determine both scales of transport were made.

Layer-to-layer mass flux gradients in the snow

Comparison of snow on the ground and on tables

The existence of layer-to-layer mass flux gradients in the Fairbanks snow cover, and an estimate of their magnitude, can be determined by comparing the end-of-winter density profiles from the ground and the tables (Fig. 8). Over a 20-year period, the snow on the table was denser at the base than the snow on the ground; conversely the top snow layers on the ground were denser than the top layers on the tables. These density contrasts could only be the result of a net upward transfer of vapor from the bottom to the top of the snow cover on the ground. They imply that there was a vapor flux gradient of about 3×10^{-6} kg m^{-2} s^{-1} m^{-1} (see below).

Consider the average density curves in the center of Figure 8. The greater density at the base of the snow on the tables could be partially the result of more rapid compaction on the tables than the ground because of textural differences in the snow, a net upward transfer of mass in the snow on the ground, or a combination of both. But the density contrast at the top of the snow can only be explained by a net upward transfer of mass. At the top, the snow on both the tables and on the ground had initial densities of approximately 100 kg m^{-3}, but the snow on the ground became more dense than the corresponding snow on the table. With little or no overburden stress at the top of the snow cover, it is unlikely that differing rates of compaction were responsible for the density contrast, which in any case would have resulted in the opposite density contrast, since the snow on the ground was composed almost entirely of depth hoar that was more resistant to compaction than the snow on the tables, as described in Section 3. A net accumulation of mass in the upper part of the ground snow cover is the only reasonable mechanism to produce the increased density, as pointed out by Trabant and Benson (1972). The mass must have come from the lower part of the snow cover.

In comparing the density profiles of snow on the ground with those on the tables, it can be seen that the gain in the upper part of the ground snow cover was roughly equal to the loss from the lower part. If in the course of a winter (175 days) the mass (11 kg m^{-2}) moved up and none moved out the top of the snow cover, it would require a layer-to-layer mass flux gradient of 3×10^{-6} kg m^{-2} s^{-1} m^{-1}, assuming the top half of the snow cover was a layer 0.25 m thick.

Due to the low air temperatures present throughout the winter in Fairbanks, the snow surface is usually the location of the minimum temperature. Consequently, it is a site of condensation rather than sublimation. Therefore, it is reasonable to assume that little or no water vapor escapes from the snow.

Calculations from layer density and thickness measurements

Layer density and thickness measurements made in 1986–1987 allow layer-to-layer mass flux gradients to be calculated in a more detailed manner than in the preceding section. For each of the 10 marked layers of snow the continuity equation was solved to determine the mass flux gradient. The continuity equation for a compacting layer of snow is (Appendix F):

$$\frac{\bar{\rho}}{h}\frac{Dh}{Dt} + \frac{D\rho}{Dt} \approx -\frac{\overline{\partial J}}{\partial z} \tag{6}$$

where $\bar{\rho}$ is the bulk density of the snow, t is time, h is the thickness of the snow layer, z is the vertical coordinate, and J is a vertical mass flux, here limited to a vapor flux. Both J and z are positive upward. The minus sign accounts for the fact that when more vapor enters through the bottom than exits through the top of layer (a negative flux gradient) it increases the mass of the layer.

From density and layer thickness data (see Section 3, Tables 5 and 6), empirical linear relationships:

$$\begin{aligned} h(t) &= a_1 t + b_1 \\ \rho(t) &= a_2 t + b_2 \end{aligned} \tag{7}$$

were fitted to the compaction [$h(t)$] and densification [$\rho(t)$] curves for each snow layer (Fig. 38). The compaction and densification were rapid immediately after the snow was deposited, but this was followed by a longer period of reduced rates, therefore the data for the initial and secondary periods were fit with separate linear relationships. From the functional relationships (eq 7), the derivatives $D\rho/Dt$ and Dh/Dt, $\bar{\rho}$, and h were evaluated for the midpoint of each line segment, and eq 6 was solved for an early- and late-winter value for the mass flux gradient for each layer (Table 9). Uncertainties in thickness (±3 mm) and density (about ±5 kg m^{-3}) made the uncertainty in the calculated value of the mass flux gradient relatively large (Appendix F).

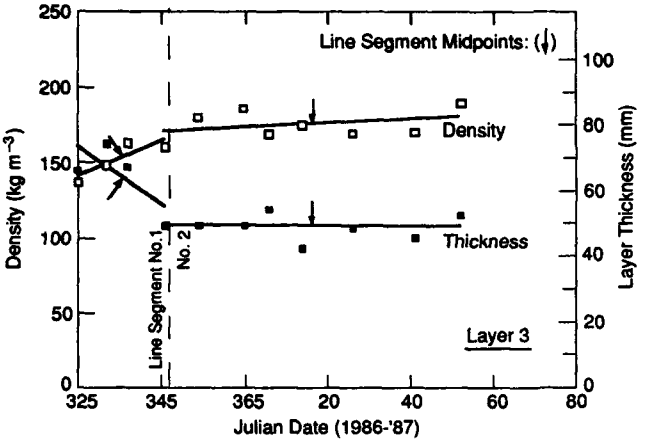

Figure 38. Line segments fit to a compaction and densification curve for a snow layer on the ground, 1986–1987. The midpoint of each line segment is marked (→). h and ρ were evaluated at this point.

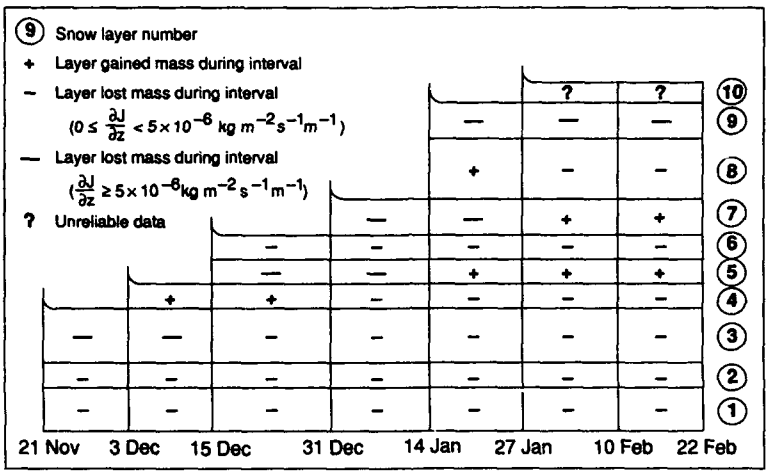

Figure 39. Layer-to-layer mass flux gradients for Fairbanks snow cover, 1986–1987 (see also Table 9). Minus signs indicate that a layer was losing mass ($\partial J/\partial z \ge 0$), plus signs that it was gaining mass ($\partial J/\partial z \le 0$).

The results of the calculations for individual snow layers suggest that the redistribution of mass in the snow took place in a complex and episodic manner (Fig. 39, Table 9). For example, the maximum 1986–1987 layer-to-layer mass flux gradient (26×10^{-6} kg m^{-2} s^{-1} m^{-1}), though it only existed for a short interval in a single layer of snow, was an order of magnitude greater than the 20-year average gradient. Several other layers also had flux gradients that were greater than average for at least part of the winter. These brief periods with strong gradients suggest some of the mass transport may have occurred during short, intense bursts of high flux. In several snow layers (i.e. layers 4, 5, 7, and 8) the flux gradient even changed sign during the winter.

Mass flux gradients calculated for individual snow layers (1986–1987) are broadly consistent with the net transfer of mass from the base to the top of the snow implied by the end-of-winter density profiles. In fact, the 1986–1987 end-of-winter profiles are nearly identical with the 20-year average profiles (Fig. 8). In addition, the average mass flux gradient for the lower half of the snow cover (layers 1 through 4) calculated from the values for individual layers (a weighted average, where the layer thickness and the time interval were used as weighting factors) was approximately 2×10^{-6} kg m^{-2} s^{-1} m^{-1}, which is reasonably consistent with the 20-year average.

Table 9. Calculated values of the layer-to-layer mass flux gradient and flux for snow on the ground, 1986–1987. ρ and h were evaluated on the Julian date indicated.

Layer	Interval	Δ (days)	h (mm)	ρ (kg m^{-3})	Julian date	$\overline{\partial J/\partial z}$ (kg m^{-2} s^{-1} m^{-1})	J (kg $m^{-2}s^{-1}$)
1	21 Nov–21 Feb	91	59	165	14	5.5×10^{-7}	2.9×10^{-7}
2	21 Nov–21 Feb	91	19	168	14	18.9×10^{-7}	3.3×10^{-7}
3	21 Nov–15 Dec	24	64	155	337	79.4×10^{-7}	8.4×10^{-7}*
3	15 Dec–21 Feb	67	49	177	17	35.7×10^{-7}	5.0×10^{-7}*
4	3 Dec–31 Dec	28	37	163	350	-70.7×10^{-7}	5.8×10^{-7}*
4	31 Dec–21 Feb	52	32	193	33	14.0×10^{-7}	5.5×10^{-7}
5	15 Dec–14 Jan	30	26	192	1	263.9×10^{-7}	12.6×10^{-7}*
5	14 Jan–21 Feb	38	22	199	33	-17.6×10^{-7}	5.1×10^{-7}
6	15 Dec–21 Feb	67	22	194	17	10.5×10^{-7}	5.3×10^{-7}
7	31 Dec–27 Jan	27	36	135	13	109.0×10^{-7}	9.3×10^{-7}*
7	27 Jan–21 Feb	24	27	180	39	-58.0×10^{-7}	3.8×10^{-7}*
8	14 Jan–27 Jan	13	80	157	20	207.2×10^{-7}	-7.2×10^{-7}*
8	27 Jan–21 Feb	24	68	181	39	28.6×10^{-7}	5.7×10^{-7}*
9	14 Jan–21 Feb	37	50	170	32	67.2×10^{-7}	9.1×10^{-7}*
10	27 Jan–10 Feb	14	12	117	34	?	?

See Appendix F for the methods of calculation.

See also Tables 5 and 6 and Figures 12 and 39.

* Significant value: not due to uncertainties in calculations.

? Top layer of snow difficult to work with; values unreliable.

Two details of the layer-to-layer mass transport for 1986–1987 are not consistent with the pattern suggested by 20 years of end-of-winter density profiles. First, the calculated flux gradients in the lowest two layers of the snow, which were expected to be the source of much of the water vapor transported to the top of the snow, were quite small (Fig. 39, Table 9). This may have been because these two layers were deposited in October and had been on the ground nearly 40 days at the time that they were first measured. They were already depth hoar and there might have been significant vapor flux out of the layers before they were measured. Second, zones of mass accumulation (+ signs in Fig. 39) were not always near the snow surface. This is puzzling. Nyberg (1938) has shown that minimum temperatures are usually found at the snow/air interface, a fact confirmed by measurements made during this study. Due to this temperature minimum, the interface is a preferential site for the condensation of water vapor from below and above. Condensation from above results in the formation of surface hoar (Lang et al. 1984, Colbeck 1988), but the data from 1986–1987 indicate that the snow/air interface was not always the locus for accumulation of mass from below.

The average flux gradient for 1986–1987 is about three times greater than the value obtained by Yosida et al. (1955) for snow under much weaker temperature gradients and about 30% of the value reported by Trabant and Benson (1972) for the Fairbanks snow cover (Table 1). Trabant and Benson

(1972) calculated the mass flux gradient without measuring changes in the thicknesses of snow layers. Instead they used the compaction rate of the snow on the tables to evaluate the rate at which snow layers on the ground compacted. It was assumed that a snow layer on the table was subject only to compaction, because there was no strong temperature gradient to induce a vapor flux. In that case, in eq 6 $(\partial J/\partial z)_{TABLE}$ was 0, and $(-D\rho/Dt)_{TABLE}$ equaled $(\rho/h \cdot Dh/Dt)_{TABLE}$. It was further assumed that the compaction rate, Dh/Dt, and the ratio, $\bar{\rho}/h$, were the same on the tables as on the ground, so that $(\bar{\rho}/h \cdot Dh/Dt)_{TABLE}$ equaled $(\bar{\rho}/h \cdot Dh/Dt)_{GROUND}$. The flux gradient on the ground could then be evaluated by subtracting the densification rate on the table from the densification rate on the ground:

$$\left(\frac{D\rho}{Dt}\right)_{GROUND} - \left(\frac{D\rho}{Dt}\right)_{TABLE} \approx -\frac{\partial \bar{J}}{\partial z}. \tag{8}$$

Unfortunately, the critical assumption behind this method is incorrect. Figure 11 shows that for two stratigraphically equivalent layers, the layer on the table compacted more quickly than the layer on the ground, particularly immediately after deposition. Later in the winter their compaction rates were nearly equal. The difference in compaction rates makes the use of eq 8 appropriate only long after the snow has been deposited. The compaction rates differed because the snow deposited on the tables did not metamorphose into depth hoar, which resists vertical compaction.

The measurements of Trabant and Benson (1972) can be reinterpreted making use of the fact that measured compaction rates on the tables and the ground are nearly equal several weeks after the snow had been deposited. The available data allow recalculation only for the bottom 0.13 m of the snow. Here, the recalculated value of the mass flux gradient averaged 5×10^{-6} kg m^{-2} s^{-1} m^{-1} for four winters, which is about twice the average value calculated in the present study for 1986–1987. It is likely that the recalculated value is high because even during the period of reduced compaction and densification rates, the snow on the tables still compacted slightly faster than the snow on the ground (Fig. 11).

It is possible to use the vapor flux measured at the snow/soil interface (0.26×10^{-6} kg m^{-2} s^{-1} m^{-1}; see Table 4) as the starting point to integrate the flux gradients layer-by-layer up through the snow cover in order to estimate the flux out of the top of each layer (Table 9 and Appendix F). The maximum flux computed in this manner was 1.26×10^{-6} kg m^{-2} s^{-1}, although for most of the layers most of the time the flux was rarely more than twice the flux at the snow/soil interface.

Estimates of grain growth rates

Data on the grain size and number of grains presented in Section 3 show that only a few selected snow grains (about 1 out of 10) grow during the development of depth hoar. The majority of grains shrink to supply mass to the growing grains. Layer-to-layer mass flux gradients can also supply mass to the growing grains. Grains must occupy favorable positions and be oriented favorably in order to grow. Even then, as conditions change within the snow cover, growing grains may undergo periods of shrinkage, or grow on one side and shrink on another (i.e., the erosion textures seen on the upper surfaces of crystals in metamorphic layer 4; see cover photo). Compaction of the snow can bring two grains into contact so that they grow together into a single grain. These physical processes make modeling grain growth difficult. To be consistent with observed growth behavior, a realistic grain growth model must be a function of 1) grain size, 2) grain size distribution, 3) grain position with respect to adjacent grains, 4) c-axis orientation, 5) temperature, and 6) over-burden stress. At present, no grain growth models are appropriate for use with the grain size distribution data collected in this study.

The data collected in this study were sufficient to make an order of magnitude estimate of the maximum growth rate of depth hoar. The masses of 20 of the largest depth hoar grains were estimated from photographs. On 8 April 1986 they averaged between 1×10^{-4} and 2×10^{-4} kg, with a maximum

value of 5×10^{-4} kg. These grains began to grow in December, at which time their mass was several orders of magnitude less than their final mass and can be considered essentially zero. Over 130 days, their average growth rate was 1×10^{-11} kg s^{-2} (0.9 mg day^{-1}), with a maximum rate of 5×10^{-11} kg s^{-1} (4.3 mg day^{-1}).

5. ANALYSIS AND DISCUSSION OF HEAT TRANSPORT IN THE SNOW COVER

In this section, the temperature data from Section 3 are used to show that air convected through the snow. The 1984–1985 data showed convection occurred (Johnson et al. 1987), though the analysis was limited to a single, 10-day record early in the winter. Here, the data are used to show that convection occurred during all three winters of the study. A description of the convective circulation is developed from the patterns observed in the horizontal temperature field and by analogy with laboratory experiments. The air flow velocity during periods of convection is estimated using one-dimensional heat and mass transport equations. Using this velocity estimate and measured values of the layer-to-layer mass flux gradient, the importance of convection in moving heat and mass is discussed.

Evidence for convection in the snow cover

There is evidence for time-dependent convection in the Fairbanks snow cover. A quasi-stable convective flow, indicated by coherent temperature records, set up in early winter and evolved slowly as the basal boundary conditions changed. During 80% of the winters of 1985–1986 and 1986–1987, convection was present. It was absent only during the few brief thaws when vertical temperature gradients in the snow approached zero (Fig. 32 and 33). The flow circulation pattern was controlled by the spatial variability of the temperature along the snow/soil interface. Diffuse, plume-like updrafts developed above regions of higher temperature. As winter progressed and the soil moisture froze, the temperature distribution at the snow/soil interface changed (Fig. 35), causing the slow evolution of the convective circulation pattern (Fig. 32).

During brief periods (a total of about 15% of the winter), a more vigorous convective circulation developed. In some cases, it coincided with clearly identifiable external forcing mechanisms such as high wind or rapid changes in air temperature that perturbed the convection (Fig. 30 and 31). During these periods, the flow circulation pattern remained relatively unchanged (Fig. 32), but the strength of the convection (i.e., the flow speed) increased. The perturbations in the convection resulted in incoherent temperature records (see Section 3 and Fig. 29c). These showed greater horizontal temperature gradients than the coherent temperature records characteristic of the quasi-stable convective flow (16°C m^{-1} vs 10°C m^{-1}). Crossing of thermistor traces and the simultaneous warming and cooling of different thermistors on a single horizontal string, distinctive features of the incoherent temperature records (Fig. 29c), were the result of thermal disequilibrium in the snow as it adjusted to the new flow conditions. (These features may also have been in part the result of natural spatial variations in forcing mechanisms, such as small-scale spatial variations in wind speed.) When external forcing ceased, quasi-stable convective flow resumed, and thermal equilibrium was re-established, resulting in a gradual change from incoherent to coherent temperature records. In contrast, the onset of incoherent records was abrupt (Fig. 30 and 31).

Incoherent temperature records as evidence of convection

The key feature of the incoherent records was that warming and cooling occurred simultaneously at different points on a horizontal thermistor string (Fig. 29c, 30). The only plausible explanation for this behavior was air movement through the snow. The thermistors that warmed were located in warm updrafts, while those that cooled were located in cold downdrafts.

The fact that half of the incoherent records coincided with periods of strong wind (Table 8) suggests that forced convection occurred in some cases. Dubrovin (1961) and Gjessing (1977) have observed what may be wind-pumping in snow, and Clarke et al. (1987) and Colbeck (1989) have concluded theoretically that wind-caused pressure fluctuations can pump air through the snow.

The cause of the incoherent records that occurred during calm conditions is not known. One speculation is that they were caused by other forcing mechanisms, such as rapid changes in air temperature (see Fig. 31; record B). Another possible mechanism is pressure fluctuations caused by synoptic-scale weather systems or gravity waves. Wilson and Nichparenko (1967) and Wilson and Fahl (1969) have measured gravity waves in Fairbanks that produced atmospheric pressure fluctuations of 10 to 30 μbar. Colbeck (1989), however, indicates that the frequency of pressure fluctuations necessary to perturb the temperature field would have to be considerably higher than the frequency of either synoptic or gravity pressure fluctuations.

Coherent temperature records as evidence of convection

The possibility that conditions other than convection could have produced coherent temperature records was examined. Several points in the following analysis also apply to incoherent temperature records.

In the absence of convection, coherent temperature records could have arisen from:

1) Improper thermistor calibration,
2) Horizontal variation of the thermal conductivity,
3) Variations in thermistor heights,
4) Variations in the thickness of the snow cover, and
5) Relatively warm and cold spots at the snow/soil interface.

Possibility 1 can be dismissed, because the thermistors were accurate to ±0.03°C, 500 times more sensitive than the observed temperature range (see Section 2 and Appendix C).

Possibility 2 is unlikely because there is no evidence to suggest horizontal variations in the thermal conductivity of the snow. Moreover, considering that the total measured range in thermal conductivity was quite small (Appendix D), any horizontal variations in the thermal conductivity, if they had existed, would have been insignificant.

Possibilities 3 and 4 were known to be potential problems at the start of the study, so considerable effort was taken to avoid them. The height of each thermistor was measured when it was installed and when it was excavated at the end of the winter. The observed variations in height were compared with the variations in height that would have been required to produce the temperature records by conduction. From the vertical thermistor strings, the temperature gradient at the height of the horizontal strings was determined. The range in temperature along the horizontal strings was measured, and the vertical misplacement that would have been required to produce the full range was computed. For example, if the vertical gradient was 100°C m^{-1} at the height of the thermistors, then a horizontal temperature range of 10°C would require a vertical misplacement of 0.1 m. Johnson et al. (1987) analyzed the 1984–1985 data in this manner; Table 10 lists the results for 1985–1986 and 1986–1987. For all three winters, the measured vertical misplacements were 1/3 to 1/10 the amount necessary to produce the observed temperature range. Not only were the misplacements too small, but also the relative thermistor misplacements would have had to change with time, which is physically unreasonable. Therefore, it is unlikely that coherent or incoherent temperature records were the result of thermistors at different heights.

Since the snow/soil interface was level, possibility 4 (local variations in the snow depth) could only have been the result of surface drifting, which rarely exceeded 0.01 m (Fig. 34a). The effects of surface drifts were examined using a steady-state, two-dimensional finite difference conduction model. Results from the model showed that drifts in excess of 0.06 m would have been required to produce the observed range of horizontal temperatures, and as more snow accumulated during the winter, the

height of the drifts would have had to increase, making drifting an unlikely cause of the observed temperature records.

The poor correlation between relative warm and cold zones in the snow with a) the thermistor heights and b) the snow depth reinforces that these two factors were not the cause of the coherent temperature records. If differences in the heights of the thermistors or the amount of snow above the thermistors had affected their temperatures, the correlation coefficients would have been high, but instead they never exceeded 0.36.

As for possibility 5, the significant spatial variations in the temperature of the snow/soil interface (Fig. 35) could not have produced the observed temperature signals by conduction alone. However, they may have had a profound effect on the stability of the air in the snow and the initiation of convection, as discussed in Onset of Convection, below. The maximum range in temperature at the interface was 4°C, while the maximum range in temperature on the horizontal strings 0.1 to 0.2 m above the interface was often greater than 5°C, occasionally as high as 16°C. Clearly, the temperature range at the thermistor strings could not have exceeded the temperature range at the interface if only conductive processes were taking place. Results from a steady-state, finite difference model showed that. For a 0.6-m-deep snow cover with a basal boundary containing a 1-m-wide spot elevated 3°C above the normal interface temperature, the maximum temperature contrast that would be observed 0.1 m above the interface would be 1.5°C. For smaller warm zones the temperature contrast would be even less. The observed horizontal variations in temperature were almost an order of magnitude greater than 1.5°C, and could not have been produced by conduction.

Table 10. Observed vs required vertical misplacement of thermistors.

Julian date	*$\partial T/\partial z$ at thermistor ($°C\ m^{-1}$)*	*Observed temperature range (°C)*	*Required vertical misplacement (m)*
		1986	
Avg. end-of-winter thermistor height:			0.119 m
Std. deviation:			± 0.010 m
Number of thermistors:			145
341	−41.9	5.0	0.060
349	−45.0	5.0	0.056
2	−37.2	3.0	0.040
13	−34.4	6.0	0.087
41	−13.8	2.5	0.091
		1987	
Avg. end-of-winter thermistor height:			0.110 m
Std. deviation:			± 0.007 m
Number of thermistors:			152
330	−187.0	8.0	0.021
345	1.0	0.1	0.063
358	−106.3	5.0	0.024
8	−19.8	1.0	0.025
36	−41.6	2.5	0.030

The argument could be made that combinations of possibilities 1 through 5 produced the observed temperature signals by conduction, but this is unlikely. It would have required the alignment of the crests of snow drifts above just the thermistors that had been displaced downward and directly above warm spots at the snow/soil interface. If snow drifts, warm spots, and displaced thermistors occurred randomly, the chances of this sort of alignment would be low. One is forced to conclude that the coherent temperature records were the result of air convecting through the snow.

The rapidity with which the snow responded to changes in air temperature is also strong evidence for convection during both coherent and incoherent records. The snow at the depth of the horizontal thermistor strings responded to changes in air temperature 10 times faster than it should have by heat conduction alone. In the absence of convection, the bulk thermal diffusivity ($\alpha = k/\rho c$) was approximately $1 \times 10^{-7}\ m^2\ s^{-1}$. Because there was little variation in either k or ρ with height (Fig. 9 and 27), the bulk thermal diffusivity for the entire snow cover was approximately the same as for each layer. The time necessary for a change in air temperature to propagate to a depth L in the snow is approximately $\tau = (L^2/\alpha)$ (Turcotte and Schubert 1982). Using measured values of the snow depth (h) and horizontal thermistor string height (z_t) to calculate L ($L = h - z_t$), the conductive response time of a number of rapid changes in air temperature have been calculated and compared to the actual response

Table 11. Response time of snow to changes in air temperature, 1984–1987. Predicted lag time was calculated assuming conduction as only mode of heat transport.

Julian date	*Type of temperature record*	*No. of obs.*	*Snow depth (m)*	*Therm. height (m)*	*Predicted lag* (s)*	*Observed lag (s)*	*Ratio***
1984–1985							
344 –351	Incoherent	6	0.24	0.18	36,000	7,200	5
351 –360	Coherent	2	0.84	0.18	4,400,000	132,500	33
42 – 52	Incoherent	1	0.73	0.18	3,000,000	59,500	51
74 – 84	Coherent(?)	1	0.75	0.17	3,400,000	125,000	27
1985–1986							
345 –350	Coherent(?)	7	0.26	0.18	64,000	5,400	12
350 –355	Coherent	7	0.26	0.18	64,000	5,400	12
355 –360	Coherent & incoherent	5	0.25	0.17	64,000	3,900	16
360 –365	Coherent	8	0.25	0.17	64,000	6,900	9
365 – 5	Coherent & incoherent	3	0.25	0.17	64,000	7,500	9
55 – 65	Coherent & incoherent	13	0.28	0.16	144,000	14,800	10
1986–1987							
345 –350	Coherent	7	0.23	0.14	81,000	3,200	25
350 –355	Coherent	7	0.28	0.14	196,000	6,000	32
355 –360	Coherent	11	0.22	0.13	85,000	8,900	10
360 –365	Coherent	9	0.24	0.12	132,200	6,600	20
365 – 5	Incoherent	2	0.24	0.12	139,000	4,900	28
25 – 30	Coherent & incoherent	2	0.42	0.12	900,000	32,300	28

* Calculated using a bulk thermal diffusivity, α, equal to 1×10^{-7} m^2 s^{-1}

** Predicted lag time divided by the observed lag time.

time (Table 11). In all cases, during coherent or incoherent records the response was one to two orders of magnitude faster than predicted. To respond this fast to changes in temperature, the air in the snow must have been in motion. The rapidity with which the snow responds to changes in air temperature has been noted by other authors (Bey 1951, Benson 1962, Fay 1973), which suggests that convection occurs elsewhere.

In laboratory experiments, the presence of convection is usually indicated by an increase in heat transfer. This is shown using the Nusselt number (Nu), which is the ratio of total heat transfer to conductive heat transfer; it can be expressed as:

$$\mathrm{Nu} = \frac{k_{\mathrm{eff}}}{k} \tag{9}$$

In the absence of convection, Nu equals 1; when there is convective heat transfer, it is greater than 1. In the present study, the Nusselt number was calculated by comparing the effective bulk thermal conductivity of snow measured by heat flow meters (Fig. 25) to the average effective thermal conductivity measured by needle probe. The effective bulk conductivity ranged from 0.1 to 0.2 $W\ m^{-1}\ K^{-1}$; the average thermal conductivity ranged from 0.04 to 0.10 $W\ m^{-1}\ K^{-1}$. Comparing these values suggests that the Nusselt number was about 2, which is consistent with the conclusion reached above that convection was prevalent in the Fairbanks snow cover.

The nature of convective circulation

One of the striking characteristics of the temperature field in the snow is that relative warm and cold zones developed and remained nearly stationary throughout the winter (Fig. 32 and 33). During the

winter these zones evolved slowly, with their relative temperatures changing through time. Their evolution was independent of the snowfall history and snow settlement (Fig. 12), suggesting that the zones were caused by a mechanism that was not in the snow. In addition, where it was possible to compare the location of the zones with the temperature at the snow/soil interface, it was found that warm zones coincided with the higher temperatures. These facts suggest that the warm and cold zones in the snow were caused by variations in temperature at the snow/soil interface due to unevenly distributed surface moisture. Since the variation in temperature at the interface could not account for the warm and cold zones by conduction, we suggest that it generated a plume-like convective circulation system. Diffuse plumes of warm, rising air were centered over the warmer areas of the interface, while cold downdrafts formed elsewhere. As shown below, this hypothesis is consistent with the temperature observations and with the results of laboratory studies of convective plumes.

Convective circulation

The temperature fields shown in Figure 32 do not indicate the periodic spatial repetition that would result from cellular or roll convection (Rayleigh 1916, Combarnous and Bories 1975, Powers et al. 1985). In 1984–1985, the spatial resolution of the thermistor grid was insufficient to rule out cellular circulation, but the temperature patterns developed during the next two winters show no repetition, even on the scale of expected cell size (cells of about 0.5 m). It is likely that conditions in the snow in 1984–1985 were similar.

Instead, the temperature patterns suggest that there were at most three convective plumes, and usually only one or part of one convective plume intersected by the thermistor grid. The plumes were diffuse, with diameters of about a meter or less (Fig. 32). Downdrafts had slightly smaller diameters of about 0.3 m. Plume updrafts were between 2°C and 16°C warmer than nearby downdrafts, and both up- and downdrafts were relatively fixed in space throughout the winter (see correlation analysis, Fig. 33). When plumes were present, they generated either coherent or incoherent records. Presumably, plumes were better developed during incoherent records, because the temperature contrasts between up- and downdrafts were greater. In 1986–1987, when snow/soil interface temperatures were measured at the south end of the horizontal thermistor array (Fig. 35), plume updrafts were linked to the higher temperatures. Similar coupling between plumes and warm spots at the snow/soil interface is assumed to have existed elsewhere.

Laboratory experiments support the hypothesis that convective plumes developed above warm spots at the base of the snow. Experimental and theoretical studies in porous media by Elder (1967) and El-Khatib and Prasad (1986) indicate that a circulation pattern similar to the one shown in Figure 40 would develop above a warm spot. Plumes or updrafts would be narrow and of higher velocity than downdrafts, so in horizontal cross-section, downward flow would occupy a larger area than upward flow. Recharge and discharge would occur through the permeable upper surface of the medium, possibly resulting in a net gain or loss of mass and a recirculation of about 30% of the fluid. Flow lines would be predominantly vertical, except along the base where they would be horizontal.

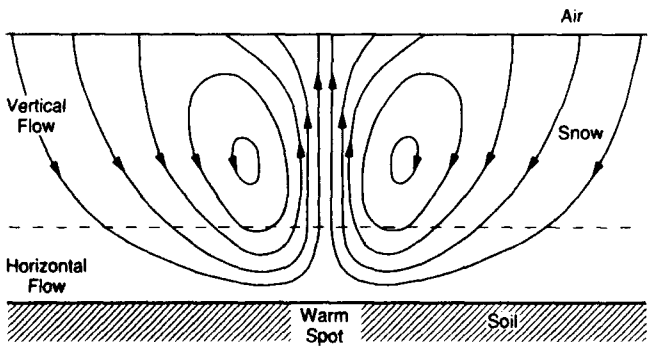

Figure 40. Hypothetical air flow circulation over a warm spot, based on Elder (1967). Flow lines are predominately vertical except at the base of the snow. 30% of the air recirculates; there is discharge from the plume above the warm spot.

Laboratory and theoretical studies also support the hypothesis that the convective circulation system that developed in the snow cover was time-dependent. For example, Schubert and Straus (1982) have shown that varying the boundary conditions of a porous medium, such as occurs during rapid fluctuations in air temperature, can produce transient convection states with distinct oscillatory regimes. These regimes can change from polyhedral cellular convection to a state in which circulation cells appear and disappear rapidly (Combarnous and Bories 1975). Even with constant conditions, long periods are required to achieve steady state, during which transitory circulation patterns come and go (Elder 1967). Even small perturbations in the snow may have had large effects on the circulation system. Meyer et al. (1987) showed that the circulation patterns that formed in a Benard cell were different each time the experiment was run, pointing to the importance of stochastic effects on the flow pattern.

Onset of convection

Convection occurs when the buoyant forces exceed the viscous resistance of a fluid. The ratio of buoyant to viscous forces is usually presented as a dimensionless ratio, the Rayleigh number (Ra), which, for uniform boundary conditions, can be written:

$$\mathrm{Ra} = \frac{g\,\beta\,(\rho c)_f\,\Delta T\,h\,\kappa_i}{\nu\,k_m} \tag{10}$$

where g equals the acceleration of gravity, $\beta = (1/V)(\partial V/\partial T)_p$ is the isobaric coefficient of thermal expansion, $(\rho c)_f$ is the volumetric heat capacity of the fluid (moist air), ΔT is the temperature difference across the snow layer, h is the layer thickness, κ_i is the coefficient of air permeability, ν is the kinematic viscosity, and k_m is the thermal conductivity of the porous medium (Lapwood 1948, Katto and Masuoka 1967, Akitaya 1974, Combarnous and Bories 1975, Turcotte and Schubert 1982).

The formulation includes several approximations, among which the most critical are:

1) The system is in steady-state,
2) The boundaries are horizontal and isothermal, and
3) There is no latent heat transfer (a source term).

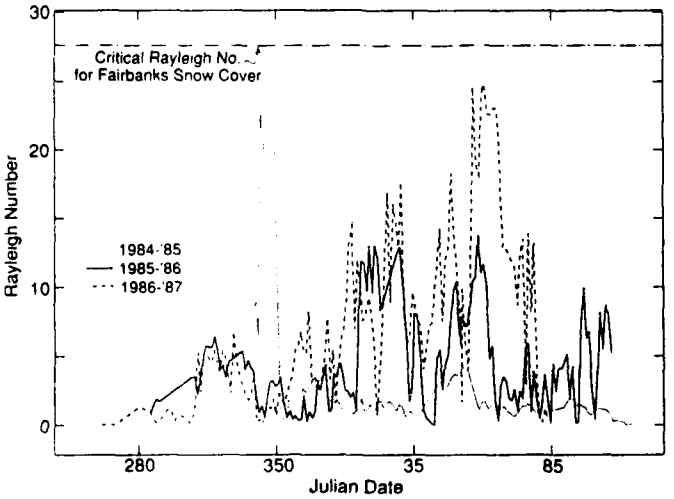

Figure 41. Rayleigh number, 1984–1987, calculated using measured values for the Fairbanks snow cover. The theoretical critical Rayleigh number for the onset of convection thought to be applicable for the Fairbanks snow is 27.

For porous media consistent with these approximations, the critical Rayleigh number (Ra_{cr}) (i.e., the Rayleigh number at which convection begins) can be determined. Lapwood (1948) and Nield (1968) found that Ra_{cr} equaled about 27 for a horizontal porous layer heated from below with isothermal, impermeable upper and lower boundaries. Ribando (1977) found Ra_{cr} equaled 40 for a constant temperature, permeable top, and a constant heat flux, impermeable base. Based on a critical Rayleigh number between 27 and 40, it has been concluded that convection is unlikely in most natural snow covers (Palm and Tveitereid 1979, Powers et al. 1985a, b; see Section 1).

However, the Rayleigh number given by eq 10 is not valid for a natural snow cover because the three critical assumptions fail. Rayleigh numbers calculated using eq 10 never exceeded 27 during this study, despite the fact that air was convecting in the snow almost continuously (Fig. 41). Convection was observed for Rayleigh numbers as low as 4 (for example on 1 March 1985).

The presence of spatial variations in temperature at the snow/soil interface were undoubtedly the chief cause for the lowering of the critical Rayleigh number. Kelly and Pal (1978) and Rees and Riley (1986, 1989) have shown that spatial variations in boundary temperatures of a convecting system can dramatically lower the critical Rayleigh number. In some cases, they found that the system was unconditionally unstable.

Convective flow velocity

The convective flow velocity is estimated in this section. It is a necessary step in determining the importance of convection in heat and mass transfer in snow. An order-of-magnitude estimate is made using measured values of the mass flux gradient. A second estimate is made by combining heat and mass transport equations and solving for the velocity.

Mathematical framework

For a small volume of snow, assuming the air and ice are in local thermal equilibrium, the heat transport is given by:

$$\nabla \cdot \left(k_{dry} \nabla T\right) + L_s \left.\frac{\partial \rho}{\partial t}\right]_v - \phi \, (\rho c)_f \, \vec{v} \cdot \left(\nabla T\right) = (\rho c)_m \frac{\partial T}{\partial t} \tag{11}$$

where T is temperature, L_s is latent heat of sublimation, $\partial\rho/\partial t]_v$ is the densification rate of the snow due to the vapor flux, ϕ is the porosity, $\vec{v}$ is the air flow velocity through the pores of the snow, $(\rho c)_f$ is the volumetric heat capacity of air, and $(\rho c)_m$ is the volumetric heat capacity of the bulk snow ($[\rho c]_s$ is the volumetric heat capacity of ice) (Table 12). The appropriate thermal conductivity, k_{dry}, is that of snow measured in a way that precludes convection, and at temperatures low enough that there is no latent heat transfer. For depth hoar, it is approximately 0.025 W m^{-1} K^{-1}.

The mass transport for a snow layer that is not compacting is given by

$$\left.\frac{\partial \rho}{\partial t}\right]_v = \nabla \cdot \left(\phi F D_0 \nabla \rho_v\right) - \frac{\partial\left(\rho_v \phi\right)}{\partial t} - \nabla \cdot \left(\phi \rho_v \vec{v}\right) \tag{12}$$

where ρ is the bulk density of the snow, ρ_v is the water vapor density, F is an enhancement factor discussed at eq 21, and D_0 is the diffusion coefficient of water vapor in air (Table 12).

Due to limitations in the data, eq 11 and 12 must be simplified to one dimension to determine the velocity. This can be justified because in many areas in the snow, flow lines and temperature gradients are primarily vertical (Fig. 40). In one dimension, the equations become:

$$k_{dry} \frac{\partial^2 T}{\partial z^2} + L_s \left.\frac{\partial \rho}{\partial t}\right]_v - \phi (\rho c)_f v_z \frac{\partial T}{\partial z} = \left[\phi \, (\rho c)_f + \left(1 - \phi\right)(\rho c)_s\right] \frac{\partial T}{\partial t} \tag{13}$$

Table 12. Physical parameters of the Fairbanks snow cover.

Thermal conductivity (k)

New snow	k	= 5	× 10^{-2}	W m^{-1} K^{-1}	($\rho \approx 50$ kg m^{-3})
Depth hoar	k	= 4	× 10^{-2}	W m^{-1} K^{-1}	($\rho \approx 200$ kg m^{-3})
"Dry" snow	k_{dry}	= 2.5	× 10^{-2}	W m^{-1} K^{-1}	
Air	k_{air}	= 2.3	× 10^{-2}	W m^{-1} K^{-1}	at –10°C
Ice	k_{ice}	= 2.3		W m^{-1} K^{-1}	at –10°C

Thermal diffusivity (α)

Air	α_{air}	= 1.556	× 10^{-5}	m^2 s^{-1}	$\frac{\alpha_{air}}{\alpha_{snow}} = 156$
Ice	α_{ice}	= 1.280	× 10^{-6}	m^2 s^{-1}	
Snow	α_{snow}	= 1	× 10^{-7}	m^2 s^{-1}	for ρ = 200 kg m^{-3} at –10°C

Latent heat of sublimation (L_s)

$L_s = 2.834 \times 10^6$ J kg^{-1}

Diffusion coefficient of water vapor in air (D_o)

$D_o = 2.1 \times 10^{-5}$ m^2 s^{-1}

Specific heat (c)

Air	$c = 1.01 \times 10^3$ J kg^{-1} °C^{-1}	for	0 to –0°C
Ice	$c = 2.09 \times 10^3$ J kg^{-1} °C^{-1}	at	0°C
	$c = 1.97 \times 10^3$ J kg^{-1} °C^{-1}	at	–20°C
	$c = 1.80 \times 10^3$ J kg^{-1} °C^{-1}	at	–40°C

Density (ρ)

Air	ρ_{air}	=	1.5	kg m^{-3} at –10°C
Ice	ρ_{ice}	=	916.0	kg m^{-3}
Depth hoar	ρ	≈	200	kg m^{-3}

Porosity (ϕ)

$$\phi = \left(1 - \frac{\rho}{\rho_{ice}}\right)$$

Volumetric heat capacity (ρc)

Air	$(\rho c)_f$	=	1.507×10^3 J m^{-3} °C^{-1}	$\frac{(\rho c)_f}{(\rho c)_s} \approx 0.001$ $\quad \frac{(\rho c)_m}{(\rho c)_f} \approx 280$
Ice	$(\rho c)_s$	=	1.805×10^6 J m^{-3} °C^{-1}	
Snow	$(\rho c)_m$	=	$(\rho c)_s(1-\phi) + (\rho c)_f \phi$:	where ϕ = porosity, f = fluid, s = solid

Saturation water vapor density (empirical fit to data [List 1951])

$\rho_v(T) = A\, e^{BT}$ where T is in °C; ρ_v in kg m^{-3}.
$A = 0.00579$ $\quad B = 0.09658$

Dimensionless ratio of sensible to latent heat capacity $\left[\gamma = \frac{(\rho c)_f}{L_s\left(\frac{\partial \rho_v}{\partial T}\right)}\right]$

Temperature	γ
–1°C	1.5
–20°C	6.5
–40°C	48.2

$$\left.\frac{\partial \rho}{\partial t}\right]_v = \phi D_o \frac{\partial\left(F \frac{\partial \rho_v}{\partial z}\right)}{\partial z} - \phi \frac{\partial \rho_v}{\partial t} - \phi \frac{\partial (\rho_v v_z)}{\partial z} \tag{14}$$

where $(\rho c)_m$ of eq 11 is replaced by $[\phi(\rho c)_f + (1-\phi)(\rho c)_s]$ in eq 13, and the following assumptions and approximations have been made:

1) k_{dry} is assumed to be constant in the volume for which the equations are written,
2) There are no horizontal temperature gradients,
3) Horizontal components of the velocity field are zero,
4) Horizontal components of the diffusive flux are zero, and
5) Porosity (ϕ) is constant within the volume and over the time intervals for which the equations are written.

Convective velocity using the measured mass flux gradient

It is possible to make an order of magnitude estimate of the velocity using the measured layer-to-layer mass flux gradients. This can done by integrating both sides of eq 13 over a time interval, t_0 to t_1, and dividing by the elapsed time, Δt, to get time-averages of each term. The densification rate of the snow, $\partial\rho/\partial t]_v$ in eq 13, equals the negative mass flux gradient ($-\partial J/\partial z$) (Appendix F). The time average of this term ($-\overline{\partial J / \partial z}$) was measured and is listed in Table 9. The other integrations must be over the same time interval. The integral of the right-hand side of eq 13:

$$\frac{1}{\Delta t}\int_{t_0}^{t_1}\left\{\left[\phi\,(\rho c)_f + \left(1-\phi\right)(\rho c)_s\right]\frac{\partial T}{\partial t}\right\} dt \tag{15}$$

is approximately 0, since the temperature tends to fluctuate about a mean value. Assuming ϕ, k_{dry}, and $(\rho c)_f$ are constants, the integral of the first term on the left side of eq 13 is

$$\overline{\frac{\partial^2 T}{\partial z^2}} = \frac{1}{\Delta t}\int_{t_0}^{t_1}\left(\frac{\partial^2 T}{\partial z^2}\right) dt \tag{16}$$

which can be evaluated. Unfortunately, the integral of the third term:

$$\overline{\left(v_z \frac{\partial T}{\partial z}\right)} = \frac{1}{\Delta t}\int_{t_0}^{t_1}\left(v_z \frac{\partial T}{\partial z}\right) dt \tag{17}$$

cannot be evaluated directly because both v_z and $\partial T/\partial z$ are functions of t. If they were independent functions, eq 17 would equal

$$\frac{1}{\Delta t}\int v_z\, dt \int \frac{\partial T}{\partial z}\, dt\,,$$

and eq 13 could be solved for $\overline{v_z}$:

$$\overline{v_z} = \frac{1}{\phi\,(\rho c)_f \overline{\frac{\partial T}{\partial z}}}\left(k_{dry}\overline{\frac{\partial^2 T}{\partial z^2}} - L_s \overline{\frac{\partial J}{\partial z}}\right) \tag{18}$$

where

$$\overline{v_z} = \frac{1}{\Delta t} \int v_z \, dt$$

and

$$\overline{\frac{\partial T}{\partial z}} = \frac{1}{\Delta t} \int \frac{\partial T}{\partial z} \, dt .$$

But because they are not independent, an error is introduced that is approximately equal to the product of the standard deviations of v_z and $\partial T/\partial z$ multiplied by the correlation coefficient between the two functions (Davis 1973). Assuming the worst case, with the correlation coefficient equal to 1, the approximation results in no more than a 30% error in v_z.

The estimated velocity was 0.2 mm s^{-1} for the average measured values of the mass flux gradient, temperature gradient, and curvature. The maximum velocity was 1.3 mm s^{-1} (Table 13). Since this value is a time average, short periods of higher velocity flow are not precluded.

Convective velocity assuming the air in the snow is saturated

The air flow velocity can also be estimated using a method that does not require measured values of the layer-to-layer mass flux gradient. However, it does depend on the common assumption (see Bader et al. 1939, Giddings and LaChapelle 1962, de Quervain 1972, Colbeck 1982a) that the air in the snow is saturated with respect to ice. This is a reasonable assumption; if it were not, crystal growth and decay rates in the snow would be high. Instead, they are very low. For example, the maximum measured growth rate in the Fairbanks snow was 5×10^{-11} kg s^{-1}, compared to rates two orders of magnitude higher (as high as 3×10^{-9} kg s^{-1}) observed for crystals growing in a diffusion chamber where supersaturation was maintained (Lamb and Hobbs 1971).

The assumption might not be valid if air were flowing through the snow at a sufficiently high speed. However, a simple model presented below shows that the air would have to flow several times faster than the estimate given above. Consider a block of ice in which there is a vertical, cylindrical hole of radius R through which air is flowing at a velocity, v_z, and further, that there is a linear vertical temperature gradient ($\partial T/\partial z$) across the block. At any height, z, the difference between the temperature of the air in the hole (as a function of radius) and the ice is given by (Appendix E):

$$\Delta T(r) = \left(1 - \frac{r^2}{R^2}\right)\left(\frac{v_z R^2 \frac{\partial T}{\partial z}}{4\alpha_{air}}\right) \tag{19}$$

where r is the radial coordinate, and α_{air} is the thermal diffusivity of air. Applying this model to the Fairbanks snow cover, pore spaces have radii of several millimeters, vertical temperature gradients average –50°C m^{-1}, and the estimated flow velocity is less than or equal to 1.3 mm s^{-1}. The maximum difference in temperature between the center and the walls of the pore would be 0.02°C, and it is unlikely, given this minute temperature difference, that there would be significant under- or oversaturation. Therefore, we conclude that it is satisfactory to assume that the air in the pores is saturated, even when the air is convecting.

For mathematical simplicity, the data for the saturation water vapor density (List 1951) were fit with an exponential function (Fig. 4):

$$\rho_v(T) = A \, e^{BT} \tag{20}$$

Table 13. Average flow velocity calculated from layer-to-layer flux gradients measured in 1986–1987. Curvature varied as a function of z, but its average value was –100 to –500 °C m^{-2}.

Interval	Height interval (m)	$\overline{\partial T/\partial z}$ (°C m^{-1})	$\overline{\partial^2 T/\partial z^2}$ (°C m^{-2})	$\overline{\partial J/\partial z}$ (kg m^{-2}s^{-1}m^{-1})	$\overline{v_z}$ (mm s^{-1})
21 Nov–21 Feb	0–0.06	–35	–1000	6×10^{-7}	0.51
21 Nov–21 Feb	0–0.06	–35	–500	6×10^{-7}	0.27
21 Nov–21 Feb	0–0.06	–35	–100	6×10^{-7}	0.08
21 Nov–21 Feb	0.06–0.12	–50	–1000	19×10^{-7}	0.40
21 Nov–21 Feb	0.06–0.12	–50	–500	19×10^{-7}	0.24
21 Nov–21 Feb	0.06–0.12	–50	–100	19×10^{-7}	0.11
Value calculated with max. positive value of $\overline{\partial J/\partial z}$		–50	–1000	263×10^{-7}	1.32
		–50	–500	263×10^{-7}	1.16
		–50	–100	263×10^{-7}	1.02
Value calculated with avg. value of $\overline{\partial J/\partial z}$		–50	–200	30×10^{-7}	0.2

Values used in calculations:

1) $(\rho c)_f$ = 1507 J m^{-3} °C^{-1}
2) k_{dry} = 0.025 W m^{-1} K^{-1}
3) L_s = 2.834×10^6 J kg^{-1}
4) $\partial T/\partial t$ assumed to be 0
5) ϕ = 0.8

where $A = 0.00579$ and $B = 0.09658$ for T in °C and ρ_v is in kg m^{-3}. Using eq 20 and the chain rule $(\partial \rho_v/\partial z) = (\partial \rho_v/\partial T \cdot \partial T/\partial z)$, eq 14 becomes:

$$\left.\frac{\partial \rho}{\partial t}\right]_v = \phi D_o \left\{ F \left[\frac{\partial \rho_v}{\partial T} \frac{\partial^2 T}{\partial z^2} + \left(\frac{\partial T}{\partial z}\right)^2 \frac{\partial^2 \rho_v}{\partial T^2} \right] + \frac{\partial \rho_v}{\partial T} \frac{\partial T}{\partial z} \frac{\partial F}{\partial z} \right\}$$

$$- \phi \frac{\partial \rho_v}{\partial T} \frac{\partial T}{\partial t} - \phi \left(\rho_v \frac{\partial v_z}{\partial z} + v_z \frac{\partial \rho_v}{\partial T} \frac{\partial T}{\partial z} \right), \qquad (21)$$

where $\partial \rho_v/\partial T$ equals $AB\, e^{BT}$ and $\partial^2 \rho_v/\partial T^2$ equals $AB^2\, e^{BT}$.

F, $\partial F/\partial z$, and $\partial v_z/\partial z$, which appear in eq 21, are not known. The enhancement factor, F, accounts for the tortuosity of the pore spaces in the snow and the enhanced temperature gradients that result from snow-grain geometry. The tortuosity and enhanced gradients have never been measured, yet enhancement factors have been introduced in several heat and mass transport models for snow in order to bring calculated results into agreement with measurements. Most authors set F equal to approximately 5; however, F should not be a constant since it is a function of the snow-grain geometry. It should change with snow density, texture, and perhaps also temperature. However, over small distances, such as the thickness of a snow layer, we will assume it is constant and that $\partial F/\partial z$ is 0. A similar argument can be made for $\partial v_z/\partial z$. With these simplifications, eq 21 can be combined with eq 13 to give

$$k_{dry}\frac{\partial^2 T}{\partial z^2} + L_s D_o \phi F\left[AB\, e^{BT}\frac{\partial^2 T}{\partial z^2} + \left(\frac{\partial T}{\partial z}\right)^2 AB^2 e^{BT}\right] - \phi v_z \frac{\partial T}{\partial z}\left[L_s AB\, e^{BT} + (\rho c)_f\right]$$

$$= \frac{\partial T}{\partial t}\left\{\left[(1 - \phi)(\rho c)_f\right] + L_s \phi AB\, e^{BT}\right\}, \quad (22)$$

which can be solved for v_z.

To evaluate eq 22, sequential pairs of vertical temperature profiles were fit with quadratic equations using least squares regression. The fitting procedure was used to smooth the profiles. T, $\partial T/\partial z$ and $\partial^2 T/\partial z^2$ were determined from the pairs at heights of 0.05, 0.10, 0.15, 0.20, and 0.25 m in the snow. From the change between sequential pairs, $\partial T/\partial t$ was determined at each height. The air-flow velocity was then determined as a function of F.

The average velocity calculated from eq 22 was 0.4 mm s^{-1}, and the maximum was 2 mm s^{-1}. Velocities calculated for periods that exhibited coherent and incoherent records did not differ significantly. The results also indicated that there was no simple relationship between the velocity and the choice of the enhancement factor. Increasing F increased the velocity at the base of the snow cover, but decreased it at the top. For example, increasing F from 0.1 to 20 increased the velocity 1000% in the bottom 0.05 m of the snow, but decreased it 10% in the top 0.05 m. The model was highly sensitive to small uncertainties in $\partial T/\partial z$ and $\partial^2 T/\partial z^2$, suggesting that velocities less than 0.3 mm s^{-1} may not have been significant. However, the results of both methods of estimation are consistent: they indicate that the convective flow velocity in the Fairbanks snow cover averaged 0.2 mm s^{-1}, with peak velocities approximately 2 mm s^{-1}.

Importance of convection in moving heat and mass

Heat transport

Rough estimates of the heat transport in the Fairbanks snow cover are as follows: During a normal winter, about one third of the heat transported from the base to the top of the snow cover is moved by convection of sensible heat, one third is transported by conduction through the ice grains and air spaces, and the remaining third is transported as latent heat with the mass flux. However, during periods when the convective velocity is high (about 2 mm s^{-1}), convection can dominate the heat transport. As a result, during periods of convection, the time-response of the snow to changes in air temperature can be more than an order of magnitude faster than would occur by conduction alone (Table 11).

The relative contribution of the latent heat transport was estimated in the following manner: heat flow measured by heat flow meters at the base of the snow averaged 10 W m^{-2} between 1984 and 1987 (Fig. 23). It is assumed that this is approximately equal to the total heat flow through the snow. The mass flux gradient from the basal half to the top half of the snow averaged 3×10^{-6} kg m^{-2} s^{-1} m^{-1}, and the average snow depth was 0.6 m (Fig. 24). If it is assumed that mass flux out the top of the snow was negligible with most of the flux being deposited in the upper part of the snow, then the average mass flux from the base to the top was 9×10^{-7} kg m^{-2} s^{-1}, though the actual flux gradient is a strong function of depth. When multiplied by the latent heat of sublimation, the mass flux resulted in a latent heat flow at mid-height in the snow cover of approximately 2.5 W m^{-2}, which is 26% of the total heat flow. The theoretical estimates of Yosida et al. (1955), Woodside (1958), and de Quervain (1972) for the contribution of vapor diffusion to the total thermal conductivity ranged from 40% to 48%.

The estimate of the importance of the latent heat transport can be corroborated by comparing the magnitudes of the three heat transport terms in eq 13. The ratio of the latent heat term to the sum of the magnitudes of the conductive, convective, and latent heat terms can be written:

$$\frac{\overline{\frac{\partial J}{\partial z}} L_s}{\phi\,(\rho c)_f \bar{v}_z \overline{\frac{\partial T}{\partial z}} + k_{dry} \overline{\frac{\partial^2 T}{\partial z^2}} + \overline{\frac{\partial J}{\partial z}} L_s} \tag{23}$$

This ratio was evaluated from the data in Table 13. The ratio ranged from 0.04 to 0.5, but for reasonable values of the curvature of the temperature profile ($\leq -200°C\ m^{-2}$), the range was 0.3 to 0.5, which is consistent with the previous estimate that one third of the total heat was transported as latent heat.

The relative importance of conduction to convection of dry air (sensible heat) can be estimated using the Peclet number (Pe_h). It is defined as the ratio of the convective to the conductive heat transport under conditions where there is no latent heat transport, and can be written:

$$Pe_h = \left(\frac{h\, v_z\, \phi\, (\rho c)_f}{\alpha_{dry}\, (\rho c)_m}\right). \tag{24}$$

Peclet numbers less than 1 indicate that conduction dominates the heat transport, while numbers greater than 1 indicate convection dominates.

Peclet numbers, calculated using the velocity estimates of 0.2 to 2 mm s^{-1}, indicate that convection and conduction were usually of equal importance in transporting heat, except during the few periods when the convective velocity was high (~2 mm s^{-1}) (Table 14). For example, at the average velocity of 0.2 mm s^{-1}, Pe_h ranged from 0.8 to 1.6, depending on snow depth, but for the maximum velocity of 2 mm s^{-1}, it ranged from 8 to 17.

Table 14. Peclet numbers for heat transport (Pe_h).

v_z (mm s^{-1})	h (m)	Pe_h
0.01	0.15	0.05
0.1	0.15	0.4
0.2	0.15	0.8*
1.0	0.15	4.2
2.0	0.15	8.4
0.01	0.30	0.1
0.1	0.30	0.8
0.2	0.30	1.6*
1.0	0.30	8.5
2.0	0.30	17.0

v_z = Velocity
h = Snow depth
* = Peclet number for average calculated flow velocity.

Mass transport

The contribution of convection to the water vapor transport can be estimated by examining the ratio of the convective to the diffusive transport terms in eq 21. This ratio is

$$\frac{v_z \frac{\partial T}{\partial z}}{D_0 F \left[\frac{\partial^2 T}{\partial z^2} + B\left(\frac{\partial T}{\partial z}\right)^2\right]}. \tag{25}$$

For the average velocity (0.2 mm s^{-1}) and the commonly used value of the enhancement factor (F = 5; see Section 1), the ratio is 0.2 (Table 15). Even through a wide range of values of the enhancement factor ($1 \leq F \leq 10$), the ratio remains less than 1. This suggests that diffusion is the primary agent of water vapor transport in the Fairbanks snow cover most of the time. However, for the maximum estimated convective velocity (2.0 mm s^{-1}), the ratio is one to two orders of magnitude greater, ranging from 2 to 20, depending on the value of F. When F equals 5, the ratio equals 4. This indicates that considerable water vapor can be transported by convection during periods of peak air flow.

The results in Section 4 suggest that a significant percent of the layer-to-layer mass transport occurred in brief, intense intervals of enhanced flux. One might speculate that these occurred during periods of extremely low air temperatures, when temperature gradients across the snow were maximum. Under these conditions, the diffusive vapor transport is certainly enhanced, since it is a

function of the temperature gradient and the curvature of the vertical temperature profile. But these low-temperature periods were also times when strong incoherent records not associated with wind occurred. Following the interpretation that the convective flow velocity was high during these periods, the ratio in eq 25 may have been significantly greater than 1, and convection could have increased the already enhanced diffusive vapor flux by a factor of 10 or more. The contribution of these brief periods of intense convective water vapor transport to the total ice mass that is moved during the winter would depend on how frequently they occurred. If they occurred each time an incoherent record was observed (about 15% of the winter), they would make a significant contribution.

Table 15. Ratio of convective to diffusive mass transport for estimated range of velocities for the Fairbanks snow cover.

v_z (mm s^{-1})	F	$\frac{\partial T}{\partial z}$ (°C m^{-1})	$\frac{\partial^2 T}{\partial z^2}$ (°C m^{-2})	*Mass transport ratio* $\frac{Convection}{Diffusion}$
0.2	1	–50	–500	1.8
0.2	2	–50	–500	1.0
0.2	5	–50	–500	0.4
0.2	10	–50	–500	0.2
2.0	1	–50	–500	20.0
2.0	2	–50	–500	10.0
2.0	5	–50	–500	4.0
2.0	10	–50	–500	1.8

Average calculated velocity ≈ 0.2 mm s^{-1}
Maximum calculated velocity ≈ 2.0 mm s^{-1}

The virtual absence of temperature profiles with positive curvature, out of the thousands that were measured, suggests that diffusion is the primary agent of water vapor transport and implies that periods when convention moves significant amounts of water vapor are infrequent. The negative curvature of the vertical temperature profiles was discussed in Section 3. It could be either 1) the result of upward diffusion of vapor and the liberation of latent heat, and/or 2) the result of upward advection of warm air. Advection of warm air, however, can cause either negative or positive curvature, depending on whether the flow direction is up or down. Based on the hypothetical circulation pattern (Fig. 40), the probability of making a temperature profile measurement in an updraft or downdraft should have been approximately equal. In contrast, the upward diffusion of water vapor will always yield negative curvature in the temperature profile. This suggests that the negative curvature was generally the result of the upward diffusion of vapor.

Though convection may be generally unimportant in moving water vapor, it may play a role in the development of the snow textures described in Section 3. There is a striking coincidence between the location of metamorphic layer 5, in which the predominant c-axis orientations are horizontal, and the zone at the base of the snow where convective flow lines are thought to be horizontal (Fig. 17 and 40). Elsewhere in the snow, flow lines are predominantly vertical, as are c-axes. Perhaps the air flow direction in the snow influences the growth direction of the crystals.

6. RESULTS, CONCLUSIONS, AND RECOMMENDATIONS

The results of the present study demonstrate that convection occurs in a natural snow cover, but they also raise many questions. In particular, what is the prevalence of convection in other types of snow covers, what is its relationship to snow metamorphism, and what conditions are necessary for the onset of convection? Results and conclusions are summarized below, and are followed by recommendations for studies that address these questions.

Summary of results and conclusions

The Fairbanks snow metamorphoses progressively until, by the end of the winter, it consists almost entirely of depth hoar. A five-layer sequence develops with a basal layer composed of extremely large crystals (≥ 10 mm) with horizontal c-axes; it is overlain by layers composed of crystals with vertical c-axes. The metamorphism results in a rapid increase in air permeability to values two to three times

higher than previously measured and a decrease in the thermal conductivity to the lowest previously measured value. The number of grains per unit volume decreases an order of magnitude as a few select grains grow and the rest of the grains shrink by sublimation.

The metamorphism is the result of strong temperature gradients caused by relatively high snow/soil interface temperatures and low air temperatures. These temperature gradients drive vapor diffusion and convection, which cause a net transfer of mass from the base to the top of the snow. Over the past 20 years, the layer-to-layer mass flux gradient averaged 3×10^{-6} kg m^{-2} s^{-1} m^{-1}, but during each winter there were occasional periods when the flux was 10 times greater. These periods of enhanced flux may have coincided with periods of vigorous convection.

Thermal convection is common in the Fairbanks snow cover. It occurred sporadically in 1984–1985, but nearly continuously in 1985–1986 and 1986–1987. The evidence for the convection is:

1) Simultaneous warming and cooling at different locations in a horizontal plane in the snow,
2) Observations of up to a 16°C range in temperature over a horizontal distance of about half a meter,
3) A 10 to 50 times faster response of the snow to rapid changes in air temperature than can be explained by diffusion, and
4) An average Nusselt number (the ratio of the total effective bulk conductivity of the snow measured by heat flow meters to the average effective thermal conductivity) equal to or greater than 2.

The convection is time-dependent. A quasi-stable mode associated with coherent temperature records is present virtually throughout the winter. Occasionally ($\leq$ 16% of the winter), this convective flow becomes more vigorous, perturbed by external conditions such as high wind (wind speed $\geq$ 5 m s^{-1}), rapid changes in temperature, or unidentified causes. At those times, the convective flow velocity probably increases, creating thermal disequilibrium in the snow and resulting in incoherent temperature records.

A plume-like convective flow pattern is suggested by relative warm and cold zones that develop in the snow and remain relatively fixed in space through the winter. The zones seem to be linked to spatial variations in the temperature of the snow/soil interface that result from uneven soil moisture or lateral variations in the thermal conductivity of the soil. By analogy with laboratory experiments of porous media, it is likely that warm, diffuse plume-like updrafts develop in the snow above the regions of the interface that are at higher temperature. The plume-like circulation pattern is characterized by vertical air flow except in a narrow layer at the base of the snow, where flow is horizontal.

The onset of convection in the snow cannot be predicted using a standard Rayleigh number formulated for a homogeneous porous medium with isothermal upper and lower boundaries. The critical Rayleigh number formulated in this manner was never exceeded during all three winters of the study, despite the fact that the system was almost continuously convecting. A system with ever-changing boundary conditions and a non-uniform basal temperature probably does not have a critical Rayleigh number, in the classic sense. Instead, the system may be unconditionally unstable. In the case of a natural snow cover, spatial variations in the temperature of the snow/soil interface, the continuously fluctuating air temperature, and on-going snow metamorphism probably all contribute to a dramatic lowering of the critical threshold for the initiation of convection.

Estimates based on one-dimensional heat and mass transport equations suggest that the average convective velocity in the Fairbanks snow cover is on the order of 0.2 mm s^{-1}, with a maximum value of 2 mm s^{-1}. Using this range of velocities, it is estimated that convection accounts for a third of the total heat transport. Latent heat transported by the vapor flux accounts for another third. Most of the time the vapor flux is primarily the result of diffusion, but during the brief periods when the convective flow velocity approaches its maximum value, it can increase the mass transport by a factor of 10 or

more. During these same periods, convection of dry air moves up to 17 times as much heat as is conducted through the ice matrix and air spaces.

Convection may be important in the development of a five-layer metamorphic sequence of snow crystals. The basal layer, which consists of crystals with horizontal c-axes, coincides with the zone where the air flow is thought to be horizontal. The overlying layers, which contain crystals with vertical c-axes, coincide with vertical flow, suggesting that the flow direction affects the crystal growth.

Recommendations for future work

Determine the prevalence of convection in other types of snow

One vertical and one horizontal thermistor string could be installed and monitored in several different types of snow covers. These must be installed over carefully prepared substrates, but they would be sufficient to indicate the presence of convection. The measurements could be made in several extreme types of snow covers, for example in the deep, dense snow found in maritime climates, in the thin, wind-blown snow found on the arctic coastal plain, and in the snow found on sea ice.

Determine the extent of convection on hillsides

In theory (Bories and Combarnous 1973, Powers et al. 1985a, b) air in the snow on hillsides always convects. An installation of thermistors in several different types of snow covers on hillsides should be able to verify and help define the extent and characteristics of the convection.

Determine the convective velocity

Convective velocities could be measured using tracer gases. Sulphur-hexafluoride or another trace gas could be introduced at the bottom of the snow during convection events by installing breakable glass vials containing the gas at the soil surface prior to the first snowfall. During the events, the vials could be broken remotely and the time it took the gas to travel from the vials to receptor tubes could be measured and used to calculate the air flow velocity. An experiment of this nature was designed and installed during the present study but never ran successfully.

Measure temperature variations at the snow/soil interface

Spatial variation in the temperature of the snow/soil interface should be measured for different substrates and moisture conditions. Because these variations affect the onset and presence of convection, it would be useful to know their range and how they change with vegetation, microtopography, and moisture content.

Create an artificial warm zone at the base of the snow
to study the relationship between convection and snow metamorphism

An artificial warm zone could be created at the base of a natural snow cover using a controllable line heater placed on the ground before the first snowfall. The heater could be adjusted during the winter to maintain it at a higher temperature than the surrounding soil surface, and at the end of winter, the snow texture above the heater and elsewhere could be compared.

Grow depth hoar with and without air flow

In a laboratory, natural new snow samples could be subjected to temperature gradients similar to those found in the Fairbanks snow. Inverted gradients (warm on top, cold on the bottom) could be applied to some samples to prevent convection, while normal gradients could be applied to other samples, allowing convection. Controlled ventilation of some samples could be used to try to determine the effect of air flow on the c-axis orientation in growing crystals.

Induce convection by creating a warm zone at the base of the snow to determine the onset conditions

One of the samples used in growing depth hoar (see above) could be instrumented with thermistors and placed on a plate that had a controllable heat pad in one section. The onset of convection in the snow could be investigated at different temperature gradients and at different stages of depth hoar metamorphism.

Develop onset criteria for porous media over a warm spot

Using existing computer models for convection in porous media, it should be possible to investigate the onset criteria for porous media with a non-uniform basal boundary temperature. It would also be useful to include in the models the effects of latent heat transfer and rapidly varying temperatures at the upper surface.

LITERATURE CITED

Adams, E. E. and R. L. Brown (1982a) Further results on studies of temperature-gradient metamorphism. *Journal of Glaciology*, **28**(98): 205–210.

Adams, E. E. and R. L. Brown (1982b) A model for crystal development in dry snow. *Geophysical Research Letters*, **9**(11): 1287–1289.

Adams, E. E. and R. L. Brown (1983) Metamorphism of dry snow as a result of temperature gradient and vapor density differences. *Annals of Glaciology*, **4**: 3–9.

Akitaya, E. (1967) Some experiments on the growth of depth hoar. In *Physics of Snow and Ice, Part 2: Proceedings of the Sapporo Conference*. Hokkaido University, Institute of Low Temperature Science, p. 713–723.

Akitaya, E. (1974) Studies on depth hoar. *Contributions from the Institute of Low Temperature Science*, A(26): 1–67.

Armstrong, R. L. (1985) Metamorphism in a subfreezing, seasonal snow cover: The role of thermal and vapor pressure conditions. Ph.D. dissertation, University of Colorado.

Bader, H., R. Haefeli, E. Bucher, J. Neher, O. Eckel and C. Thams (1939) Der Schnee und seine Metamorphose. USA Snow, Ice and Permafrost Research Establishment (SIPRE), Translation 14.

Bender, J. A. (1957) Air permeability of snow. USA Snow, Ice and Permafrost Research Establishment, SIPRE Research Report 37.

Benson, C. S. (1962) Stratigraphic studies of the snow and firn of the Greenland Ice Sheet. USA Snow, Ice and Permafrost Research Establishment, SIPRE Research Report 70.

Benson, C. S. (1982) Reassessment of winter precipitation on Alaska's arctic slope and measurements on the flux of wind blown snow. University of Alaska: Geophysical Institute Report UAG R-288.

Benson, C. S. and D. C. Trabant (1972) Field measurements on the flux of water vapour through dry snow. *The Role of Snow and Ice in Hydrology: Proceedings of the Banff Symposia, September, 1972*. UNESCO-WMO-IASH, p. 291–298.

Bergen, J. D. (1978) Some measurements of settlement in a Rocky Mountains snow cover. *Journal of Glaciology*, **20**(82): 141–148.

Bey, P. P. (1951) The heat economy of the snow pack. In *Review of the Properties of Snow and Ice*, Chapter VII (H. T. Mantis, Ed.). USA Snow, Ice and Permafrost Research Establishment, SIPRE Report 4, p. 73–85.

Blackwell, J. H. (1954) A transient-flow method for determination of thermal constants of insulating materials in bulk. *Journal of Applied Physics*, **25**(2): 137–144.

Blatt, H., G. Middleton and R. Murray (1972) *Origin of Sedimentary Rocks*. Englewood Cliffs, New Jersey: Prentice-Hall Inc.

Bories, S. A. and M. A. Combarnous (1973) Natural convection in a sloping porous layer. *Journal of Fluid Mechanics*, **57**(1): 63–79.

Bradley, C. C., R. L. Brown and T. Williams (1977a) On depth hoar and the strength of snow. *Journal of Glaciology*, **18**(78): 145–147.

Bradley, C. C., R. L. Brown and T. R. Williams (1977b) Gradient metamorphism, zonal weakening of the snow-pack and avalanche initiation. *Journal of Glaciology*, **19**(81): 335–342.

Brun, E. and F. Touvier (1987) Ètude experimentale de la convection thermique dans la neige. *Journal de Physique Terre*, **48**(C1): 257–261.

Bryson, R. A. and F. K. Hare (1974) *Climates of North America: World Survey of Climatology*, Volume 11, Amsterdam: Elsevier Scientific Publishing Company.

Carroll, T. (1977) A comparison of the CRREL 500 cc tube and the ILTS 200 and 100 cc box cutters used for determining snow densities. *Journal of Glaciology*, **18**(79): 334–337.

Chacho, E. and J. Johnson (1987) Air permeability of depth hoar. *EOS-American Geophysical Union*, **68**(44): 1271.

Christon, M., P. Burns, E. Thompson and R. Sommerfeld (1987) Water vapor transport in snow. A 2-d simulation of temperature gradient metamorphism. In *Seasonal Snowcovers: Physics, Chemistry, Hydrology* (H.G. Jones and W.J. Orville-Thomas, Eds.). Boston: D. Reidel Publishing Co., p. 37–62.

Clarke, G. K. C., D. A. Fisher and E. D. Waddington (1987) Wind pumping: A potentially significant heat source in ice sheets. *The Physical Basis of Ice Sheet Modelling*. IASH Publication 170, p. 169–180.

Colbeck, S. C. (1982a) Growth of faceted crystals in a snow cover. USA Cold Regions Research and Engineering Laboratory, CRREL Report 82-29.

Colbeck, S. C. (1982b) An overview of seasonal snow metamorphism. *Reviews of Geophysics and Space Physics*, **20**(1): 45–61.

Colbeck, S. C. (1983a) Theory of metamorphism of dry snow. *Journal of Geophysical Research*, **88**(C9): 5475–5482.

Colbeck, S. C. (1983b) Ice crystal morphology and growth rates at low super-saturations and high temperatures. *Journal of Applied Physics*, **54**(5): 2677–2681.

Colbeck, S. C. (1986) Classification of seasonal snow cover crystals. *Water Resources Research*, **22**(9): 59S–79S.

Colbeck, S. C. (1988) Ideas on the micrometeorology of surface hoar growth on snow. *Boundary-layer Meteorology*, **44**: 1–12.

Colbeck, S. C. (1989) Air movement in snow due to wind pumping. *Journal of Glaciology*, **35**(120): 209–213.

Combarnous, M. A. and S. A. Bories (1975) Hydrothermal convection in saturated porous media. *Advances in Hydroscience*, p. 231–307.

Davis, J. C. (1973) *Statistics and Data Analysis in Geology*. New York: John Wiley and Sons, Inc.

de Quervain, M. R. (1958) On metamorphism and hardening of snow under constant pressure and temperature gradient. IASH Publication 46, p. 225–239.

de Quervain, M. R. (1972) Snow structure, heat and mass flux through snow. *The Role of Snow and Ice in Hydrology*. IASH-AISH, **1**(107): 203–226.

Devaux, J. (1933) Radiation and thermal properties of snow fields and glaciers. *Annales de Physique*, **20**: 5–67.

Dubrovin, L. I. (1961) Air currents in the snow and firn layer of Lazarev Ice Shelf. *Information Bulletin of the Soviet Antarctic Expedition*, no. 26, p. 218–219.

El-Khatib, G. and V. Prasad (1986) Effects of stratification on thermal convection in horizontal porous layers with localized heating from below. In *Natural Convection in Porous Media: 4th Thermophysics and Heat Transfer Conference*, p. 61–68.

Elder, J. W. (1967) Steady free convection in a porous medium heated from below. *Journal of Fluid Mechanics*, **27**(1): 29–48.

Fay, F. H. (1973) The ecology of *Echinococcus multilocularis* Leuckart, 1863 (*Cestoda: Taeniidae*) on St. Lawrence Island, Alaska. *Annales de Parasitologie*, **48**(4): 523–542.

Fedoseeva, V. I. and N. F. Fedoseev (1988) Evaluation of the coefficient of diffusion of water vapor in the snow cover. *Soviet Meteorology and Hydrology*, no. 2, p. 132–135.

Folk, R. L. (1955) Student operator error in determination of roundness, sphericity, and grain size. *Journal of Sedimentary Petrology*, **25**(4): 297–301.

Frank, F. C. (1982) Snow crystals. *Contemporary Physics*, **23**(1): 3–22.

Friedman, G. M. and J. E. Sanders (1983) *Principles of Sedimentology*. New York: John Wiley and Sons.

Friedman, I., C. S. Benson and J. Gleason (In press) Isotopic fractionation produced by depth hoar development in snow. *Geochemica Cosmochemica Acta*.

Fukue, M. (1977) Mechanical performance of snow under loading. Ph.D. dissertation, Tokai University Press.

Giddings, J. C. and E. LaChapelle (1962) The formation rate of depth hoar. *Journal of Geophysical Research*, **67**(6): 2377–2383.

Gjessing, Y. T. (1977) The filtering effect of snow. *Isotopes and Impurities in Snow and Ice Symposium*. IASH-AISH Publication 118, p. 199–203.

Gosink, J. P., K. Kawasaki, T.E. Osterkamp and J. Holty (1988) Heat and moisture transport during annual freezing and thawing. In *Permafrost Proceedings, Vol. 1: 5th International Conference on Permafrost*. Tapir, p. 355–360.

Granberg, H. B. and R. Wener (1986) Snowpack grain size stratification at Schefferville. In *Proceedings of the 43rd Annual Eastern Snow Conference*, p. 6–10.

Griffiths, J. C. (1953) Estimation of error in grain size analysis. *Journal of Sedimentary Petrology*, **23**(2): 75–84.

Gubler, H. (1978) Determination of the mean number of bonds per snow grain and the dependence of the tensile strength of snow on stereological parameters. *Journal of Glaciology*, **20**(83): 329–341.

Gubler, H. (1985) Model for dry snow metamorphism by interparticle flux. *Journal of Geophysical Research*. **90**(C8): 8081–8092.

Hjeltström, S.A. (1890) Sur la conductibilité de la neige. *Ofversigt af den Konglige Vetenskaps-Akademiens Förhandlinger*, **46**: 669–676.

Jaafar, H. and J. J. C. Picot (1970) Thermal conductivity of snow by a transient state probe method. *Water Resources Research*, **6**(1): 333–335.

Jaeger, J.C. (1958) The measurement of thermal conductivity and diffusivity with cylindrical probes. *Transactions, American Geophysical Union*, **39**(4): 708–710.

Jansson, M. (1901) Über die Wärmeleitungsfähigkeit des Schnees. *Ofversigt af den Konglige Vetenskaps-Akademiens Förhandlinger*, no. 3, p. 207–223.

Johnson, J.B., M. Sturm, D.K. Perovich and C.S. Benson (1987) Field observations of thermal convection in a subarctic snow cover. *Avalanche Formation, Movement and Effects*. IASH-AISH Publication 162, p. 105–118.

Johnston, G. H. (1981) *Permafrost Engineering Design and Construction*. Toronto: John Wiley and Sons.

Jones, B. W. (1988) The thermal conductivity probe: development of method and application to a coarse granular medium. *Journal of Physics, E: Scientific Instrumentation*, **21**: 832–839.

Katto, Y. and T. Masuoka (1967) Criterion for onset of convective flow in a porous medium. *International Journal of Heat and Mass Transfer*, **10**: 297–309.

Keeler, C. M. (1969) Some physical properties of alpine snow. USA Cold Regions Research and Engineering Laboratory, CRREL Research Report 271.

Keller, V. W. and J. Hallett (1982) Influence of air velocity on the habit of ice crystal growth from the vapor. *Journal of Crystal Growth*, **60**: 91–106.

Kelly, R.E. and D. Pal (1978) Thermal convection with spatially periodic boundary conditions: resonant wavelength excitation. *Journal of Field Mechanics*, **86**(3): 433–456.

Knight, C. A. and A. L. DeVries (1985) Growth forms of large frost crystals in the Antarctic. *Journal of Glaciology*, **31**(108): 127–135.

Kobayashi, T. (1961) The growth of snow crystals at low supersaturations. *Philosophical Magazine*, **6**: 1363–1370.

Kojima, K. (1956) Viscous compression of natural snow-layer. II. *Low Temperature Science*, **A**(15): 117–135.

Kojima, K. (1959) The influence of temperature gradient upon the grain texture, settling rate and brittleness of snow. *Low Temperature Science*, **A**(18): 29–45.

Kojima, K. (1966) Densification of seasonal snow cover. In *Physics of Snow and Ice, Part 2. Proceedings of the Sapporo Conference*. The Institute of Low Temperature Science, p. 929–951.

Kolomyts, E. G. (1984) *Crystal Morphological Atlas of Snow*. Vladivostok: Pacific Institute of Geography, Far East Science Center, USSR Academy of Sciences.

Kondrat'eva, A. S. (1954) Thermal conductivity of the snow cover and physical processes caused by the temperature gradient. USA Snow, Ice and Permafrost Research Establishment, SIPRE Translation 22.

Kry, P. R. (1975) Quantitative stereological analysis of grain bonds in snow. *Journal of Glaciology*, **14**(72): 467–478.

Lachenbruch, A. H. (1957) A probe for measurement of thermal conductivity of frozen soils in place. *Transactions, American Geophysical Union*, **38**(5): 691–697.

Lamb, D. and P. V. Hobbs (1971) Growth rates and habits of ice crystals grown from the vapor phase. *Journal of the Atmospheric Sciences*, **28**: 1506–1509.

Lamb, D. and W. D. Scott (1972) Linear growth rates of ice crystals grown from the vapor phase. *Journal of Crystal Growth*, **12**: 21–31.

Lang, R. M., B. R. Leo, and R. L. Brown (1984) Observations on the growth process and strength characteristics of surface hoar. In *Proceedings of the International Snow Science Workshop, Mountain Rescue, Aspen*, p. 188–195.

Lange, M. A. (1985) Measurement of thermal parameters in Antarctic snow and firn. *Annals of Glaciology*, **6**: 100–104.

Lapwood, E. R. (1948) Convection of a fluid in a porous medium. In *Proceedings of the Cambridge Philosophical Society*, **44**: 508–521.

List, R. J. (1951) *Smithsonian Meteorological Tables*, 6th Edition. Washington, D.C.: Smithsonian Institution.

Ludwick, J. C. and P. L. Henderson (1968) Particle shape and inference of size from sieving. *Sedimentology*, **11**: 197–235.

Magono, C. and C. W. Lee (1966) Meteorological classification of natural snow crystals. *Journal of the Faculty of Science*, Hokkaido University, **VII**(4): 321–335.

Marbouty, D. (1980) An experimental study of temperature gradient metamorphism. *Journal of Glaciology*, **26**(94): 303–312.

Mason, B. J., G. W. Bryant, and A. P. Van den Heuvel (1963) The growth habits and surface structure of ice crystals. *Philosophical Magazine*, **8**: 505–526.

McGaw, R. W. (1984) The heating and cooling probe method for measuring thermal conductivity. Review draft for ASME 1984 Western Area meeting.

Mellor, M. (1977) Engineering properties of snow. *Journal of Glaciology*, **19**: 15–66.

Meyer, C. W., G. Ahlers and D. S. Cannell (1987) Initial stages of pattern formation in Rayleigh-Bénard convection. *Physical Review Letters*, **59**(14): 1577–1580.

Mizutani, S. (1963) A theoretical and experimental consideration on the accuracy of sieving analysis. *Journal of Earth Sciences*, Nagoya University, **11**(1): 1–27.
Nakaya, U. (1954) *Snow Crystals Natural and Artificial.* Cambridge: Harvard University Press.
National Research Council, Canada (1954) *The International Classification for Snow*, Technical Memorandum no. 31. Commission of Snow and Ice of the IAH.
Nield, D. A. (1968) Onset of thermohaline convection in a porous medium. *Water Resources Research*, **4**(3): 553–560.
Nyberg, A. (1938) Temperature measurements in an air layer very close to a snow surface. *Geografiska Annaler*, **20**: 234–275.
Okada, T. (1905) On the thermal conductivity of snow. *Journal of the Meteorology Society of Japan*, p.1–4.
Pahaut, E. and D. Marbouty (1981) Les cristaux de neige: II. Evolution. *Neige et Avalanches*, no. 25, p. 3–42.
Palm, E. and M. Tveitereid (1979) On heat and mass flow through dry snow. *Journal of Geophysical Research*, **84**(C2): 745–749.
Paulke, W. (1934a) Eisbildungen I. Der Schnee und seine Diagenese. (Translation by I. A. Langnas) *Zeitschrift fur Gletscherkunde*, **21**(4-5): 259–282.
Paulke, W. (1934b) Schnee-wachten und Lawinen. (Translation by I. A. Langnas) *Zeitschrift des Deutschen und Osterreichischen Alpenvereins*, **65**: 247–262.
Perkins, S. M. (1987) User's guide for SNOWGRAPHICS program for Hewlett Packard Model 9000 Series 200 computer. USA Cold Regions Research and Engineering Laboratory, CRREL Internal Report (unpublished).
Pitman, D. and B. Zuckerman (1967) Effective thermal conductivity of snow at –88°, –27°, and –5°C. *Journal of Applied Physics*, **38**: 2698–2699.
Powers, D. J., S. C. Colbeck, and K. O'Neill (1985a) Thermal convection in snow. USA Cold Regions Research and Engineering Laboratory, CRREL Report 85-9.
Powers, D. J., K. O'Neill and S. C. Colbeck (1985b) Theory of natural convection in snow. *Journal of Geophysical Research*, **90**(D6): 10641–10649.
Pratt, A. W. (1969) Heat transmission in low conductivity materials. In *Thermal Conductivity* (R. P. Tye, Ed.), Vol. I, Chapter 6. London: Academic Press, p. 301–405.
Pruitt, W. O., Jr. (1970) Some ecological aspects of snow. In *Ecology of the Subarctic Regions, Proceedings of the Helsinki Symposium*, UNESCO, p. 83–99.
Pruitt, W. O., Jr. (1984) Snow and living things. In *Northern Ecology and Resource Management*, (R. Olsen et al., Ed.). Alberta, Canada: The University of Alberta Press, p. 51–77.
Rayleigh, L. (1916) On convection currents in a horizontal layer of fluid, when the higher temperature is on the under side. *Philosophical Magazine and Journal of Science*, **32** (6th Series): 529–547.
Rees, D.A.S. and D.S. Riley (1986) Free convection in an undulating saturated porous layer: Resonant wavelength excitation. *Journal of Fluid Mechanics*, **166**: 503–530.
Rees, D.A.S. and D.S. Riley (1989) The effects of boundary imperfections on convection in a saturated porous layer: Non-resonant wavelength excitation. In *Proceedings of the Royal Society of London*, **421**: 303–339.
Ribando, R. J. (1977) Geothermal energy related problems of natural convection in porous media. Ph.D. dissertation, Cornell University.
Royse, C. F., Jr. (1970) *An Introduction to Sediment Analysis.* Tempe: Arizona State University.
Schubert, G. and J. M. Straus (1982) Transitions in time-dependent thermal convection in fluid-saturated porous media. *Journal of Fluid Mechanics*, **121**: 301–313.
Schwerdtfeger, P. (1970) The measurement of heat flow in the ground and the theory of heat flux meters. USA Cold Regions Research and Engineering Laboratory, CRREL Technical Report 232.

Searby, H. W. and C. I. Branton (1973) Climatic conditions in agricultural areas in Alaska. In *Climate of the Arctic* (G. Weller and S.A. Bowling, Ed.). Fairbanks: University of Alaska, p. 281–288.
Seligman, G. (1936) *Snow Structure and Ski Fields*. Cambridge: International Glaciological Society (1980 reprint).
Shimizu, H. (1970) Air permeability of deposited snow. *Contributions from the Institute of Low Temperature Science*, **A**(22): 1–32.
SIPRE (1962) Instructions for making and recording snow observations. USA Snow, Ice and Permafrost Research Establishment, SIPRE Instruction Manual 1.
Sommerfeld, R.A. (1983) A branch grain theory of temperature gradient metamorphism in snow. *Journal of Geophysical Research*, **88**(C2): 1484–1494.
Sommerfeld, R. A. and E. LaChapelle (1970) The classification of snow metamorphism. *Journal of Glaciology*, **9**: 3–17.
Sturm, M. and J. Johnson (1987) Measurements of the thermal conductivity of depth hoar. *EOS-American Geophysical Union*, **68**(44): 1271.
Trabant, D. C. (1970) Diagenesis of the seasonal snow cover of interior Alaska. M.S. thesis, University of Alaska, Fairbanks, Alaska.
Trabant, D. and C. S. Benson (1972) Field experiments on the development of depth hoar. *Geological Society of America Memoir 135*, p. 309–322.
Turcotte, D. L. and G. Schubert (1982) *Geodynamics*. New York: John Wiley and Sons.
UNESCO (1970) *Seasonal Snow Cover: A Guide for Measurement, Compilation and Assemblage of Data*. Paris: UNESCO.
Voitkovsky, K. F., V. N. Golubev, N. I. Lapteva, E. S. Troshkina, L. A. Ushakova and A. V. Pavlov (1975) Mass transfer and metamorphism in snow cover. IASH-AISH Publication 114, p. 16–23.
von Eugster, H. P. (1950) *Zür Morphologie und Metamorphose des Schnees*. Eidg. Institut fur Schnee- und Lawinenforschung, No. 113.
von Herzen, R. and A. E. Maxwell (1959) The measurement of thermal conductivity of deep-sea sediments by a needle-probe method. *Journal of Geophysical Research*, **64**(10): 1557–1563.
Wilson, C. R. and C. Fahl (1969) Infrasonic pressure waves in the auroral zone, University of Alaska Geophysical Institute Report Series, Contract E-22-27-68N, ESSA, U.S. Dept. of Commerce.
Wilson, C. R. and S. B. Nichparenko (1967) Infrasonic waves and auroral activity. *Nature*, **214**(5095): 1299–1302.
Woodside, W. (1958) Calculation of the thermal conductivity of porous media. *Canadian Journal of Physics*, **37**(7): 815–823.
Yen, Y.C. (1963) Heat transfer by vapor transport in ventilated snow. *Journal of Geophysical Research*, **68**(4): 1093–1101.
Yosida, Z. and H. Iwai (1954) Measurement of the thermal conductivity of snow cover. USA Snow, Ice and Permafrost Research Establishment, SIPRE Translation 30.
Yosida, Z. and colleagues (1955) Physical studies on deposited snow. I. *Contributions from the Institute of Low Temperature Science*, no. 7, p. 19–74.
Young, H. D. (1962) *Statistical Treatment of Experimental Data*. New York: McGraw-Hill Book Company.
YSI (1984) *Temperature, Humidity, Oxygen, Pressure Instruments and Sensors*. Yellow Springs Instrument Co., Inc.

APPENDIX A: AIR PERMEABILITY MEASUREMENTS

The air permeability measurements were made by E. Chacho. Limited measurements were made in 1984–1985 and 1985–1986. The bulk of the measurements were made in 1986–1987 using a new air permeameter designed, built, and described by Chacho and Johnson (1987). The results for 1986–1987 are listed in Table A-1. Vertical and horizontal core samples from the snow were measured and are listed separately. Figure A-1 illustrates the increase in permeability during the winter as a result of snow metamorphism.

Table A-1. Air permeability measurements for Fairbanks snow, 1986–1987. Vertical and horizontal cores of snow were measured.

	Ground			*Tables*			
Date 1987	*Sample*	*Density (kg m^{-3})*	*Permeability (darcy)*	*Date 1987*	*Sample*	*Density (kg m^{-3})*	*Permeability (darcy)*
Upper snow layerr							
Vertical							
5 Jan	4	100	2.7×10^3				
14 Jan	5	160	8.9×10^3	14 Jan	11	110	7.7×10^3
26 Jan	14	170	11.5×10^3	26 Jan	21	125	7.4×10^3
11 Feb	24	180	18.7×10^3	11 Feb	32	150	7.6×10^3
13 Mar	38	180	35.9×10^3	13 Mar	45	170	10.5×10^3
Horizontal							
14 Jan	10	160	11.6×10^3				
26 Jan	19	170	15.2×10^3				
11 Feb	30	160	9.1×10^3	11 Feb	35	150	13.3×10^3
13 Mar	43	170	18.4×10^3	13 Mar	48	145	7.7×10^3
Lower snow layer							
Vertical							
31 Dec (1986)	3	185	28.7×10^3	31 Dec	1	200	6.4×10^3
				31 Dec	2	200	5.6×10^3
14 Jan	7	175	43.5×10^3	14 Jan	13	200	7.8×10^3
26 Jan	16	175	55.5×10^3	26 Jan	22	220	7.4×10^3
11 Feb	26	180	48.2×10^3	11 Feb	33	210	8.4×10^3
11 Feb	27	180	53.0×10^3				
13 Mar	41	180	48.4×10^3	13 Mar	46	250	7.9×10^3
13 Mar	39	180	55.7×10^3				
Horizontal							
14 Jan	9	150	33.4×10^3				
26 Jan	20	160	52.8×10^3				
11 Feb	31	175	52.3×10^3				
13 Mar	44	170	56.5×10^3	13 Mar	49	230	6.4×10^3
Total snow pack							
14 Jan	8		17.7×10^3	14 Jan	12		9.6×10^3
26 Jan	18		29.0×10^3	26 Jan	23		7.1×10^3
11 Feb	28		29.0×10^3	11 Feb	34		8.3×10^3
11 Feb	29		31.4×10^3				
13 Mar	42		35.9×10^3	13 Mar	47		6.6×10^3

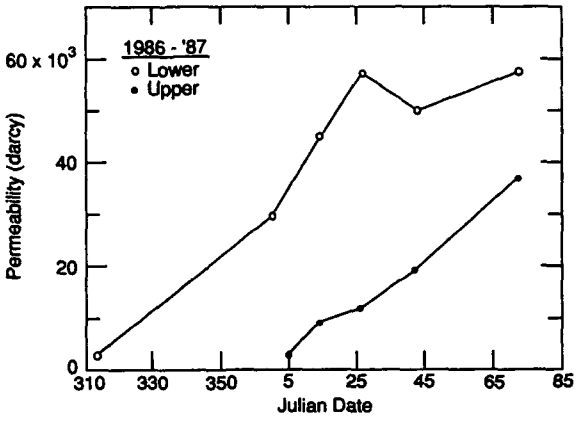

Figure A-1. Air permeability of two layers of snow on the ground, 1986–1987. The lower layer was deposited on Julian date 311; the upper layer was deposited between Julian dates 350 and 5. Measurements were made on vertical core samples.

APPENDIX B: CALCULATION OF THE NUMBER OF GRAINS IN A SNOW SAMPLE

Let a snow sample be sieved through L sieves, the bottom-most sieve actually being a pan that catches all the grains that passed through the immediately larger sieve. The total mass in the jth sieve, M_j, is equal to the sum of the masses of all the individual grains in the sieve:

$$M_j = \sum_{i=1}^{N_j} m_i \tag{B-1}$$

where there are N_j grains in the jth sieve, and the mass of the ith grain contained in the sieve is m_i. If the average mass of a grain in the jth sieve is $\overline{m}_j$, then:

$$M_j = N_j \, \overline{m}_j \tag{B-2}$$

By weighing individual grains in each sieve, a curve of average grain mass vs sieve size was established (Fig. 15). From this curve, values of $\overline{m}_j$ can be determined for any sieve size, which makes it possible to calculate the number of grains in the jth sieve using eq B-2.

The total number of grains in the sample, N_T, can be calculated by adding up the number of grains in each sieve:

$$N_T = \sum_{j=1}^{L} N_j \, . \tag{B-3}$$

In this study L equaled 9, and all samples were of a constant mass, M, rather than a constant volume. Therefore, N_T is the total number of grains per sample mass. The total number of grains per unit volume is

$$N = N_T \frac{\rho}{M} \tag{B-4}$$

where ρ is the density of the snow sample.

The uncertainties in N were large. The uncertainty in the value of $\overline{m}_j$ was probably ±20%, producing uncertainties in N of ±20%. Much of the total uncertainty in N was the result of the enormous number of grains in the pan at the bottom of the sieve stack, which caught all the grain fragments. The pan could contain as many as 3×10^8 grains per cubic meter, with a corresponding uncertainty of $\pm 6 \times 10^7$ grains per cubic meter. These uncertainties dominated the total uncertainty when there was a significant fraction of the sample in the pan. Generally, however, there was a relatively small number of grains in the pan and the corresponding uncertainty was smaller.

Some of the abrupt changes in N for the samples from the tables (Fig. 16) may have had a physical cause. Relict layers of surface hoar buried by other snow were encountered in sampling. Where possible, samples unbiased by surface hoar were preferred, but it is possible that occasional samples were contaminated with large surface hoar grains, which would have had the effect of markedly decreasing N.

APPENDIX C: INSTRUMENTATION ERRORS

The data logger system could resolve ±1 ohm when set at a full scale reading of 30 K ohms. The age and operating temperature of the logger reduced the accuracy by ±0.016% of the resistance reading, which normally ranged between 5000 and 45,000 ohms. Maximum instrumentation error was ±0.02°C. Excitation current supplied by the logger was 100 mA. In less than 180 seconds, including switching time, 250 thermistors were scanned; current was supplied to each thermistor for less than 0.5 seconds. An estimate of the possible self-heating of thermistors due to this excitation current can be determined as follows: Maximum self-heating and change in temperature will occur if the thermistors are insulated (adiabatic system). In nature, conduction of heat to the environment occurs, reducing this change in temperature. The power input to the thermistor is:

$$P = i^2 \Omega \tag{C-1}$$

where P is the power, i is the current, and Ω is the thermistor resistance. Let c_t be the specific heat capacity of the thermistor, and m_t be the mass of the thermistor. For the adiabatic case:

$$\frac{dT}{dt} = \left[P / (m_t c_t)\right] \tag{C-2}$$

or integrating from time 1 to time 2:

$$\Delta T = \left[P / (m_t c_t)\right] t \tag{C-3}$$

Using measured values ($t = 0.5$ s, $m_t = 3 \times 10^{-6}$ kg, $c_t = 800$ J kg^{-1} °C^{-1}, $i = 100$ mA, and $\Omega = 5000$ ohms),

$$\Delta T \leq 0.01 \text{ °C} \tag{C-4}$$

For the thermistors used in this study, a conservative estimate of the maximum error due to self-heating and instrumentation drift is ±0.03°C.

The data logger system could resolve 10 μV. The only transducers for which DC voltages were recorded were the heat flow meters. For these, instrument error was about ±10 μV, which gives rise to errors in heat flow of 0.3 W m^{-2}, which are insignificant compared to the order of magnitude of the results (5 to 30 W m^{-2}).

APPENDIX D: THERMAL CONDUCTIVITY MEASUREMENTS

The thermal conductivity was measured using a needle probe method that is based on the rate of warming or cooling of a sample during the transient heating of a line source embedded in the sample. It has been described by Blackwell (1954), Lachenbruch (1957), Jaeger (1958), von Herzen and Maxwell (1959), Pratt (1969), McGaw (1984), and Jones (1988) and has been used to measure the thermal conductivity of snow by Jaafar and Picot (1970), Lange (1985), and Sturm and Johnson (1987).

A stainless steel needle probe built by Custom Scientific Instruments Inc. (Model CS-48/E), 0.2 m long and containing a helical heating wire and a chromel-constantan thermocouple, was inserted along the axis of a 0.10-m-diameter cylindrical snow sample that had equilibrated to ±0.01°C at the desired temperature using a copper jacket and circulating bath. Current (using 10 to 16 V) was fed to the heater for a 5- to 10-minute heating phase, then turned off. The sample was then allowed to cool for 15 to 20 minutes. During both heating and cooling phases, the temperature of the needle was monitored. From the temperature data, a separate value of the thermal conductivity could be calculated for both the heating and cooling phase (McGaw 1984). If they agreed to ±10%, the test was considered accurate and the results averaged. If not, the test was repeated after the sample had re-equilibrated.

The tests were run using a Hewlett Packard 41-CV calculator and 3421A data logger in 1984–1985 and 1985–1986. In 1986–1987, the data logger and power supply were controlled by a Hewlett Packard Integral Computer.

The results of all measurements made between 1984 to 1987 are listed in Table D-1.

Table D-1. Summary of thermal conductivity measurements.

Date	*Snow type*	*Density* ($kg\ m^{-3}$)	*Temp.* (°C)	*Height* (m)	k_h ($W\ m^{-1}\ K^{-1}$)	k_c ($W\ m^{-1}\ K^{-1}$)	k_{avg} ($W\ m^{-1}\ K^{-1}$)	*Good test?*
1985–1986								
16 Nov	New snow	98	–13.6	—	0.049	0.098	0.049	No
16 Nov	New snow	98	–5.5	—	0.039	—	—	?
16 Nov	New snow	98	–8.2	—	0.047	—	—	?
24 Nov	Depth hoar	179	–6.8	0.03	0.031	—	0.031	Yes
24 Nov	Depth hoar	179	–10.1	0.03	0.017	—	?	No
24 Nov	Depth hoar	179	–7.0	0.03	0.030	0.031	0.031	Yes
24 Nov	Depth hoar	162	–4.8	0.03	0.034	—	0.034	?
24 Nov	Depth hoar	179	–7.5	0.03	0.049	0.115	0.049	No
30 Jan	Depth hoar	183	–24.9	0.15	0.045	—	0.045	Yes
30 Jan	Depth hoar	183	–27.0	0.15	0.048	0.068	0.058	?
30 Jan	Depth hoar	183	–21.8	0.15	0.132	—	?	No
1 Feb	Depth hoar	180	–26.1	0.15	0.067	0.101	0.084	?
6 Mar	Depth hoar	195	–14.6	0.15	0.050	0.055	0.053	Yes
6 Mar	Depth hoar	195	–13.4	0.15	0.057	—	0.057	?
6 Mar	Depth hoar	195	–12.6	0.15	0.063	—	0.063	Yes
1986–1987								
20 Dec	Depth hoar	160	–19.2	0.10	0.053	—	0.053	Yes
20 Dec	Depth hoar	160	–19.3	0.10	0.049	—	0.049	Yes
20 Dec	Depth hoar	160	–19.1	0.10	0.054	—	0.054	Yes
20 Dec	Depth hoar	160	–6.4	0.10	0.053	—	0.053	Yes
20 Dec	Depth hoar	160	–6.4	0.10	0.054	0.055	0.054	Yes
20 Dec	Depth hoar	160	–19.3	0.10	0.059	0.058	0.058	Yes

Table D-1 (cont'd). Summary of thermal conductivity measurements.

Date	Snow type	Density ($kg\ m^{-3}$)	Temp. (°C)	Height (m)	k_h ($W\ m^{-1}\ K^{-1}$)	k_c ($W\ m^{-1}\ K^{-1}$)	k_{avg} ($W\ m^{-1}\ K^{-1}$)	Good test?
1986–1987 (cont'd)								
20 Dec	Depth hoar	160	–19.8	0.10	0.064	0.067	0.066	Yes
31 Dec	Depth hoar	175	–10.3	0.03	0.065	0.060	0.063	Yes
31 Dec	Depth hoar	175	–19.8	0.03	0.043	—	0.043	?
31 Dec	Depth hoar	175	–10.3	0.03	0.049	0.056	0.052	Yes
31 Dec	Depth hoar	175	–18.6	0.03	0.049	0.065	0.057	?
31 Dec	Depth hoar	175	–19.8	0.03	0.043	0.053	0.048	Yes
31 Dec	Depth hoar	175	–10.2	0.03	0.052	0.057	0.054	Yes
6 Jan	New snow	70	–19.6	0.30	0.058	0.054	0.056	Yes
6 Jan	New snow	70	–19.2	0.30	0.060	0.054	0.057	Yes
14 Jan	Depth hoar	155	–4.9	0.07	0.049	0.048	0.049	Yes
14 Jan	Depth hoar	155	–18.8	0.07	0.049	0.050	0.049	Yes
14 Jan	Depth hoar	155	–18.9	0.07	0.049	0.043	0.046	Yes
14 Jan	Depth hoar	155	–18.9	0.07	0.050	0.053	0.047	?
14 Jan	Depth hoar	195	–19.2	0.17	0.081	0.078	0.079	Yes
14 Jan	Depth hoar	195	–19.0	0.17	0.092	0.078	0.085	?
14 Jan	Depth hoar	195	–19.0	0.17	0.096	0.085	0.091	?
14 Jan	Depth hoar	195	–19.3	0.17	0.086	0.079	0.082	Yes
14 Jan	Depth hoar	195	–5.0	0.17	0.105	0.099	0.102	Yes
14 Jan	Depth hoar	195	–5.0	0.17	0.098	0.098	0.098	Yes
26 Jan	Depth hoar	168	–18.4	0.07	0.053	0.051	0.052	Yes
26 Jan	Depth hoar	168	–18.4	0.07	0.057	0.046	0.052	?
26 Jan	Depth hoar	168	–18.6	0.07	0.052	0.049	0.051	Yes
26 Jan	Depth hoar	168	–12.3	0.07	0.080	0.084	0.082	Yes
26 Jan	Depth hoar	168	–12.4	0.07	0.077	0.080	0.078	?
26 Jan	Depth hoar	201	–19.7	0.17	—	—	—	—
26 Jan	Depth hoar	201	–19.6	0.17	0.078	0.068	0.073	?
26 Jan	Depth hoar	201	–19.5	0.17	0.093	0.071	0.082	No
26 Jan	Depth hoar	201	–19.5	0.17	0.084	0.082	0.083	Yes
26 Jan	Depth hoar	201	–11.1	0.17	0.057	0.054	0.055	?
26 Jan	Depth hoar	201	–11.1	0.17	0.069	0.056	0.063	No
26 Jan	Depth hoar	201	–4.8	0.17	0.079	0.090	0.085	No
26 Jan	Old Stellars	169	–19.2	0.29	0.059	0.055	0.057	Yes
26 Jan	Old Stellars	169	–19.3	0.29	0.061	0.055	0.058	?
26 Jan	Old Stellars	169	–18.9	0.29	0.056	0.056	0.056	Yes
26 Jan	Old Stellars	169	–12.9	0.29	0.063	0.057	0.060	Yes
26 Jan	Old Stellars	169	–12.8	0.29	0.062	0.055	0.058	?
10 Feb	Depth hoar	170	–19.2	0.07	0.045	0.042	0.044	Yes
10 Feb	Depth hoar	170	–18.5	0.07	0.043	0.046	0.044	Yes
10 Feb	Depth hoar	200	–20.0	0.17	0.071	0.059	0.065	?
10 Feb	Depth hoar	168	–19.9	0.27	0.063	0.065	0.064	Yes
13 Mar	Depth hoar	154	–19.6	0.04	0.028	0.023	0.021	No
13 Mar	Depth hoar	154	–19.8	0.04	0.076	0.069	0.072	Yes
13 Mar	Depth hoar	154	–19.7	0.04	0.076	0.071	0.073	Yes
13 Mar	Depth hoar	154	–19.9	0.04	0.079	0.074	0.077	Yes
13 Mar	Depth hoar	190	–20.1	0.17	0.093	0.086	0.090	Yes
13 Mar	Depth hoar	190	–20.1	0.17	0.086	0.083	0.084	Yes
13 Mar	Depth hoar	190	–20.1	0.17	0.093	0.085	0.089	Yes
13 Mar	Depth hoar	190	–20.2	0.25	0.096	0.086	0.091	Yes
13 Mar	Depth hoar	160	–20.3	0.31	0.086	0.092	0.089	Yes

Table D-1 (cont'd).

Date	Snow type	Density (kg m^{-3})	Temp. (°C)	Height (m)	k_h (W m^{-1} K^{-1})	k_c (W m^{-1} K^{-1})	k_{avg} (W m^{-1} K^{-1})	Good test?
1986–1987 (cont'd)								
26 Mar	Depth hoar	160	–18.2	0.05	0.056	0.051	0.053	Yes
26 Mar	Depth hoar	160	–18.1	0.05	0.055	0.050	0.053	Yes
26 Mar	Depth hoar	160	–18.5	0.05	0.057	0.049	0.053	No
26 Mar	Depth hoar	160	–18.8	0.05	—	—	—	—
26 Mar	Depth hoar	220	–18.9	0.16	0.042	0.038	0.040	Yes
26 Mar	Depth hoar	220	–19.1	0.16	0.045	0.040	0.042	Yes
26 Mar	Depth hoar	220	–19.2	0.16	0.045	0.044	0.044	Yes
26 Mar	Depth hoar	190	–18.5	0.26	0.070	0.056	0.063	?
26 Mar	Depth hoar	190	–18.4	0.26	0.064	0.061	0.062	Yes
26 Mar	Depth hoar	190	–11.5	0.26	0.075	0.066	0.070	?
26 Mar	Depth hoar	190	–6.7	0.26	0.083	0.074	0.079	Yes
26 Mar	Depth hoar	190	–6.7	0.26	0.084	0.081	0.083	Yes
26 Mar	Depth hoar	190	–3.6	0.26	0.089	0.074	0.082	?
FOAM STANDARD (1987–1988)								
2 Jan, 1987	Foam	—	Room	—	0.009	0.013	0.0	No
14 Jan, 1987	Foam	—	Room	—	0.010	0.012	0.011	Yes
5 Feb, 1987	Foam	—	Room	—	0.012	0.014	0.013	Yes
16 Mar, 1987	Foam	—	Room	—	0.012	0.011	0.011	Yes
16 Mar, 1987	Foam	—	Room	—	0.012	0.015	0.014	?
15 May, 1987	Foam	—	Room	—	0.013	0.015	0.014	Yes
21 July, 1988	Foam	—	Room	—	0.014	0.017	0.016	?

APPENDIX E: TEMPERATURE DISTRIBUTION IN A CYLINDRICAL HOLE IN AN ICE BLOCK

Consider an ice block of thickness H through which there is a vertical, cylindrical hole of radius R. Air flows up the hole at a velocity v_z. There is a vertical temperature gradient across the block, $\partial T/\partial z$, where z is the vertical coordinate, positive upward. In steady-state, the heat equation for the moving air in the hole is

$$\frac{\partial^2 T}{\partial z^2} + \frac{1}{r}\left\{\frac{\partial}{\partial r} r \frac{\partial T}{\partial r}\right\} + \frac{v_z}{\alpha_{air}} \frac{\partial T}{\partial z} = 0 \qquad \text{(E-1)}$$

where α_{air} is the thermal diffusivity of the air and r is the radial coordinate from the center of the hole. Assuming that the temperature gradient is a constant, it can be shown by differentiation that a solution to eq E-1 is

$$T(z,r) = \frac{\partial T}{\partial z} z + \left(1 - \frac{r^2}{R^2}\right)\left(\frac{v_z R^2 \frac{\partial T}{\partial z}}{4\alpha}\right). \qquad \text{(E-2)}$$

The difference in the temperature of the air at a height z from that of the walls of the hole is

$$\Delta T(r) = \left(1 - \frac{r^2}{R^2}\right)\left(\frac{v_z R^2 \frac{\partial T}{\partial z}}{4\alpha}\right) \qquad \text{(E-3)}$$

APPENDIX F: THE CONTINUITY EQUATION FOR A COMPACTING LAYER OF SNOW

Conservation of mass for a small volume of snow, ΔV, from which there is mass flux divergence, $\nabla \cdot \vec{J}$, can be written as:

$$\lim_{\Delta V \to 0} \left\{ \frac{1}{\Delta V} \frac{Dm}{Dt} \right\} = - \left(\nabla \cdot \vec{J} \right) \tag{F-1}$$

where t is time and Dm/Dt is the material derivative that is used because the volume is moving. The flux divergence, $\nabla \cdot \vec{J}$ is primarily the result of the movement of water vapor into and out of the volume by diffusion and convection. If we set the mass (m) equal to ($\rho \, \Delta V$), eq F-1 can be written

$$\lim_{\Delta V \to 0} \left[\rho \frac{1}{\Delta V} \frac{D(\Delta V)}{Dt} \right] + \frac{D\rho}{Dt} = - \left(\nabla \cdot \vec{J} \right) \tag{F-2}$$

The first term in brackets is the density (ρ) times the volumetric strain rate ($\dot{e}$), so eq F-2 becomes

$$\dot{e}\rho + \frac{D\rho}{Dt} = - \left(\nabla \cdot \vec{J} \right) \tag{F-3}$$

Assuming that the small volume is in a horizontal snow layer of great extent, there will be no strain in the x and y direction. Then

$$\dot{e} \to \dot{e}_{zz} = \lim_{h \to 0} \left\{ \frac{1}{h} \frac{Dh}{Dt} \right\} \tag{F-4}$$

where h is the thickness of the snow layer. Further, assuming that water vapor flows into or out of this layer only in a vertical direction (the predominant temperature gradients are in that direction), then $\nabla \cdot \vec{J}$ simplifies to $\partial J/\partial z$. Eq F-3 becomes:

$$\lim_{h \to 0} \left\{ \frac{\rho}{h} \frac{Dh}{Dt} \right\} + \frac{D\rho}{Dt} = - \frac{\partial J}{\partial z} \tag{F-5}$$

If h is finite, then this is:

$$\frac{\bar{\rho}}{h} \frac{Dh}{Dt} + \frac{D\rho}{Dt} \approx - \frac{\overline{\partial J}}{\partial z} \tag{F-6}$$

where z is the vertical coordinate, positive upward, and the overbar indicates the spatial average over the layer thickness.

The uncertainty in the calculated value of $\overline{\partial J/\partial z}$ can be determined by considering the uncertainties (e) in the measured values of h, ρ, Dh/Dt, and $D\rho/Dt$:

snow layer thickness (h): $e_h = \pm 3$ mm
snow layer density (ρ): $e_\rho = \pm 5$ kg m^{-3}
slope of compaction curve (Dh/Dt): $e_{Dh} = \pm 6 \times 10^{-10}$ m s^{-1}
slope of densification curve ($D\rho/Dt$): $e_{D\rho} = \pm 1 \times 10^{-6}$ kg m^{-3} s^{-1}

This produces an uncertainty in the calculated value of $\partial J/\partial z$ equal to (Young 1962):

$$e = \left[\left(\frac{\frac{Dh}{Dt}}{h} e_\rho \right)^2 + \left(\frac{\frac{Dh}{Dt}(\rho)}{h^2} e_h \right)^2 + \left(\frac{\rho}{h} e_{Dh} \right)^2 + \left(e_{D\rho} \right)^2 \right]^{1/2} \quad \text{(F-7)}$$

where $h(t)$ and $\rho(t)$ are the curves fit to compaction and densification data (see Section 4). The uncertainty in $\partial J/\partial z$ (using reasonable values of h, ρ, and $h(t)$ for purposes of calculation [$h = 0.05$ m, $\rho = 180$ kg m^{-3}, and $Dh/Dt = 50 \times 10^{-10}$ m s^{-1}]) shown as a function of e_h and e_ρ in Figure F-1 indicates that the flux gradient is more sensitive to errors in thickness than errors in density.

The flux gradient, $\partial J/\partial z$, can be integrated starting at the snow/soil interface in order to calculate the flux at the top of each snow layer:

$$J(z) = \int_0^h \left(\frac{\partial J}{\partial z} \right) dz \quad \text{(F-8)}$$

The flux out of the bottom layer of snow (thickness h_b) is:

$$J(h_b) = h_b \frac{\partial J}{\partial z} + J_{\text{snow/soil}} \quad \text{(F-9)}$$

where $J_{\text{snow/soil}}$ is the flux measured at the snow/soil interface. The integration can be repeated for successively higher layers in the snow cover.

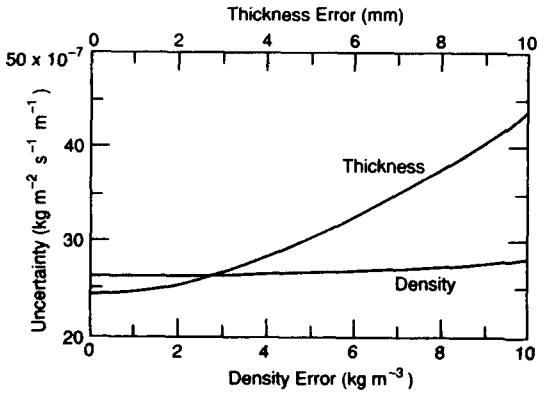

Figure F-1. The relationship between the uncertainty (e) in the calculated value of the layer-to-layer mass flux gradient ($\partial J/\partial z$) and errors in measurements of snow density (ρ) and layer thickness (h).

REPORT DOCUMENTATION PAGE

Form Approved
OMB No. 0704-0188

Public reporting burden for this collection of information is estimated to average 1 hour per response, including the time for reviewing instructions, searching existing data sources, gathering and maintaining the data needed, and completing and reviewing the collection of information. Send comments regarding this burden estimate or any other aspect of this collection of information, including suggestion for reducing this burden, to Washington Headquarters Services, Directorate for Information Operations and Reports, 1215 Jefferson Davis Highway, Suite 1204, Arlington, VA 22202-4302, and to the Office of Management and Budget, Paperwork Reduction Project (0704-0188), Washington, DC 20503.

1. AGENCY USE ONLY (Leave blank)	2. REPORT DATE	3. REPORT TYPE AND DATES COVERED
	October 1991	

4. TITLE AND SUBTITLE
The Role of Thermal Convection in Heat and Mass Transport in the Subarctic Snow Cover

5. FUNDING NUMBERS
PE: 6.11.01A
PR: 4A161101A91D
TA: ILIR
WU: 524

6. AUTHORS
Matthew Sturm

7. PERFORMING ORGANIZATION NAME(S) AND ADDRESS(ES)
U.S. Army Cold Regions Research and Engineering Laboratory
72 Lyme Road
Hanover, New Hampshire 03755-1290

8. PERFORMING ORGANIZATION REPORT NUMBER
CRREL Report 91-19

9. SPONSORING/MONITORING AGENCY NAME(S) AND ADDRESS(ES)
U.S. Army Cold Regions Research and Engineering Laboratory
72 Lyme Road
Hanover, New Hampshire 03755-1290

10. SPONSORING/MONITORING AGENCY REPORT NUMBER

11. SUPPLEMENTARY NOTES

12a. DISTRIBUTION/AVAILABILITY STATEMENT
Approved for public release; distribution is unlimited.

Available from NTIS, Springfield, Virginia 22161

12b. DISTRIBUTION CODE

13. ABSTRACT (*Maximum 200 words*)

The purpose of this study was to investigate the role of air convection in moving heat and water vapor in snow. To detect convection, the three-dimensional temperature field in the Fairbanks snow cover was measured hourly during three winters (1984–1987). Measurements of snow density, compaction, and grain size were made monthly to determine the water vapor flux and textural changes.

The snow metamorphosed into depth hoar, producing a sequence of five layers, including a basal layer with horizontal c-axes. C-axes in the overlying layers were vertical or randomly oriented. As the depth hoar developed, its air permeability increased to a value several times higher than previously measured for any snow, while the number of snow grains per unit volume decreased by an order of magnitude as a few select grains grew while others sublimated away. Simultaneously, there was a net transfer of mass from the base to the top of the snow due to mass flux gradients that averaged 3×10^{-6} kg m^{-2} s^{-1} m^{-1}, but were occasionally 10 times higher.

Convection occurred sporadically in the winter of 1984–85 and continuously in the winters of 1985–86 and 1986–87. The evidence was 1) simultaneous warming and cooling at different locations in a horizontal plane in the snow, and 2) horizontal temperature gradients of up to 16°C m^{-1}. The convection was time-dependent, with perturbations such as high wind or rapid changes in air temperature triggering periods when horizontal temperature gradients were strongest, suggesting these were also periods when the air flow was fastest. During the winter, warm and cold zones developed in the snow and remained

14. SUBJECT TERMS			15. NUMBER OF PAGES
Air flow	Snow	Thermal conductivity	93
Convection	Snow metamorphism	Vapor flux	16. PRICE CODE
Depth hoar	Temperature		

17. SECURITY CLASSIFICATION OF REPORT	18. SECURITY CLASSIFICATION OF THIS PAGE	19. SECURITY CLASSIFICATION OF ABSTRACT	20. LIMITATION OF ABSTRACT
UNCLASSIFIED	UNCLASSIFIED	UNCLASSIFIED	UL

NSN 7540-01-280-5500

☆ U. S. GOVERNMENT PRINTING OFFICE: 1991--600-063--42032

Standard Form 298 (Rev. 2-89)
Prescribed by ANSI Std. Z39-18
298-102

13. Abstract (cont'd).

relatively fixed in space. The zones were probably the result of a diffuse plume-like convection pattern linked to spatial variations in the temperature of the snow/soil interface. Air flow was inferred to have been horizontal near the base of the snow and vertical elsewhere. Flow averaged 0.2 mm s^{-1}, with a maximum of 2 mm s^{-1}. During average flow conditions, convection moved about a third of the total heat, but did not move significant mass. However, the coincidence of crystals with horizontal c-axes and the horizontal flow lines at the base of the snow suggests that convection may have affected crystal growth direction.